NASA TECHNICAL MEMORANDUM

NASA TM X-72702

NASA TM X-72702

FLOW VISUALIZATION OF LEADING-EDGE VORTEX ENHANCEMENT BY SPANWISE BLOWING

By Gary E. Erickson - George Washington University,
Joint Institute of Acoustics and Flight Sciences and
James F. Campbell - NASA Langley Research Center

NATIONAL AERONAUTICS AND SPACE ADMINISTRATION
LANGLEY RESEARCH CENTER, HAMPTON, VIRGINIA 23665

1. Report No.	2. Government Accession No.	3. Recipient's Catalog No.
NASA TM X-72702		

4. Title and Subtitle	5. Report Date
FLOW VISUALIZATION OF LEADING-EDGE VORTEX ENHANCEMENT BY SPANWISE BLOWING	SEPTEMBER 1975
	6. Performing Organization Code
7. Author(s)	8. Performing Organization Report No.
Gary E. Erickson and James F. Campbell	
	10. Work Unit No.
9. Performing Organization Name and Address	
NASA Langley Research Center Hampton, Virginia 23665	11. Contract or Grant No.
	13. Type of Report and Period Covered
12. Sponsoring Agency Name and Address	Technical Memorandum
National Aeronautics and Space Administration Washington, DC 20546	14 Sponsoring Agency Code

15. Supplementary Notes

16. Abstract

Flow visualization studies were conducted in a small pilot wind tunnel at the NASA Langley Research Center to determine qualitative effects of blowing a discrete jet essentially parallel to the leading edge of a 45° -swept trapezoidal wing featuring leading- and trailing-edge flaps. Test parameters included wing angle-of-attack, jet momentum coefficient, leading- and trailing-edge flap deflections, and nozzle chordwise displacement. Results of this study indicated that blowing from a reflection plane over the wing was found to enhance the leading-edge vortex and to delay vortex bursting to higher angles-of-attack and greater span distances. Increased blowing rates decreased vortex size, growth rate, and vertical displacement above the wing surface at a given span station and also extended the spanwise effectiveness of lateral blowing. Deflection of a leading-edge flap delayed the beneficial effects of spanwise blowing to higher angles-of-attack. Nozzle chordwise locations investigated for the wing with and without leading-edge flap deflection appeared equally effective in enhanchng the separated leading-edge flow. Observations also suggest that spanwise blowing in conjunction with deflection of a leading-edge flap may possibly enhance trailing-edge flap effectiveness.

17. Key Words (Suggested by Author(s)) (STAR category underlined)	18. Distribution Statement
Spanwise blowing Leading-edge vortex	Unclassified-Unlimited

19. Security Classif. (of this report)	20. Security Classif. (of this page)	21. No. of Pages	22. Price*
Unclassified	Unclassified	105	

*Available from { The National Technical Information Service, Springfield, Virginia 22151
STIF/NASA Scientific and Technical Information Facility, P.O. Box 33, College Park, MD 20740

NATIONAL AERONAUTICS AND SPACE ADMINISTRATION

FLOW VISUALIZATION OF LEADING-EDGE VORTEX ENHANCEMENT BY SPANWISE BLOWING

By Gary E. Erickson and James F. Campbell
Langley Research Center
Hampton, Virginia

SUMMARY

Flow visualization studies were conducted in a small pilot wind tunnel at the NASA Langley Research Center to determine qualitative effects of blowing a discrete jet essentially parallel to the leading edge of a 45° -swept trapezoidal wing featuring leading- and trailing-edge flaps. Test parameters included wing angle-of-attack, jet momentum coefficient, leading- and trailing-edge flap deflections, and nozzle chordwise displacement. Results of this study indicated that blowing from a reflection plane over the wing was found to enhance the leading-edge vortex and to delay vortex bursting to higher angles of attack and greater span distances. Increased blowing rates decreased vortex size, growth rate, and vertical displacement above the wing surface at a given span station and also extended the spanwise effectiveness of lateral blowing. Deflection of a leading-edge flap delayed the beneficial effects of spanwise blowing to higher angles-of-attack. Nozzle chordwise locations investigated for the wing with and without leading-edge flap deflection appeared equally effective in enhancing the separated leading-edge flow. Observations also suggest that spanwise blowing in conjunction with deflection of a leading-edge flap may possibly enhance trailing-edge flap effectiveness.

INTRODUCTION

Stable leading-edge vortices are characteristic of the flow over thin, highly-swept wings at moderate to high angles of attack. This flow situation is illustrated in Figure 1 and occurs because the favorable spanwise pressure gradient causes the separated leading-edge flow to form into a stable spiral vortex. Many researchers have investigated sharp-edge delta and delta-related planforms and have shown that a fully developed leading-edge vortex produces substantial increases in lift beyond that obtainable with attached flow (See Reference 1 for example). For moderately- swept, higher aspect ratio wings typical of fighter aircraft these vortex-induced effects are not achieved due to vortex breakdown at low angles of attack.

One technique of delaying the breakdown of the leading-edge vortex on moderately swept wings consists of blowing a concentrated jet spanwise over the wing's upper surface. A sketch of this concept is shown in Figure 2 and illustrates how air is drawn over the leading-edge vortex and reattaches behind the jet, much like the reattachment behind a two-dimensional separation bubble. Spanwise blowing induces a flow along the vortex axis which delays vortex breakdown to greater span stations and higher wing angles-of-attack. A stable flow can thus be maintained over a wider range of flight attitudes and Mach numbers.

Studies have been performed which confirm the augmentation of lift by spanwise blowing (References 2-7). An example of data is presented in Figure 3 which illustrates the magnitude of the vortex-induced lift increments for a delta planform at a jet momentum coefficient and Mach number of 0.3 and 0.2, respectively. The nonlinear character of the vortex-induced lift and the

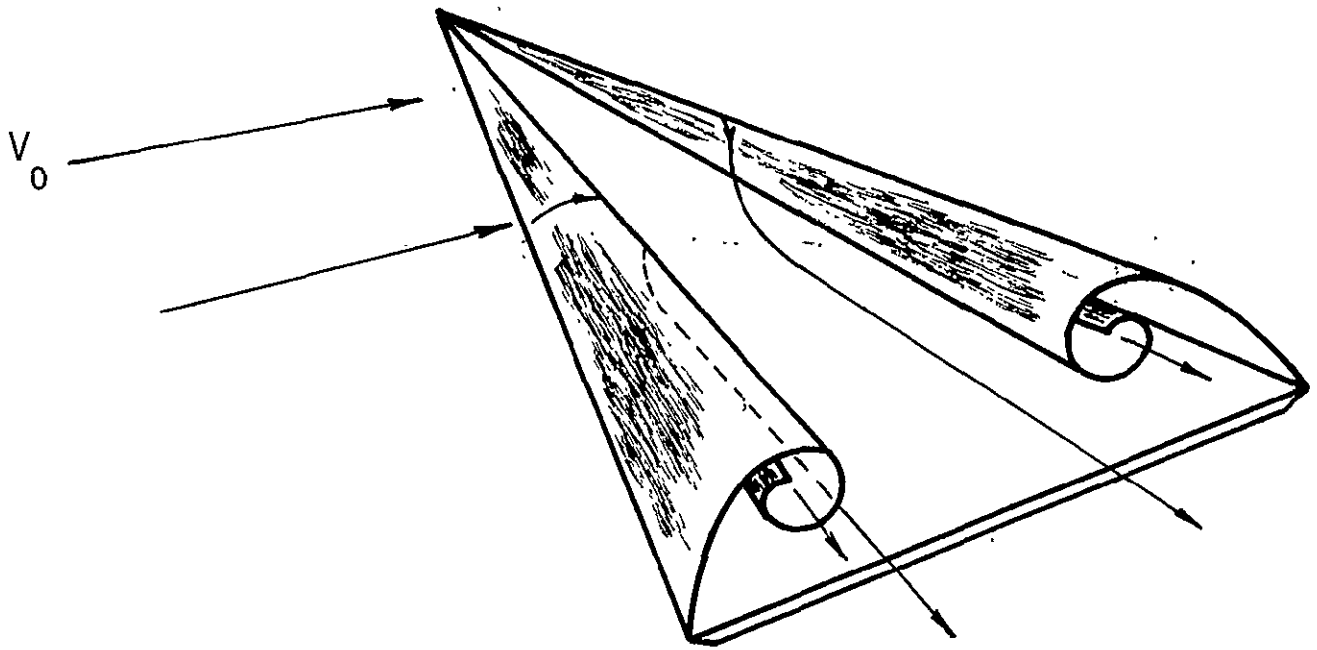

Figure 1.- Stable leading-edge vortices over a slender wing.

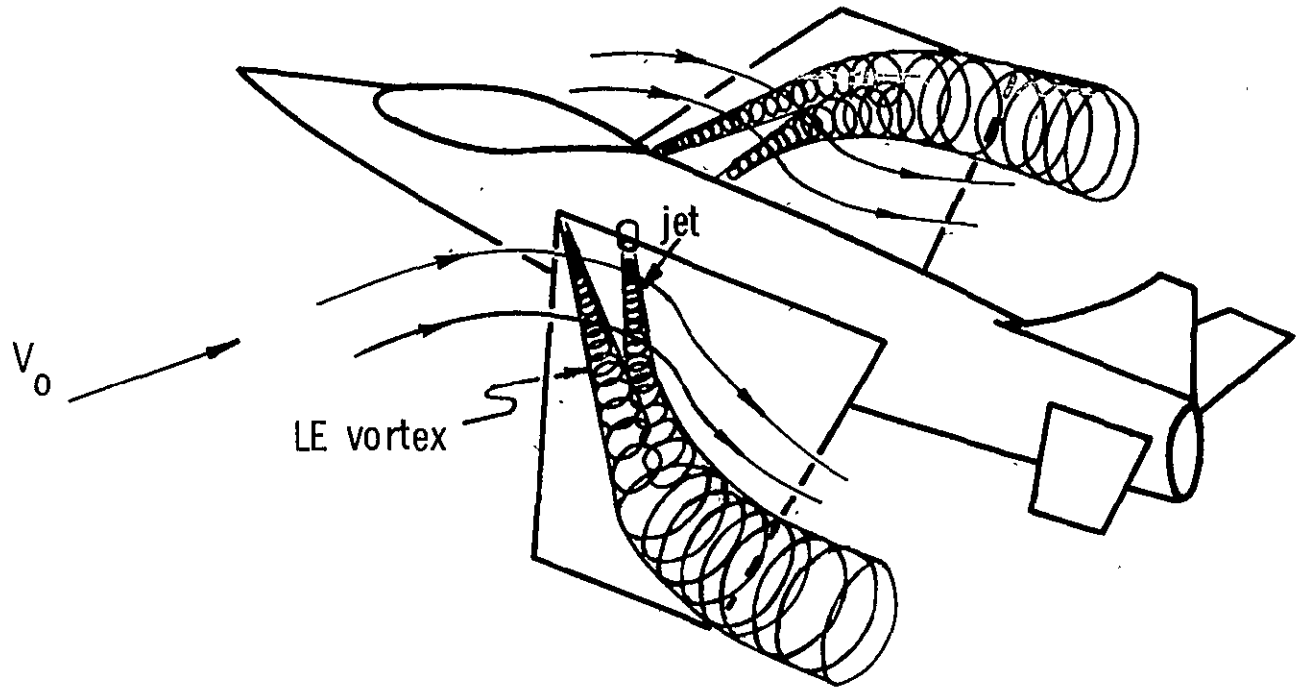

Figure 2.- Leading-edge vortex enhancement by spanwise blowing.

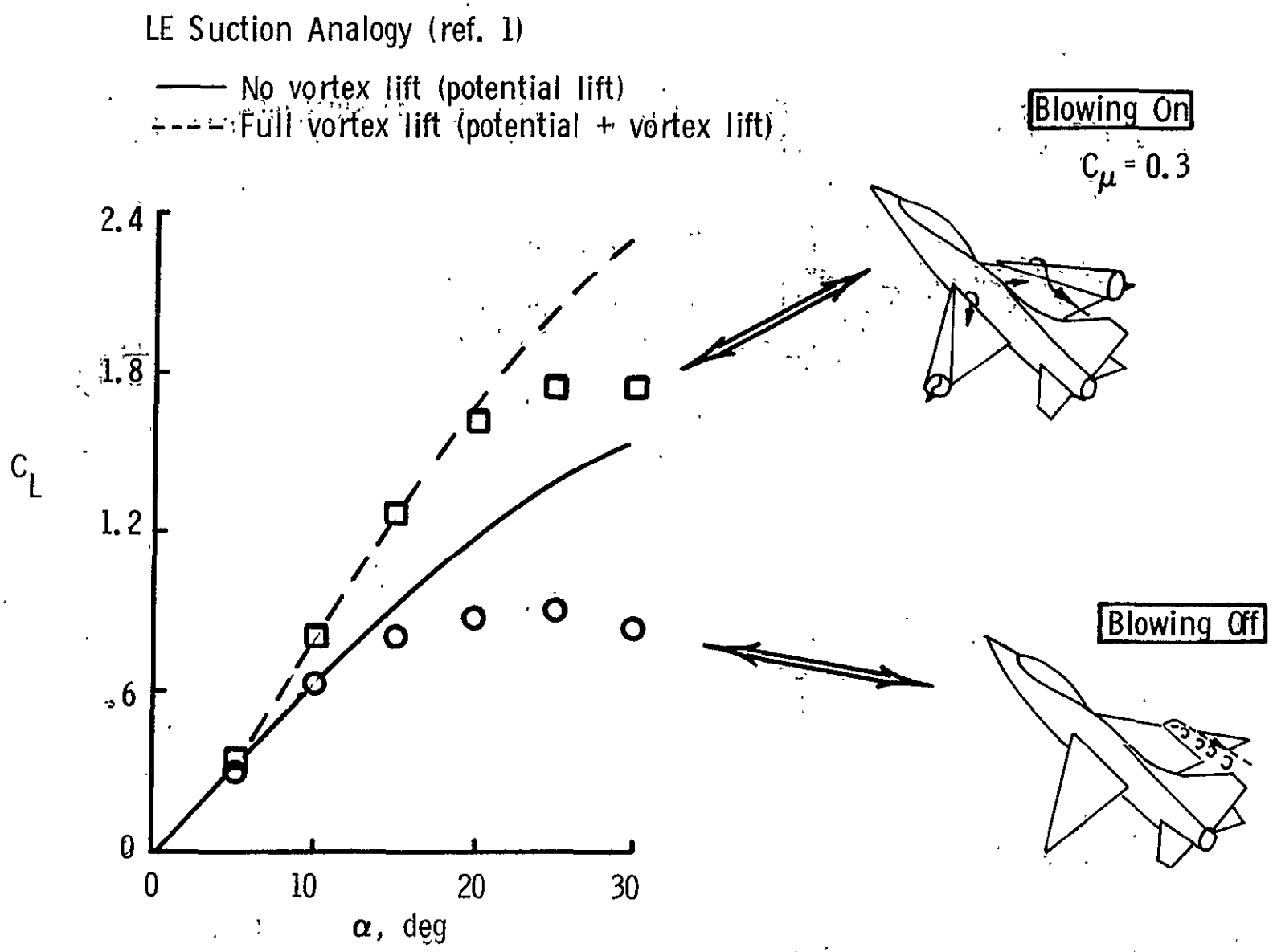

Figure 3.- Lift augmentation by spanwise blowing on a 30^0 swept delta wing at $M_0 = 0.2$ (data are from ref. 2).

substantial increase over the potential flow values are evident.

The objective of the present flow visualization study was to provide a systematic qualitative study of the nature of the leading-edge vortex flow and its enhancement by spanwise blowing over wings suitable for fighter aircraft. Low speed wind tunnel tests were conducted using a helium bubble generator to visualize the flow over a 45^{o} -swept trapezoidal wing having leading- and trailing-edge flaps. The test parameters included angle-of-attack, jet momentum coefficient, flap deflection angle, and jet chordwise location.

NOMENCLATURE

a_e	sonic velocity at nozzle exit
A_e	nozzle exit area
AR	aspect ratio
b	wing span
c_r	wing root chord
c_t	wing tip chord
C_μ	jet momentum coefficient, $\equiv \dfrac{2\left(\rho_e A_e V_e\right) V_e}{\rho_o V_o^2 S}$
d_n	nozzle diameter
LE	wing leading edge
M_e	Mach number at nozzle exit
p_e	static pressure at nozzle exit
p_o	free-stream static pressure
$p_{t,e}$	total pressure at nozzle exit
S	wing planform area

T	nozzle thrust
TE	wing trailing edge
V_e	jet exit velocity (See eq. (1))
V_o	free-stream velocity
x_n	nozzle chordwise location measured from wing apex
α	wing angle-of-attack
γ	ratio of specific heats (air: γ = 1.4)
δ_{LE}, δ_{TE}	leading- and trailing-edge flap deflection angles, respectively
ρ_e	air density at jet exit (assumed equal to ρ_o)
ρ_o	air density of free stream
2y/b	wing span station

WIND TUNNEL TESTS

Flow visualization tests were conducted in a small pilot wind tunnel at the NASA Langley Research Center. The semispan wing model was mounted on a vertical reflection plane located in the tunnel test section and which provided angle-of-attack capability by means of a circular insert. A free-stream dynamic pressure of 1.5 psf and free-stream velocity of 35.5 fps were maintained throughout the tests.

MODEL

The model used in the experiments consisted of the wing and jet assembly illustrated in Figure 4(a). The 45^o -swept trapezoidal wing was constructed of 0.25-in. thick plexiglass which was beveled to provide a sharp LE and TE. The flap had a constant-chord dimension of 0.10 c_r, while the TE flap had a chord

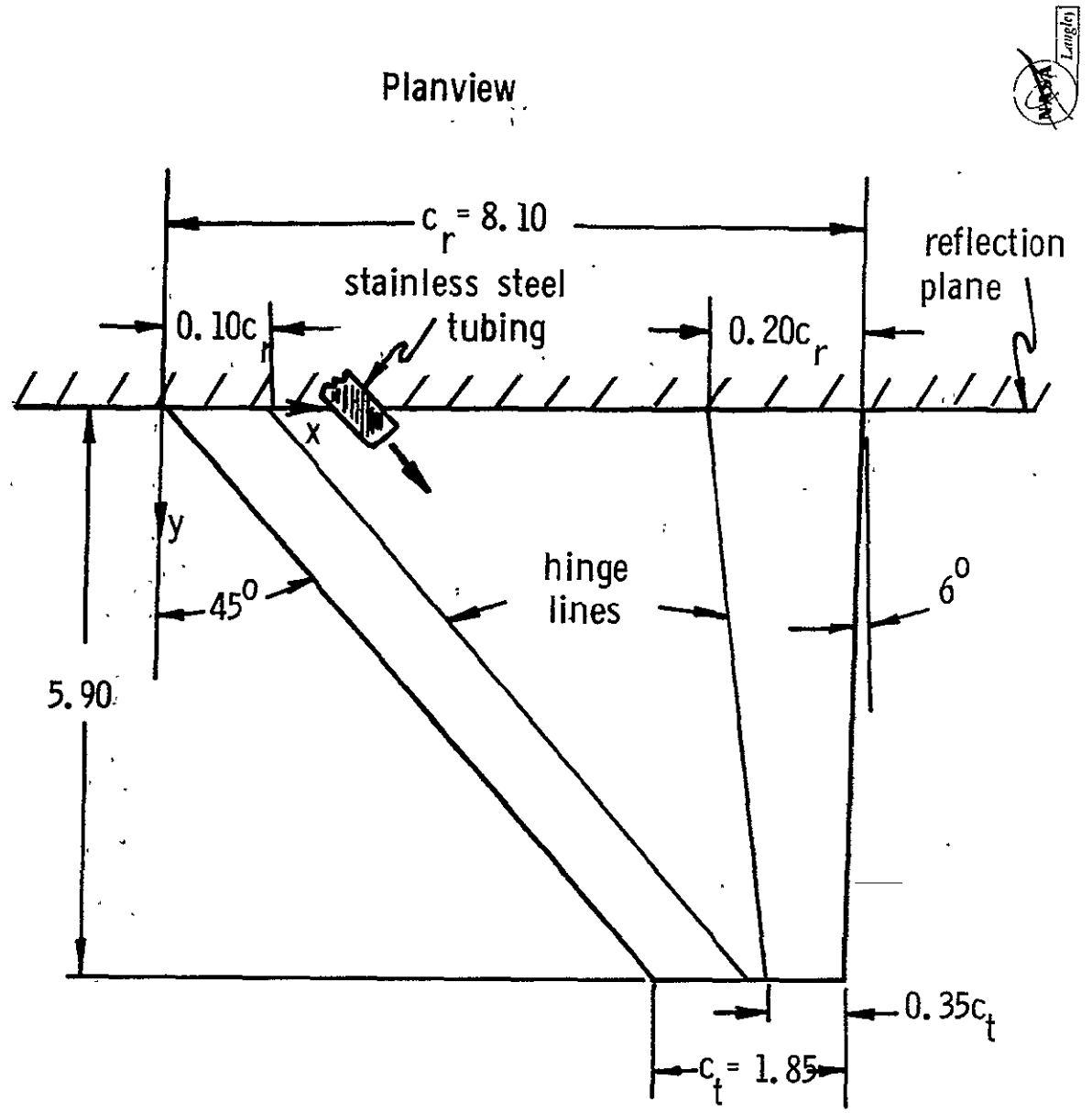

(a) Flow visualization model. (all dimensions in inches)

Figure 4.

which tapered linearly from 0.20 c_r at the root to 0.35 c_t at the tip. Test configurations considered in the flow visualization study are illustrated in Figure 4(b).

Compressed air was brought over the wing through flexible tubing coupled to a length of stainless steel tubing (0.17" I.D.) which extended outward slightly from the reflection plane and in a direction parallel to the wing leading edge.

INSTRUMENTATION

A flow meter indicated the volume flow rate (CFM) through the air supply system and the flow was regulated by a valve between the flow meter and nozzle. The volume flow rate and the compressed air pressure were adjusted to provide the desired nozzle flow conditions.

The total pressure at the nozzle exist ($p_{t,e}$) was measured with a pitot tube, and jet exit velocities were calculated using the following compressible flow equation:

$$V_e = a_e M_e = \left(\frac{2}{\gamma - 1}\right) \left\{ \left[1 - \left(\frac{p_e}{p_{t,e}}\right)^{\frac{\gamma-1}{\gamma}} \right] \left(\frac{p_e}{p_{t,e}}\right)^{\frac{\gamma-1}{\gamma}} \right\}^{1/2} \qquad (1)$$

V_e is the jet velocity that results when the flow expands isentropically from $p_{t,e}$ to p_e, where it is assumed that $p_e = p_o$.

Nozzle thrust was estimated by suspending the nozzle vertically at one end of a platform balance and measuring the thrust for a range of blowing rates. This measured thrust is plotted as a function of C_μ in Figure 5 along with the thrust calculated from the following equation:

$$T = \left(\rho_e A_e V_e\right) V_e \qquad (2)$$

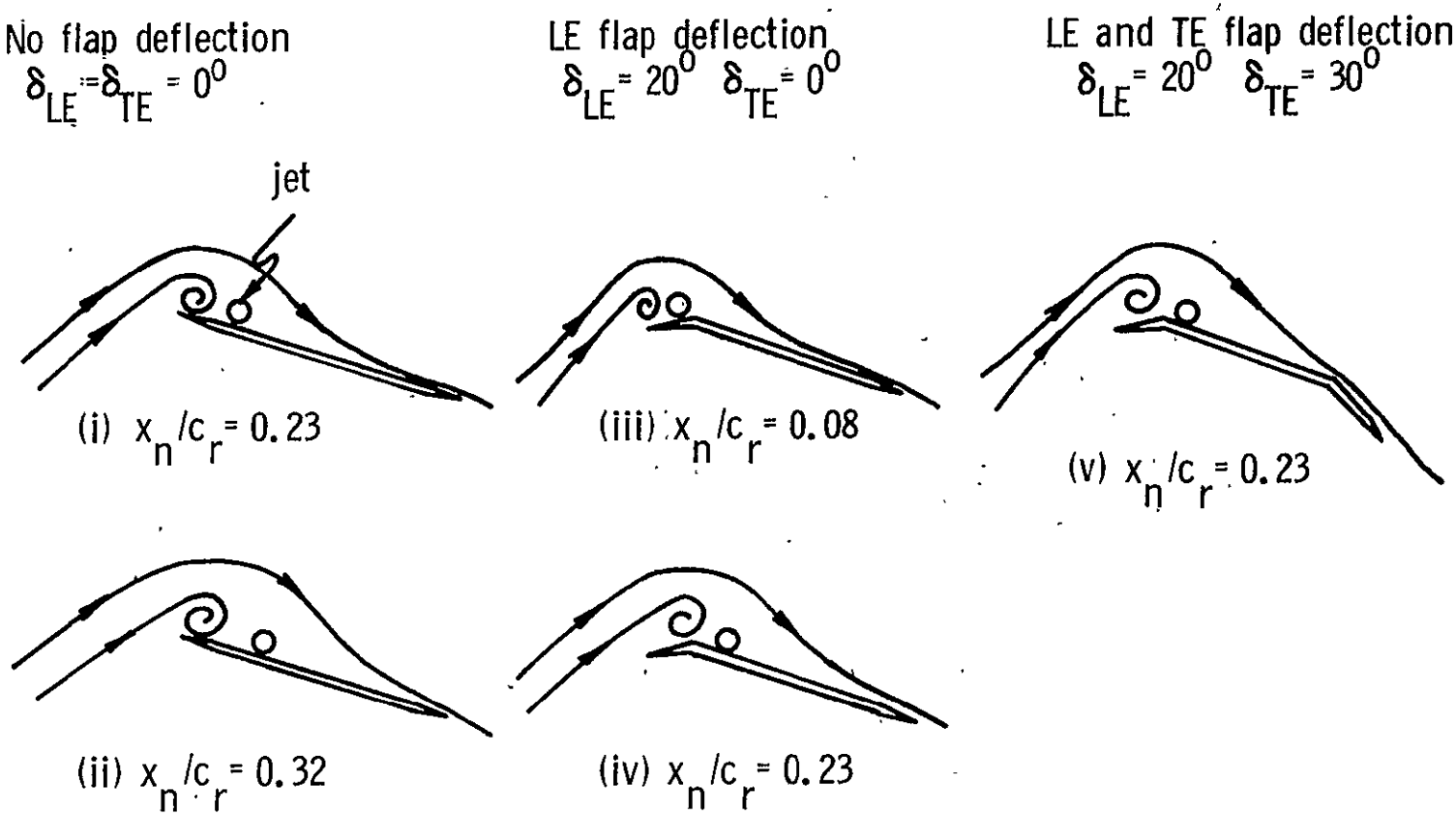

(b) Test configurations for flow visualization tests.

Figure 4.- Concluded.

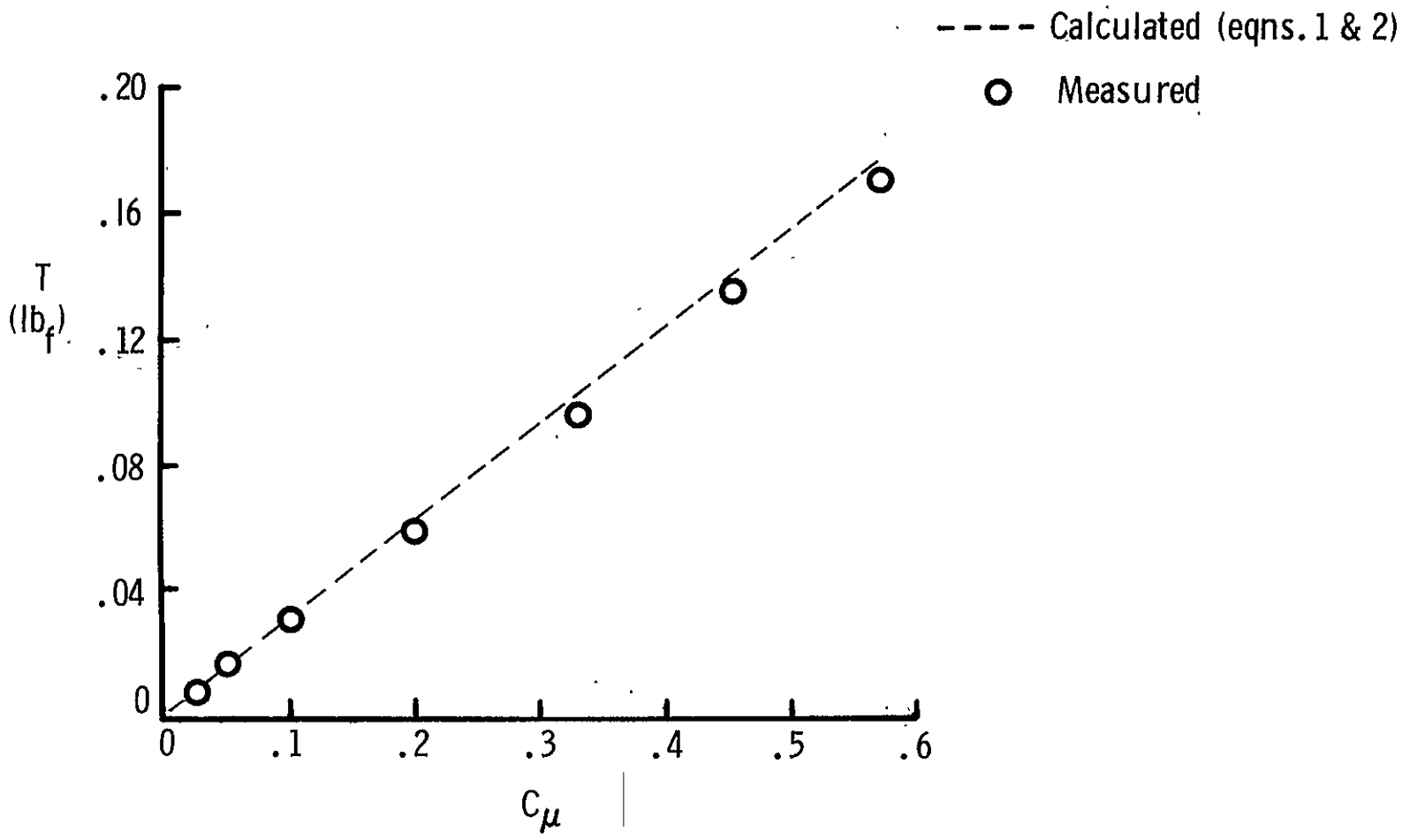

Figure 5.- Nozzle thrust versus jet momentum coefficient.

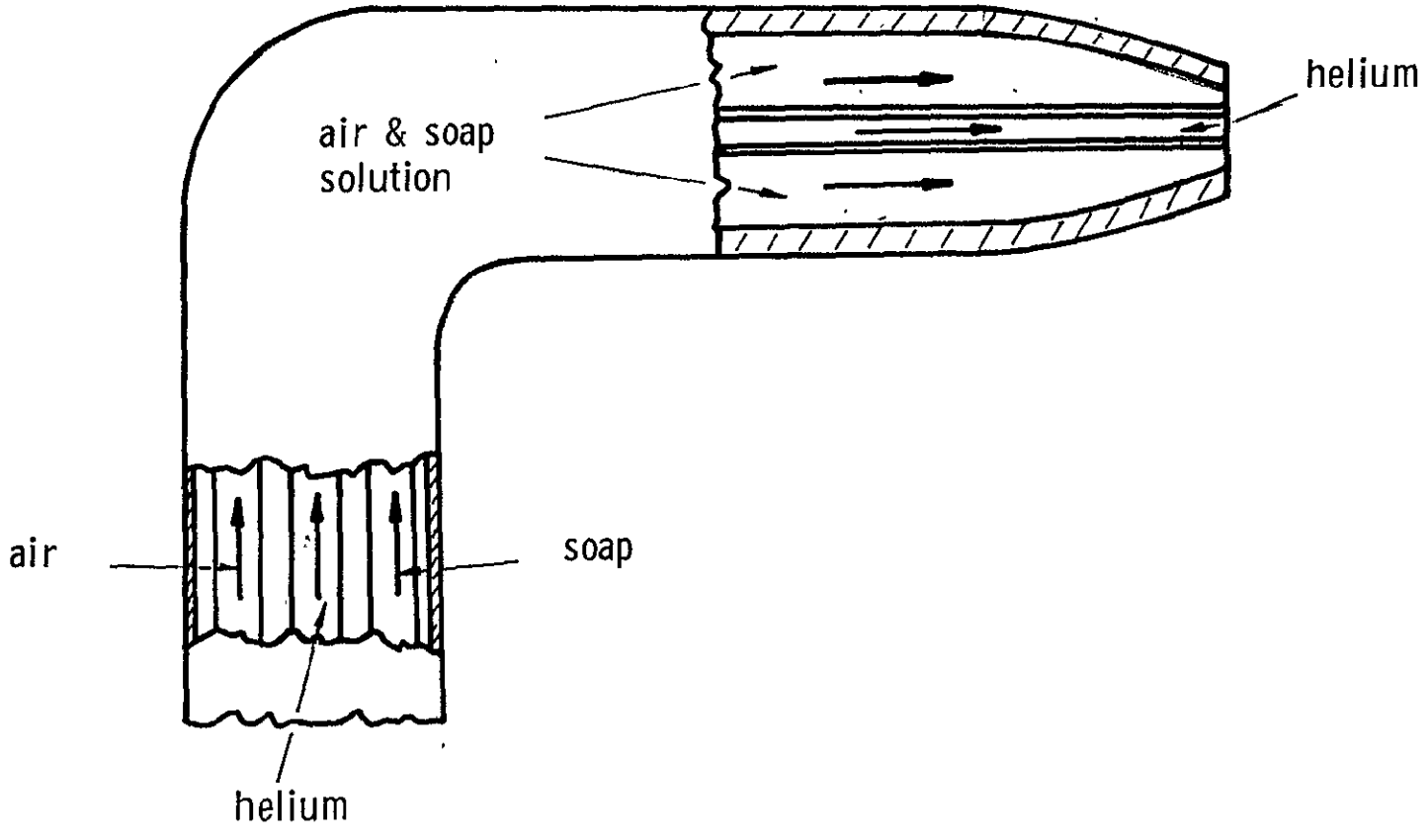

Figure 6.- Helium-filled bubble nozzle and supply lines.

A helium bubble generator was used to produce neutrally-buoyant helium-filled bubbles which, when exposed to the flow, would reveal the general flow about the model. A mixture of air, helium, and soap solution ejected at the end of a converging nozzle produced bubbles, the diameter of which could be varied by adjusting the air, helium, and soap supplies. A sketch of the nozzle arrangement is presented in Figure 6. The flow at any wing station could be examined by moving the bubble nozzle to the desired location.

A high-intensity light source was placed behind the model and facing upstream such that the bubbles would appear white in contrast to the black surfaces of the model and reflection plane.

A Hasselblad 500 EL-M (70mm) camera was used in the tests. F-stop and shutter speed settings were 5.6 and 1/8 second, respectively, which enabled each bubble to appear as a streakline in the foregoing photographs. The development process of the Kodak Tri-X Pan film (ASA 400) increased the ASA rating to 1000 to heighten the contrast between the helium-filled bubbles and the wing and reflection plane surfaces.

RESULTS AND DISCUSSION

The results of this study are in the form of photographs which were taken of the flow visualization process for the variety of test configurations illustrated in Figure 4(b). In all of these photographs, the free-stream flow is from left to right. The general effects of spanwise blowing on the wing with no flap deflections are discussed in the following section for a range of angle-of-attack and blowing rate. Observations of the effects of spanwise blowing on the wing with leading-edge and trailing-edge flap deflections will be presented in later sections.

Effect of Spanwise Blowing on Wing with No Flap Deflections ($\delta_{LE} = \delta_{TE} = 0$)

The results obtained for the wing with no flap deflection are presented in Figures 7-53 for angles-of-attack from 15^{o} to 35^{o} and C_{μ} values from 0.0 to 0.088. Unless otherwise noted, the information presented in this section was acquired with the nozzle at a chordwise location of $x_n/c_r = 0.23$.

With no blowing ($C_{\mu} = 0$) and $\alpha = 15^{o}$, the separated leading-edge flow rolled up into a weak vortex originating at the wing apex (Figure 7). Increasing angle-of-attack to 20^{o} (Figure 12) and 25^{o} (Figure 23) weakened the vortex even further until at $\alpha = 30^{o}$ (Figure 33) and 35^{o} (Figure 42) the flow over the wing became completely separated, resulting in a large, slowly rotating mass.

Figures 8 and 9 illustrate the enhancement of the LE vortex by spanwise blowing at $\alpha = 15^{o}$ and $C_{\mu} = .026$ and .057, respectively, where the nozzle is located at $x_n/c_r = .23$. At the higher blowing rate, it is evident that vortex bursting is delayed to a greater span distance and the apparent vortex strength is increased at a given span station. Figures 10 and 11 are side views which illustrate the flow at $\alpha = 15^{o}$ and $C_{\mu} = .057$ at $2y/b = .1$, $2y/b = .5$, respectively. The separated leading-edge flow is drawn over the jet and reattaches behind the jet. Furthermore, the reattachment point behind the jet moves aft towards the trailing edge as span distance is increased.

The flow visualization tests suggest that spanwise blowing effectiveness is dependent on separated flow at the leading-edge. Figures 12-22 illustrate the progressive enhancement of the separated leading-edge flow at $\alpha = 20^{o}$ for the range of blowing rates $0.0 \leqslant C_{\mu} \leqslant .088$. It appears that

maintaining a stable leading-edge vortex is dependent on sufficient axial flow in the vortex core. The deflected streaklines over the jet-vortex system appear similar to potential flow about a wing of increased camber and thickness. Vortex instability is indicated in Figures 13-19 by a significant increase in vortex size and growth rate and consequent vortex bursting. A leading-edge "bulb," or closed turbulent region which includes both the vortex and jet flows, is shown in Figure 20 at $\alpha = 20^{\circ}$ and $C_{\mu} = .057$. The leading-edge "bulb" acts essentially as a solid body which induces an effective increase in wing camber. Also, at low angles-of-attack at which spanwise blowing effectiveness is minimal, a jet camber effect, as discussed in References 2 and 3, occurs which induces a positive lift increment. Referring again to Figure 20, there appeared to be a dividing streamline between the vortex and jet, from which flow moved forward towards the leading-edge. The co-rotation of the vortex and jet also suggests that the jet feeds mass and momentum into the underside of the vortex. The jet is analogous to a spanwise line sink and the separated leading-edge flow to a feeding vortex sheet, the outer layers of which are entrained into the vortex core region. A second stagnation line behind the jet was also observed, behind which a forward flow was induced by jet entrainment. Figures 21 and 22 show the flow at 2y/b = .5 and .75, respectively, at $\alpha = 20^{\circ}$, $C_{\mu} = .057$. The flow reattachment point behind the jet at 2y/b = .50 is near mid-chord. At 2y/b = .75, flow reattachment on the wing surface does not occur.

Comparison of Figures 12-22 at $\alpha = 20^{\circ}$ with Figures 23-32 at $\alpha = 25^{\circ}$ illustrate the increase in vortex size, growth rate and vertical displacement above the wing surface at a given C_{μ} as α is increased. Further investigation of Figures 23-32 reveal that the enhancement of the LE vortex by spanwise

blowing at $\alpha = 15^{\circ}$ and 20° is also evident at $\alpha = 25^{\circ}$, but to a lesser degree. This implies that higher blowing rates are required to maintain a stable leading-edge vortex to a given span station as angle-of-attack is increased. The photographs also suggest that blowing a discrete jet in a spanwise direction induces an equivalent sweep and sufficient axial flow to augment the LE vortex. The strong, stable LE vortex and the flow reattachment behind the jet, as seen in Figures 17 and 18 at $\alpha = 20^{\circ}$, with $C_{\mu} = .057$ and .075, respectively, and also in Figures 29 and 31 at $\alpha = 25^{\circ}$, with $C_{\mu} = .057$ and .075, respectively, imply that at moderate to high angles-of-attack the vortex lift increment should be significant.

Figures 33-41 at $\alpha = 30^{\circ}$ and Figures 42-49 at $\alpha = 35^{\circ}$ further illustrate the inboard displacement of the vortex bursting point at a given C_{μ} as α is increased. As seen in the photographs, vortex breakdown was very rapid at these high angles-of-attack. It has been observed in the experimental investigations of References 3 and 7 that spanwise blowing is a jet decay problem. This is well illustrated in Figures 9, 14, 25, 41, and 48 at $\alpha = 15^{\circ}$, 20°, 25°, 30°, and 35°, respectively. These photographs show that due to boundary layer interaction and surface friction, the spanwise jet decay is rapid and vortex characteristics consequently degenerate. When the local cross flow effects become dominant, the vortex-jet system is deflected downstream which is indicated in Figures 15, 28, and 35 at $\alpha = 20^{\circ}$, 25°, and 30°, respectively.

The effect of displacing the nozzle in the chordwise direction from $x_n/c_r = 0.23$ to 0.32 is seen in Figures 50 and 51 at $\alpha = 25^{\circ}$ and Figures 52 and 53 at $\alpha = 30^{0}$. These photographs were obtained for $C_{\mu} = .088$ and are representative of the results obtained for the range of angles-of-attack

($15^{\circ} \leq \alpha \leq 35^{\circ}$) and blowing rates ($0 \leq C_{\mu} \leq .088$) considered. Chordwise displacement of the nozzle to $x_n/c_r=0.32$ yielded results similar to those previously observed for blowing at $x_n/c_r=0.23$. Both nozzle locations appeared equally effective in enhancing the separated LE vortical flow.

In summary, the results of this section have shown that spanwise blowing enhanced the LE separation vortex by inducing a flow along the vortex axis. At a given angle-of-attack, vortex bursting was delayed to greater span distances, and vortex size, growth rate, and vertical displacement above the wing surface at a given span station were decreased. Increased blowing rates further enhanced the LE vortex and extended blowing effectiveness outboard. Increasing angle-of-attack increased the blowing rate required to maintain a stable vortex to a given span station.

Effect of Spanwise Blowing on Wing with LE Flap Deflection $\left(\delta_{LE}= 20^{\circ}\ ,\ \delta_{TE}= 0^{\circ}\right)$

The results obtained for the wing with a leading-edge flap deflection of 20° are presented in Figures 54-85 for the angles-of-attack from 30° to 40° and C_{μ} values of 0.0 to 0.10.

Deflection of a LE flap, which effectively increases wing camber, tended to maintain attached flow at the LE at $\alpha= 20^{\circ}$ for $C_{\mu} = 0$ as shown in Figure 54. The higher angle-of-attack range, namely $30^{\circ} \leq \alpha \leq 40^{\circ}$, at which LE separation occurred, was therefore investigated.

Figures 55, 64, and 75 show the separated flow that exists over the entire wing for $C_{\mu} = 0$ at $\alpha= 30^{\circ}$, 35°, and 40°, respectively. A large rotating mass of air was observed above and behind the wing in all cases.

Blowing over the LE flap was accomplished by positioning the nozzle at $x_n/c_r = .08$. The resulting effects are shown in Figures 56-59 at $\alpha = 30^\circ$, Figures 65-68 at $\alpha = 35^\circ$, and Figures 76-80 at $\alpha = 40^\circ$. The discussion of the preceding section concerning LE vortex enhancement by spanwise blowing on a wing with no flap deflections applies equally well to the observations discussed in this section. The roll-up of the separated LE flow ahead of the jet for a range of blowing rates, the decay characteristics of the LE vortex, and the flow reattachment point aft of the jet at various span stations are illustrated in the photographs.

The nozzle was moved aft to $x_n/c_r = .23$ to achieve blowing behind the flap hinge-line. The results are illustrated in Figures 60-63 at $\alpha = 30^\circ$, Figures 69-74 at $\alpha = 35^\circ$, and Figures 81-85 at $\alpha = 40^\circ$. These photographs show, in a manner analogous to the case for $x_n/c_r = .08$, the enhancement of the LE vortex for a range of C_μ and α, and also indicate the flow about the wing at different span stations. Since deflection of a leading-edge flap tends to maintain attached flow at the leading-edge, the beneficial effects obtained by blowing on the wing with no flap deflection are delayed to higher wing incidence at which separated flow occurs at the flap leading-edge or at the flap shoulder. Blowing over the leading-edge flap and also behind the flap hinge-line appeared equally effective in enhancing the separated leading-edge flow.

Effect of Spanwise Blowing on Wing with LE and TE Flap Deflections $\left(\delta_{LE} = 20^{o}\ ,\ \delta_{TE} = 30^{o}\right)$

Figures 86-89 indicate a possible method of increasing TE flap effectiveness by coupling deflection of a leading-edge flap with a nominal amount of spanwise blowing behind the LE flap hinge-line. For this case the nozzle was located at $x_n/c_r = 0.23$. Figures 86 and 87 reveal the reattached flow behind the jet at $\alpha = 25^{o}$ at two span stations for $\delta_{LE} = 20^{o}$, $\delta_{TE} = 30^{o}$ and $C_\mu = .011$. Figures 88-89 show in a similar manner the smooth flow over the TE flap at $\alpha = 30^{o}$ and $C_\mu = .026$.

POSSIBLE AREAS OF INVESTIGATION

Experimental observations and, also, original work performed in References 2-7, suggest that spanwise blowing could provide a means of direct lift control, a method of improving flap effectiveness and the flow about horizontal and vertical tails, improving directional stability, and a means of varying the effective wing camber and thickness. The simplicity of spanwise blowing is attractive since blowing from the fuselage requires no wing ducting or wing design modifications.

Due to vortex decay and breakdown at outboard stations, it appears necessary to provide some means of enhancing the separated leading-edge flow outboard. Distributed blowing at two span stations has been investigated in Reference 7, but wing ducting poses severe problems. A method of passively inducing a spanwise flow would avoid the problems associated with wing ducting. An alternative configuration might be a wing with a segmented leading-edge flap system coupled with spanwise blowing from the wing root. Reattachment of the separated LE flow by the highly effective jet inboard and maintainance of

attached flow at the LE by differential flap deflections outboard is a possible configuration.

Flow test observations and results obtained in Reference 6 suggest that a nominal amount of spanwise blowing associated with a small leading-edge flap deflection (e.g., 10^{o}) might induce positive lift increments and drag-due-to-lift reduction comparable to those induced by a large amount of blowing on a wing with no LE flap deflection. Spanwise blowing near the LE may improve TE flap effectiveness by maintaining smooth flow over the TE. Thus, for a given TE flap deflection, a positive increment in lift and drag-due-to-lift reduction may result and, furthermore, the effective range of TE flap deflections might be extended. Blowing over a trailing-edge flap might also be a viable method of improving flap effectiveness. A jet located in this region is shielded from crossflow effects that influence spanwise blowing near the leading-edge and necessarily acts over a smaller wing surface area.

Since the spanwise jet acts essentially as a solid body in the flow, location of a jet in the region of the LE and/or TE might induce the same aerodynamic effects as a LE and/or TE flap. The necessity of physical LE and TE flaps might thus become less significant. The reduction of weight associated with physical flaps is an appealing design consideration.

For low blowing rates at which LE vortex augmentation is nominal, spanwise blowing might be a possible boundary layer control device by inducing favorable spanwise flow gradients in the boundary layer.

Concentrated lateral blowing is a possible means of alleviating or delaying buffet during maneuver. The latter phenomenon is related to leading-edge separation and/or wing stall and creates serious problems for highly-

maneuverable aircraft.

The encouraging qualitative results obtained in the experiments illustrate the need for extensive quantitative evaluation of the applications of leading-edge vortex enhancement by spanwise blowing. Investigation of the effects of concentrated lateral blowing on maneuvering lift and stability and control characteristics are necessary. Possible areas of investigation concerning leading-edge vortex enhancement are:

1. Roll control by differential nozzle thrust.
2. Increased jet vectoring to enable higher engine thrust recovery and maintain the beneficial effects of blowing.
3. Blowing over trailing-edge flaps and in the regions of horizontal and vertical tails.
4. Blowing over canards and canard-wing configurations.
5. Spanwise blowing associated with strake-wing configurations.
6. Mach number effects on blowing effectiveness.

CONCLUDING REMARKS

Flow visualization studies were conducted in a small pilot wind tunnel at the NASA Langley Research Center to determine qualitative effects of blowing a discrete jet essentially parallel to the leading-edge of a 45^{o} -swept trapezoidal wing featuring leading- and trailing-edge flaps. Results of this investigation indicated that blowing from a reflection plane over the wing enhanced the leading-edge vortex and delayed vortex bursting to higher angles-of-attack and greater span distances. Increased blowing rates decreased vortex size, growth rate, and vertical displacement above the wing surface at a given span station and also extended the spanwise effectiveness of lateral blowing. Greater values of blowing were required to maintain a stable vortex to a given span station as angle-of-attack was increased. Concentrated blowing associated with deflection of a leading-edge flap also appeared effective in enhancing the separated LE flow. Since deflection of a LE flap tended to maintain attached flow at the LE, spanwise blowing effectiveness was delayed to higher wing angles-of-attack at which separation occurred, either at the LE or the flap shoulder. The results obtained for wing configurations with and without LE flap deflection indicated no discernible variation of LE vortex enhancement by spanwise blowing for a small range of nozzle chordwise displacements. Deflection of a LE flap coupled with spanwise blowing behind the LE flap hinge-line also appeared a viable method of improving TE flap effectiveness.

REFERENCES

1. Polhamus, Edward C.: Predictions of Vortex-Lift Characteristics by a Leading-Edge Suction Analogy. Journal of Aircraft, April 1971.
2. Bradley, R. G., et. al.: An Experimental Investigation of Leading-Edge-Vortex Augmentation by Blowing. NASA CR-132415, April 1974.
3. Campbell, James F.: Effects of Spanwise Blowing on the Pressure Field and Vortex-Lift Characteristics of a 44° Swept Trapezoidal Wing. NASA TN D-7907, August 1975.
4. Dixon, C. J.: Lift Augmentation by Lateral Blowing Over a Lifting Surface. AIAA Paper No. 69-193, February 1969.
5. Cornish, J. J.: High-Lift Applications of Spanwise Blowing. ICAS Paper No. 70-09, September 1970.
6. Bradley, R. G., et. al.: Leading-Edge-Vortex Augmentation In Compressible Flow. AIAA Paper No. 75-124, January 1975.
7. Dixon, C. J., et. al.: Theoretical and Experimental Investigations of Vortex-Lift Control by Spanwise Blowing. Vol. I, Experimental Research, LG73ER-0169, September 1973.

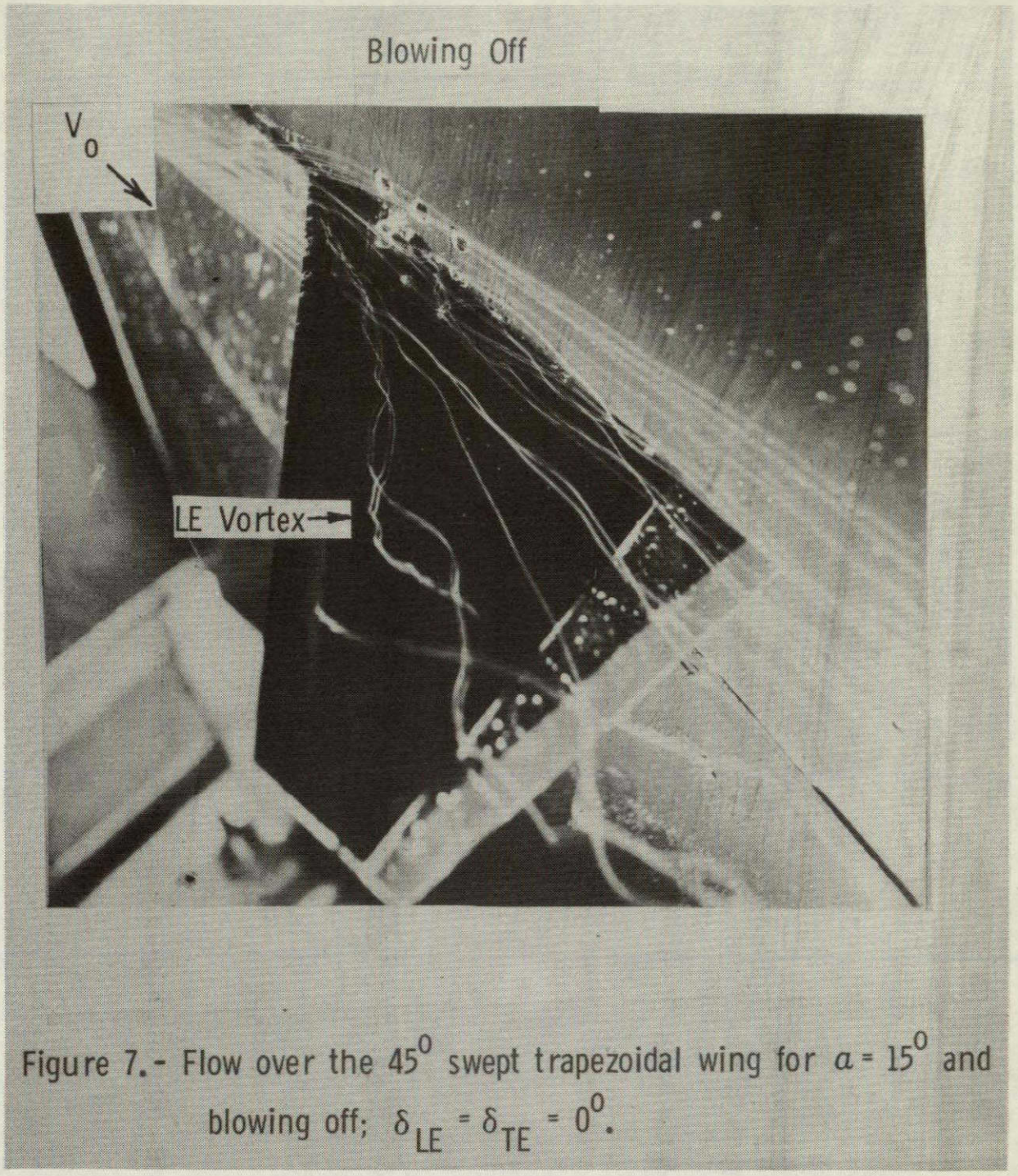

Figure 7.- Flow over the 45^o swept trapezoidal wing for $\alpha = 15^o$ and blowing off; $\delta_{LE} = \delta_{TE} = 0^o$.

PAGE INTENTIONALLY BLANK

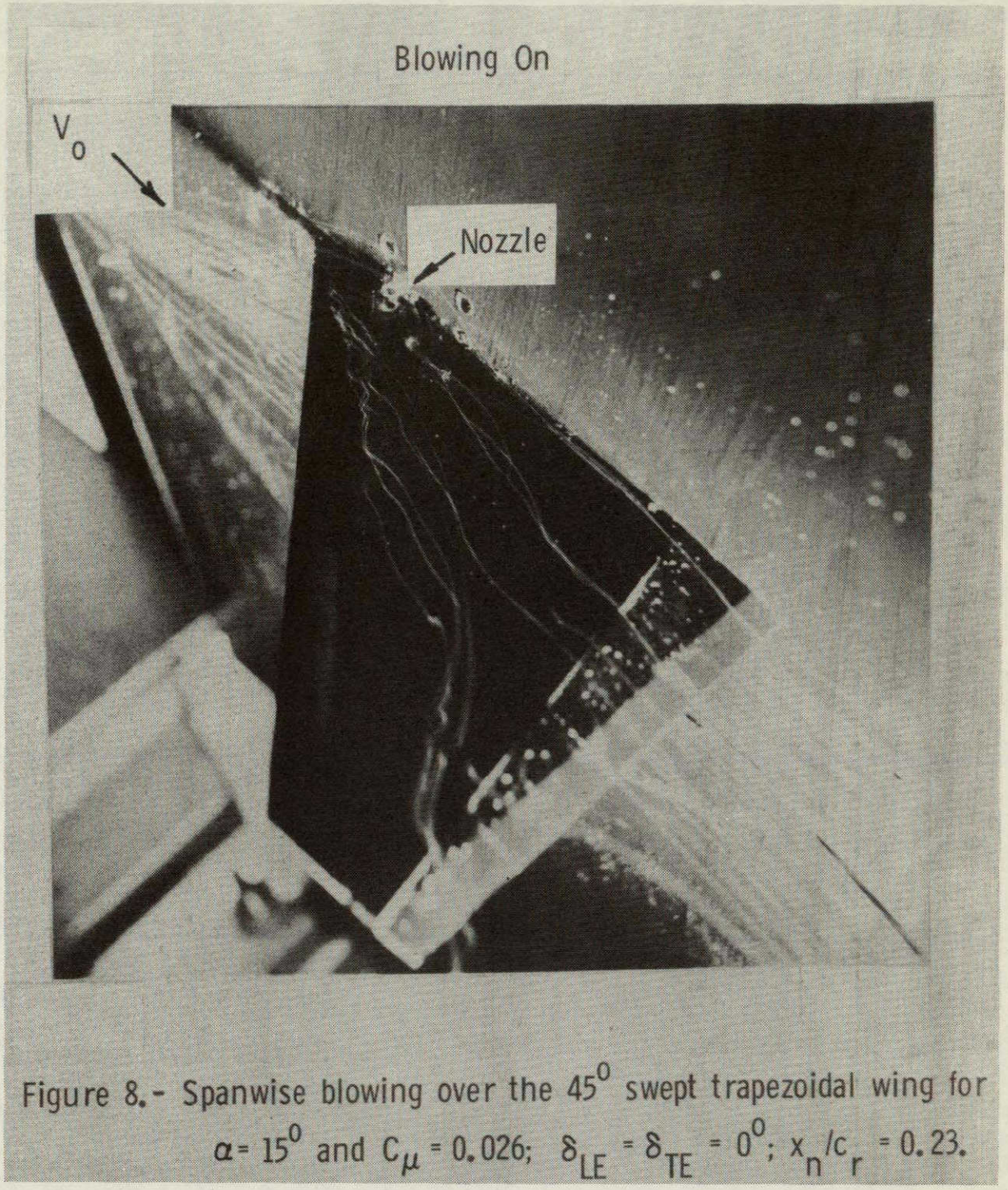

Figure 8.- Spanwise blowing over the 45^0 swept trapezoidal wing for $\alpha = 15^0$ and $C_\mu = 0.026$; $\delta_{LE} = \delta_{TE} = 0^0$; $x_n/c_r = 0.23$.

PAGE INTENTIONALLY BLANK

Blowing On

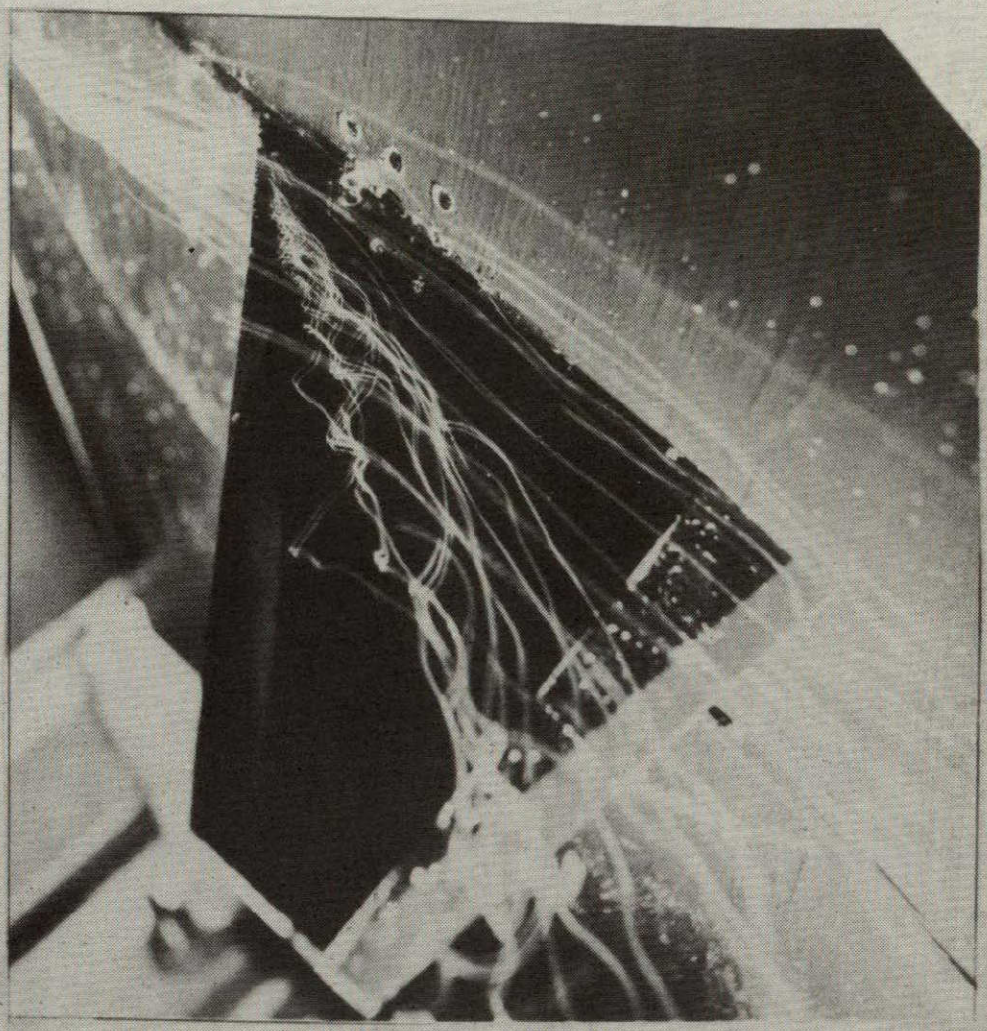

Figure 9.- Spanwise blowing over the 45^{o} swept trapezoidal wing for $\alpha = 15^{o}$ and $C_{\mu} = 0.057$; $\delta_{LE} = \delta_{TE} = 0^{o}$; $x_n/c_r = 0.23$.

PAGE INTENTIONALLY BLANK

Figure 10.- Spanwise blowing over the 45^0 swept trapezoidal wing for $\alpha = 15^0$ and $C_\mu = 0.057$; $\delta_{LE} = \delta_{TE} = 0^0$; $x_n/c_r = 0.23$.

PAGE INTENTIONALLY BLANK

Blowing On

Streaklines At Mid-Span

Figure 11.- Spanwise blowing over the 45^{o} swept trapezoidal wing for $\alpha = 15^{o}$ and $C_{\mu} = 0.057$; $\delta_{LE} = \delta_{TE} = 0^{o}$; $x_n/c_r = 0.23$.

PAGE INTENTIONALLY BLANK

Blowing Off

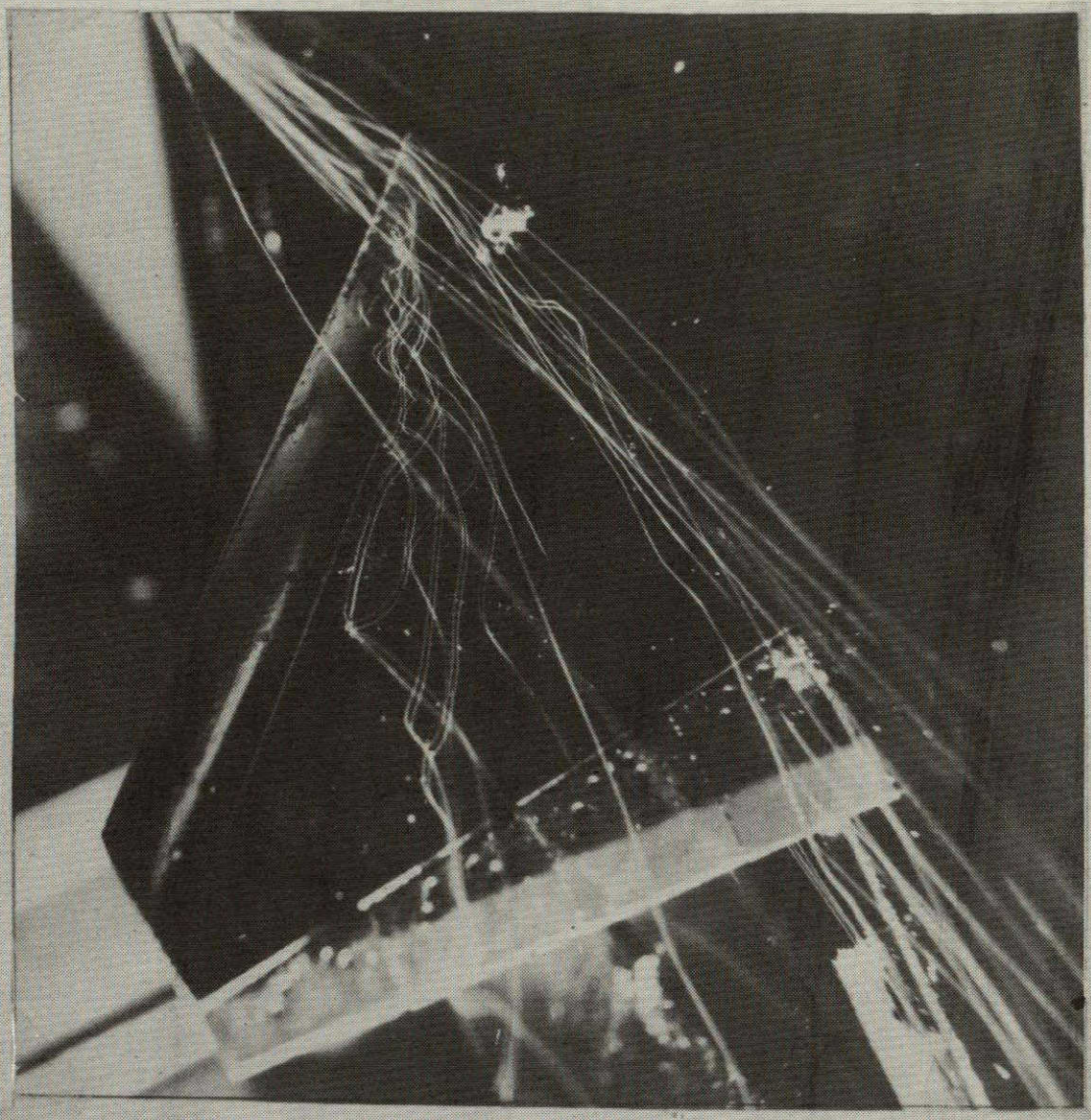

Figure 12.- Flow over the 45° swept trapezoidal wing for $\alpha = 20^{\circ}$ and blowing off; $\delta_{LE} = \delta_{TE} = 0^{\circ}$.

PAGE INTENTIONALLY BLANK

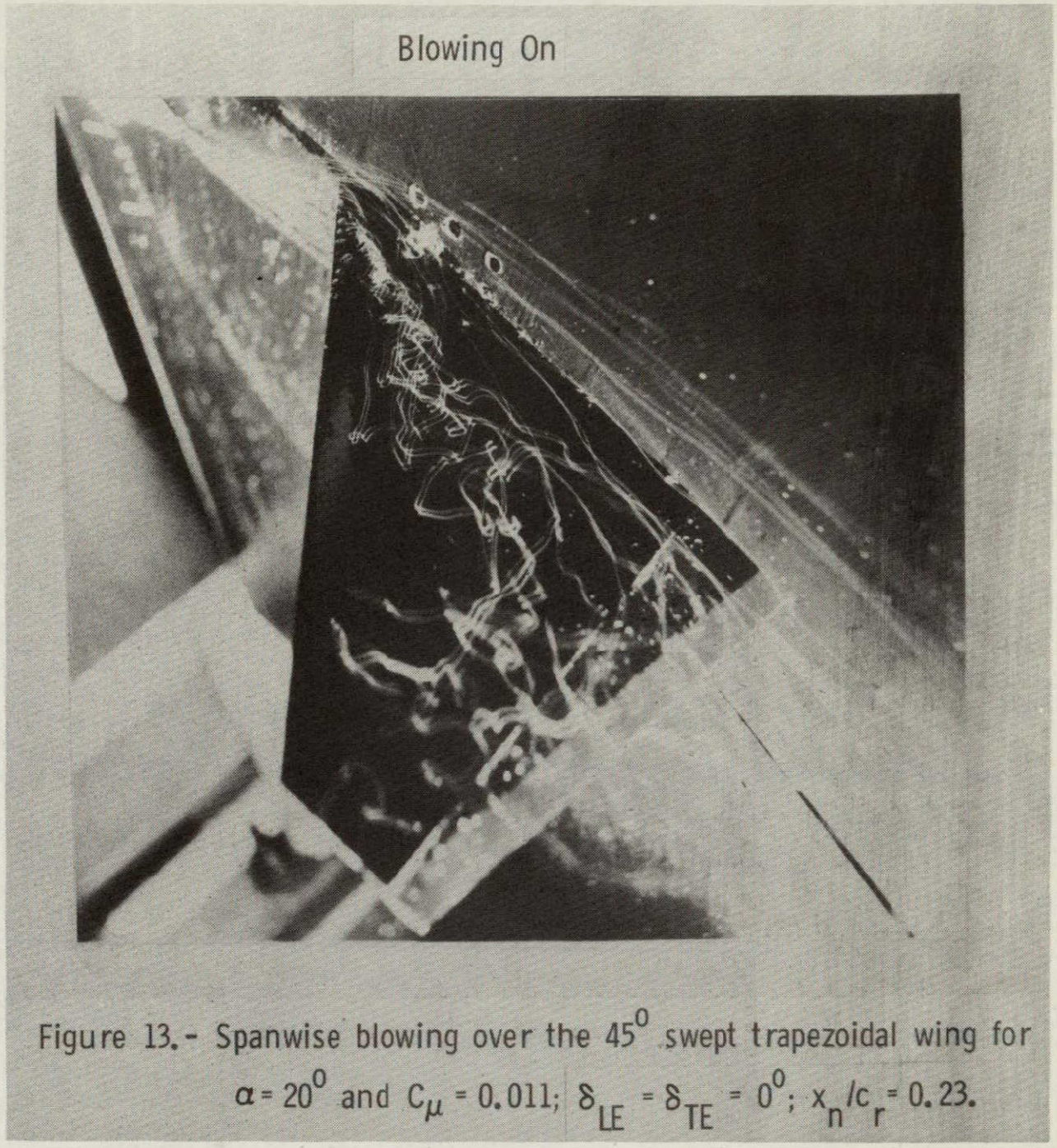

Figure 13.- Spanwise blowing over the 45^{0} swept trapezoidal wing for $\alpha = 20^{0}$ and $C_{\mu} = 0.011$; $\delta_{LE} = \delta_{TE} = 0^{0}$; $x_n/c_r = 0.23$.

Blowing On

Figure 14.- Spanwise blowing over the 45^{o} swept trapezoidal wing for $\alpha = 20^{o}$ and $C_{\mu} = 0.026$; $\delta_{LE} = \delta_{TE} = 0^{o}$; $x_n/c_r = 0.23$.

PAGE INTENTIONALLY BLANK

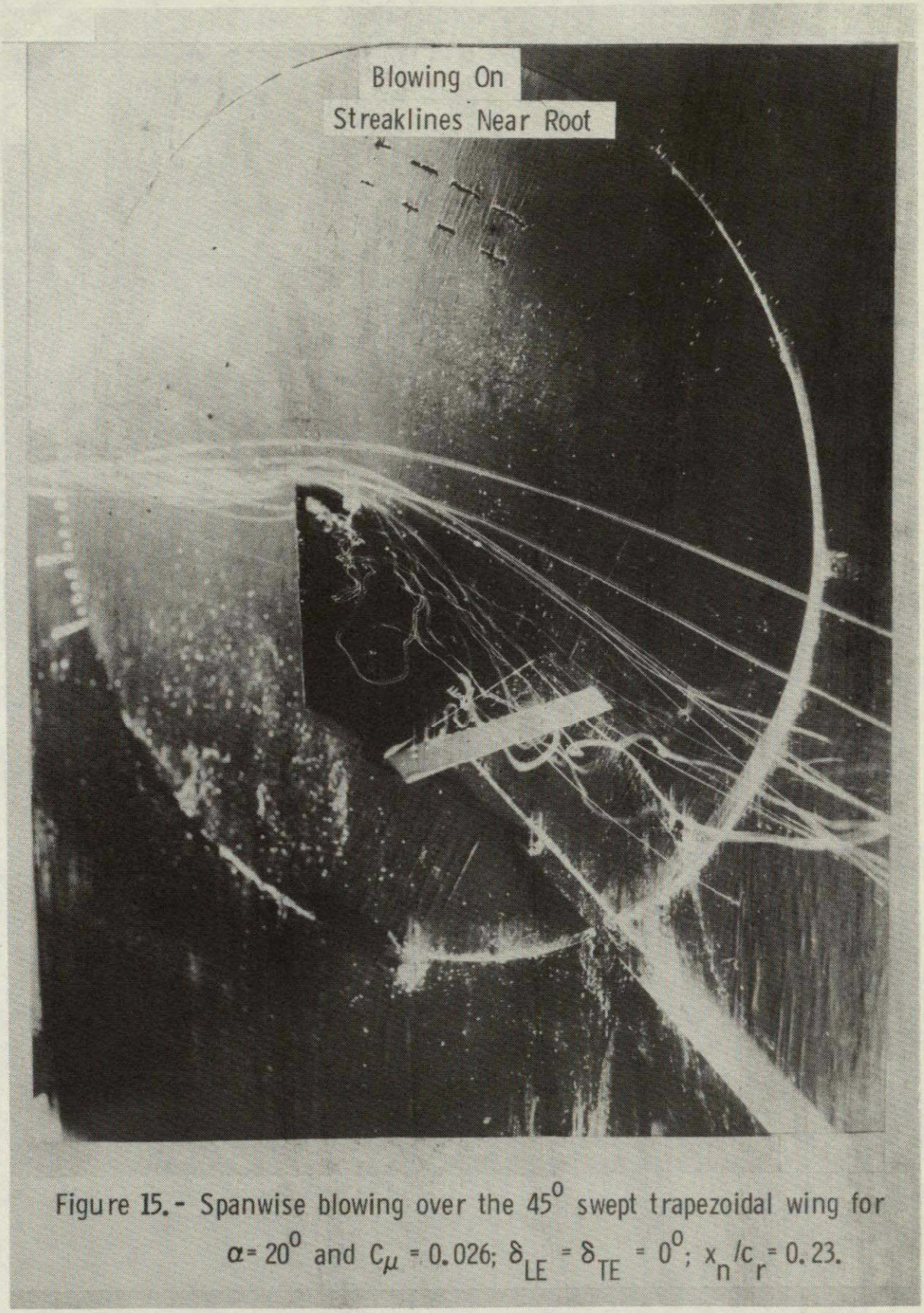

Figure 15.- Spanwise blowing over the 45° swept trapezoidal wing for $\alpha = 20^{\circ}$ and $C_{\mu} = 0.026$; $\delta_{LE} = \delta_{TE} = 0^{\circ}$; $x_n/c_r = 0.23$.

PAGE INTENTIONALLY BLANK

Blowing On

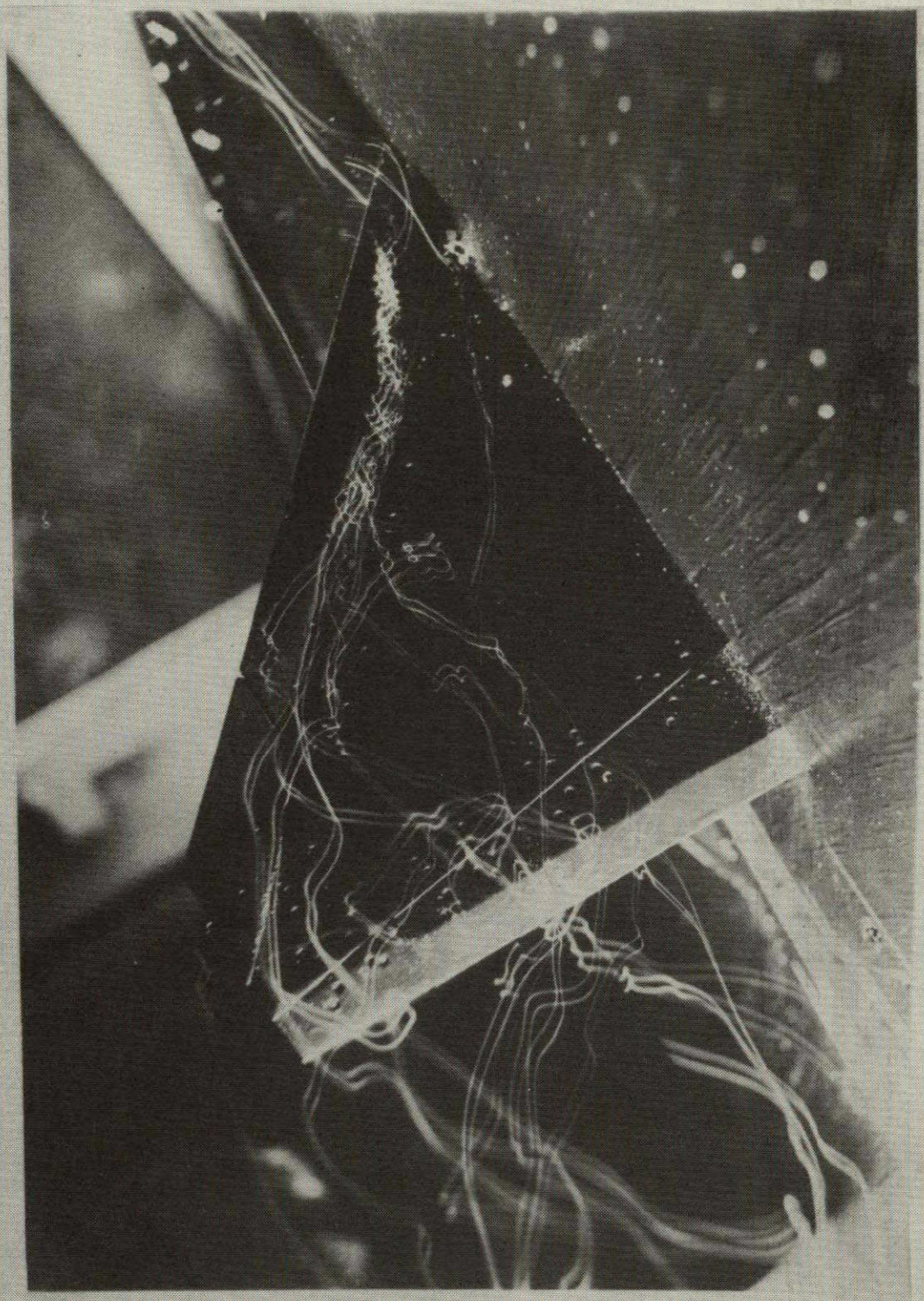

Figure 16.- Spanwise blowing over the 45^{0} swept trapezoidal wing for $\alpha = 20^{0}$ and $C_{\mu} = 0.042$; $\delta_{LE} = \delta_{TE} = 0^{0}$; $x_n/c_r = 0.23$.

Blowing On

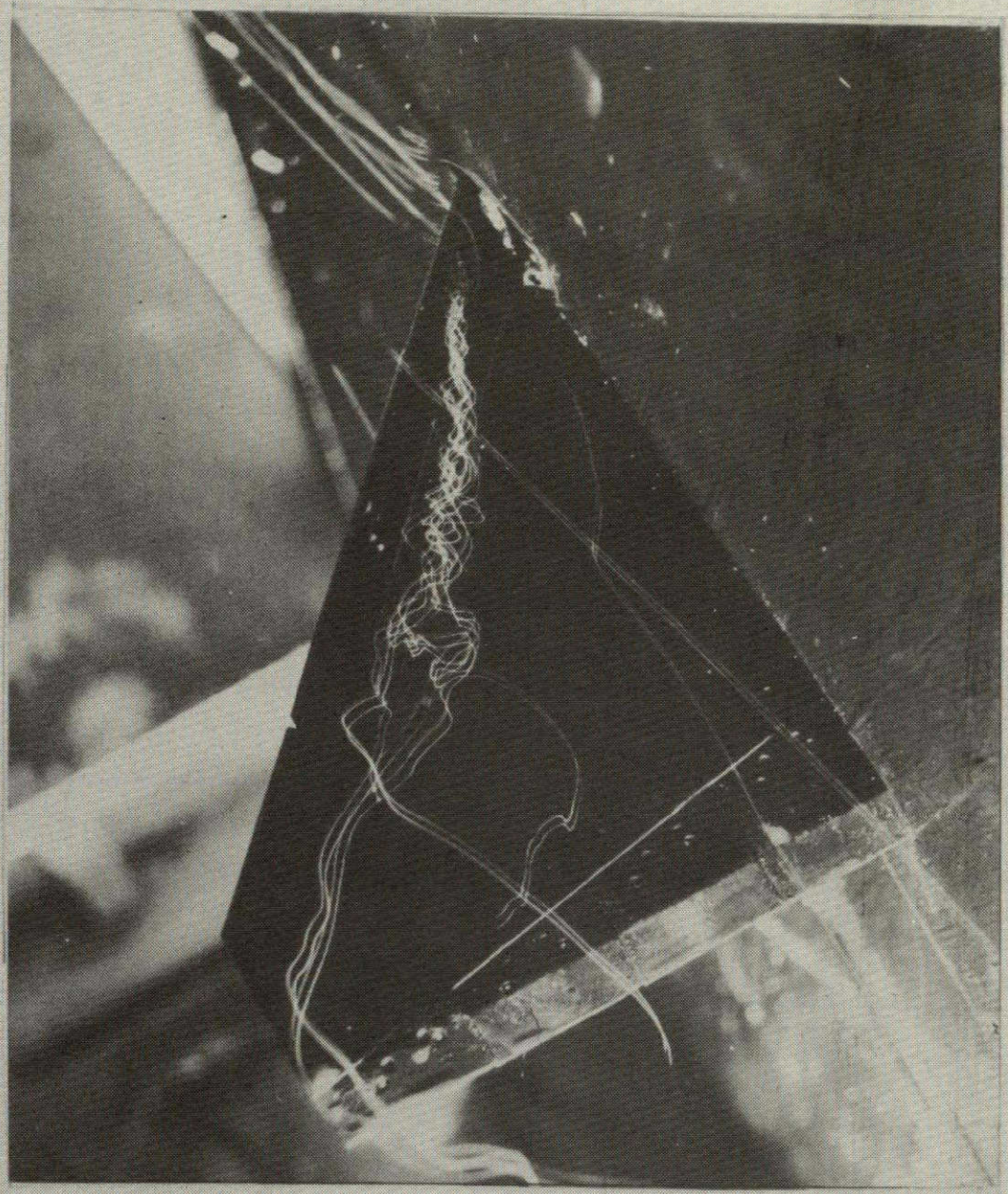

Figure 17.- Spanwise blowing over the 45^{o} swept trapezoidal wing for $\alpha = 20^{o}$ and $C_{\mu} = 0.057$; $\delta_{LE} = \delta_{TE} = 0^{o}$; $x_n/c_r = 0.23$.

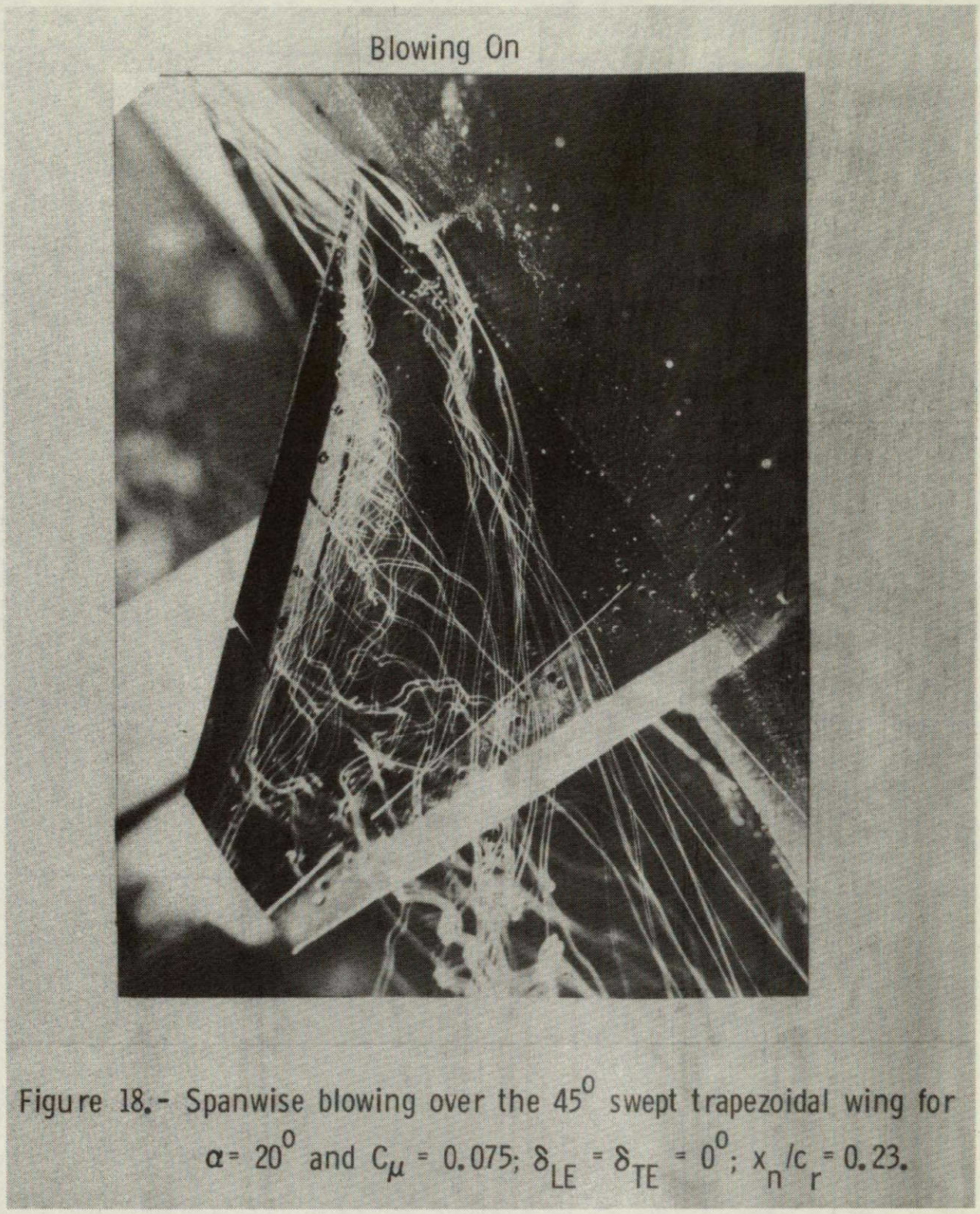

Figure 18.- Spanwise blowing over the 45° swept trapezoidal wing for $\alpha = 20^{\circ}$ and $C_{\mu} = 0.075$; $\delta_{LE} = \delta_{TE} = 0^{\circ}$; $x_n/c_r = 0.23$.

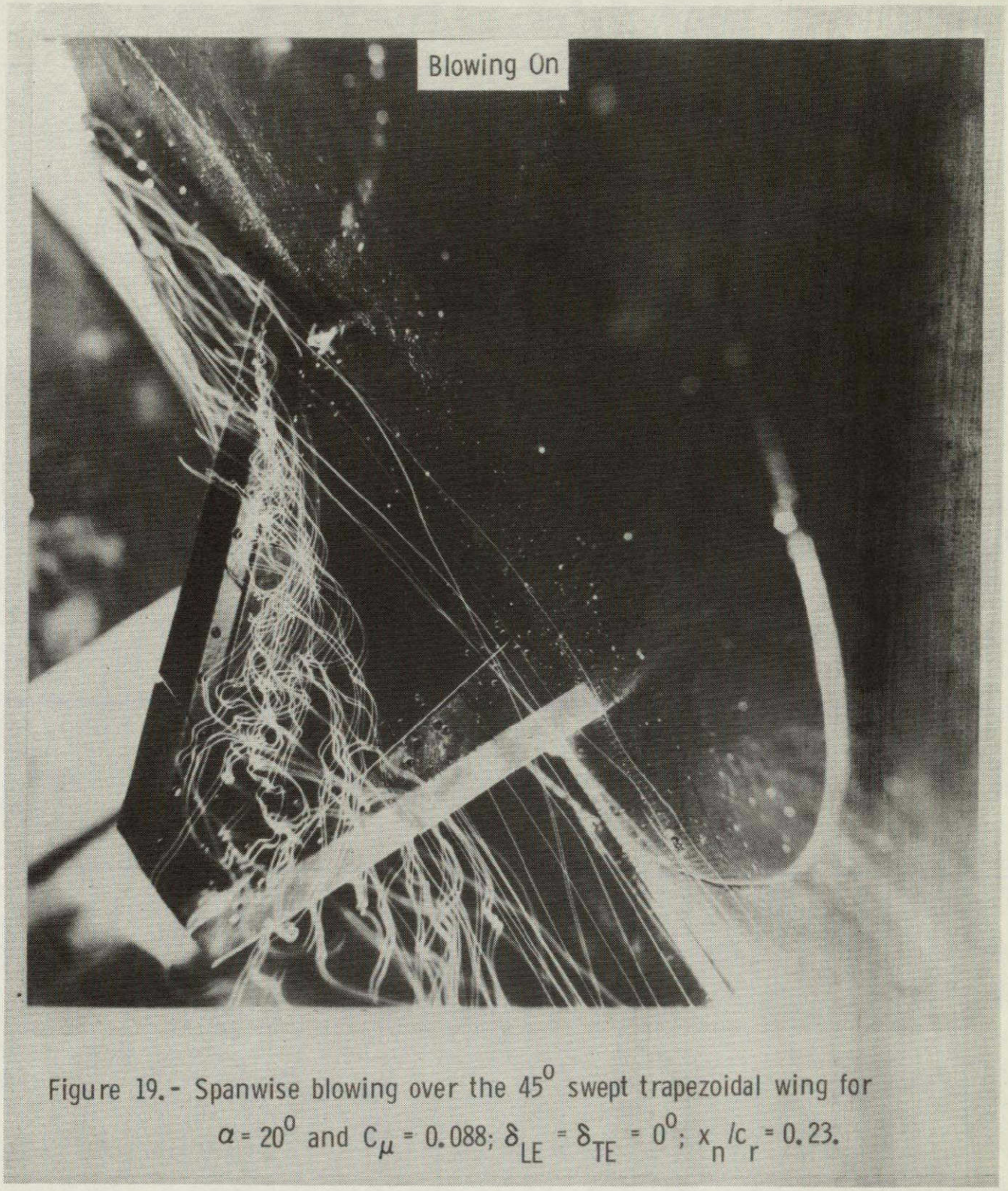

Figure 19.- Spanwise blowing over the 45^{o} swept trapezoidal wing for $\alpha = 20^{o}$ and $C_{\mu} = 0.088$; $\delta_{LE} = \delta_{TE} = 0^{o}$; $x_n/c_r = 0.23$.

Blowing On

Streaklines Near Root

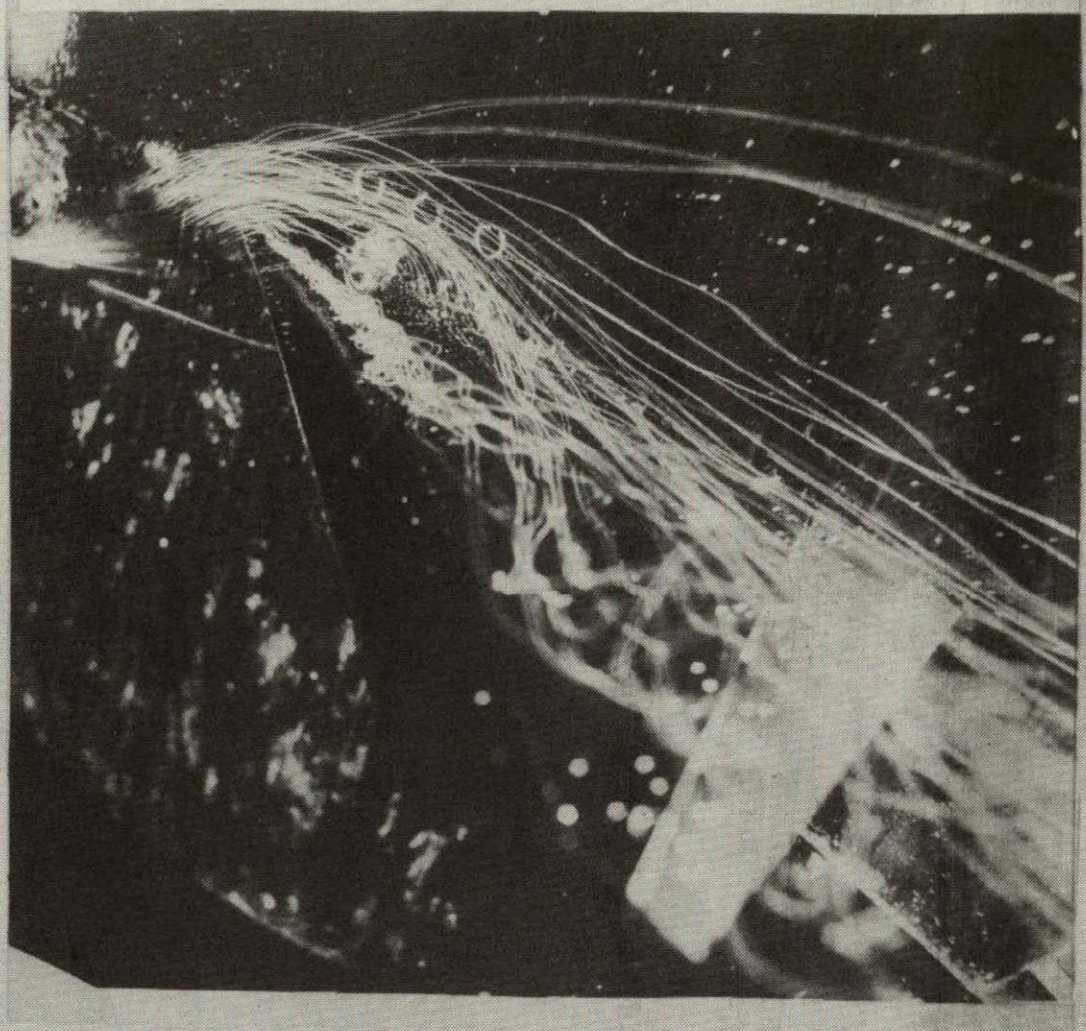

Figure 20.- Spanwise blowing over the 45^{0} swept trapezoidal wing for $\alpha = 20^{0}$ and $C_{\mu} = 0.057$; $\delta_{LE} = \delta_{TE} = 0^{0}$; $x_n/c_r = 0.23$.

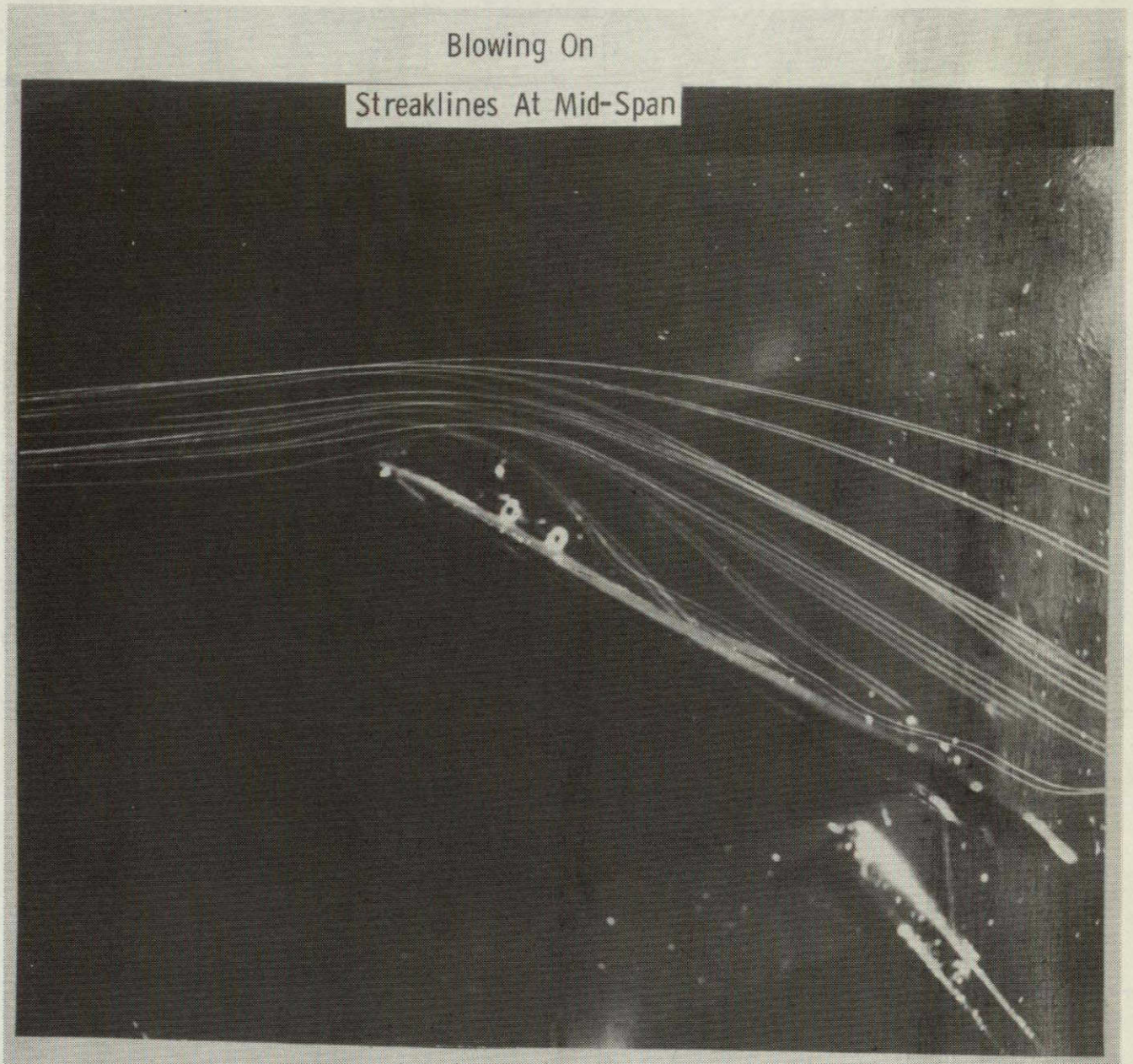

Figure 21.- Spanwise blowing over the 45^{0} swept trapezoidal wing for $\alpha = 20^{0}$ and $C_{\mu} = 0.057$; $\delta_{LE} = \delta_{TE} = 0^{0}$; $x_n/c_r = 0.23$.

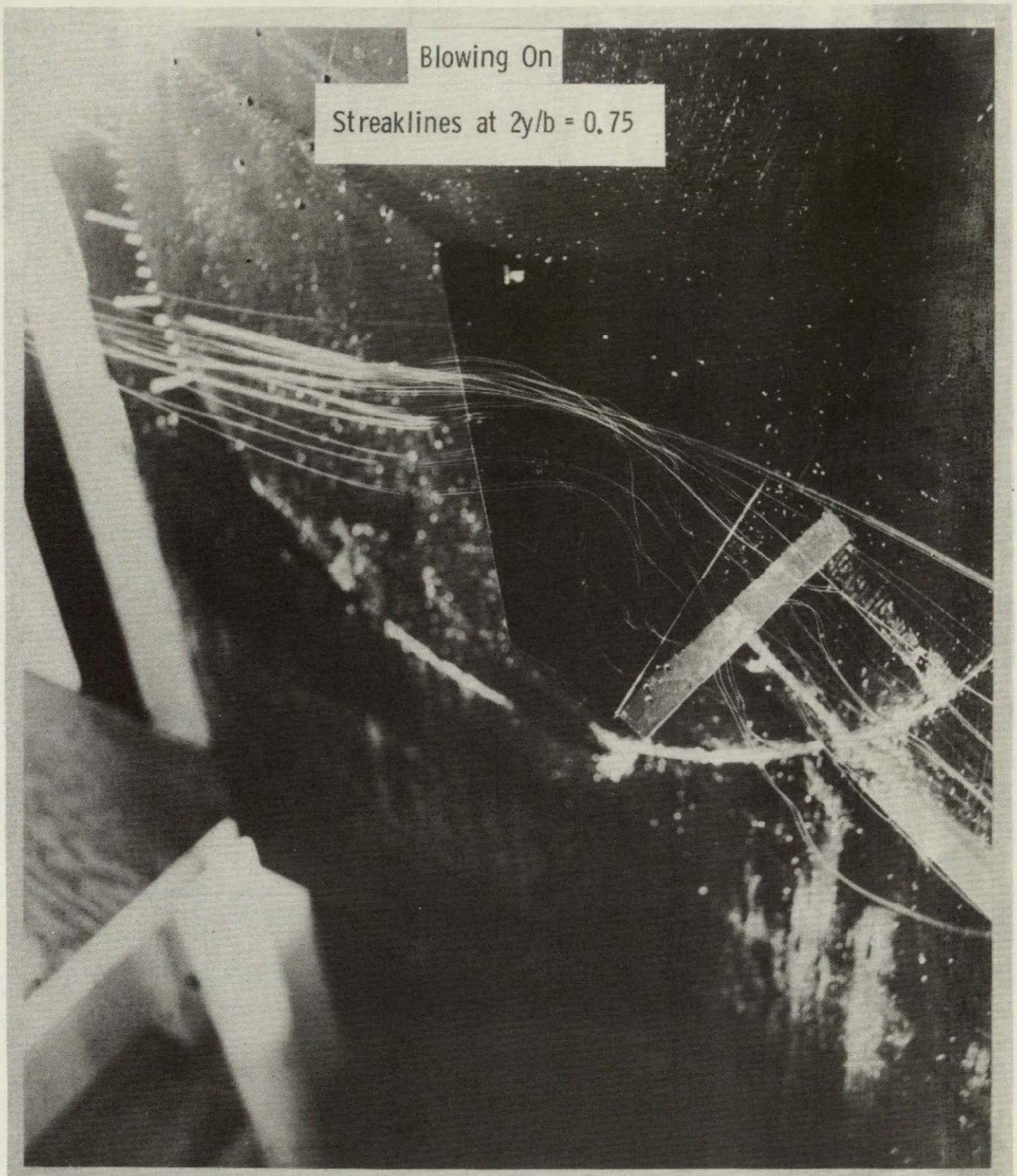

Figure 22.- Spanwise blowing over the 45° swept trapezoidal wing for $\alpha = 20^0$ and $C_\mu = 0.057$; $\delta_{LE} = \delta_{TE} = 0^0$; $x_n/c_r = 0.23$.

Blowing Off

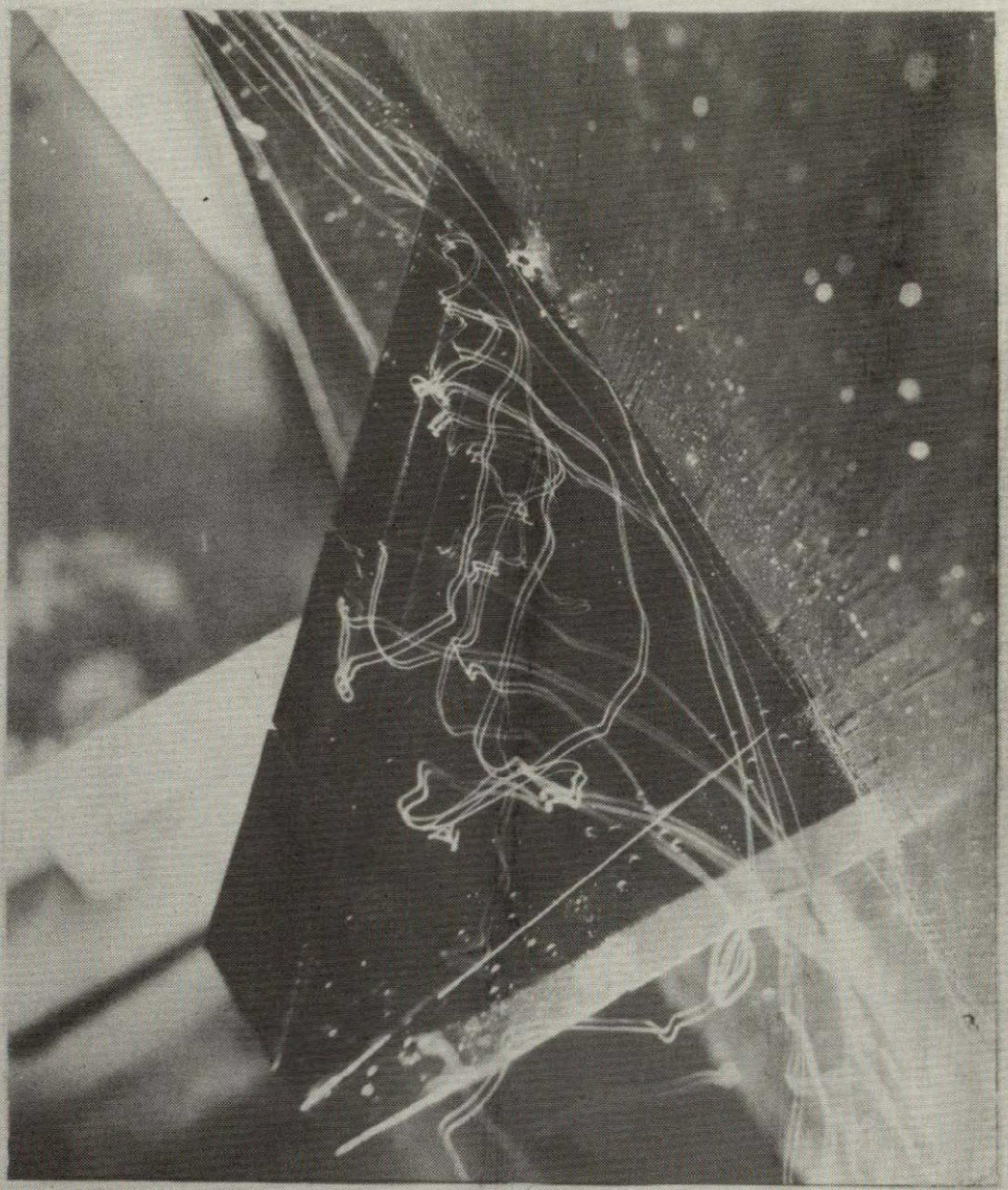

Figure 23.- Flow over the 45^{o} swept trapezoidal wing for $\alpha = 25^{o}$ and blowing off; $\delta_{LE} = \delta_{TE} = 0^{o}$.

Figure 24.- Spanwise blowing over the 45^{0} swept trapezoidal wing for $\alpha = 25^{0}$ and $C_{\mu} = 0.011$; $\delta_{LE} = \delta_{TE} = 0^{0}$; $x_n/c_r = 0.23$.

Blowing On

Figure 25.- Spanwise blowing over the 45^{0} swept trapezoidal wing for $\alpha = 25^{0}$ and $C_{\mu} = 0.026$; $\delta_{LE} = \delta_{TE} = 0^{0}$; $x_n/c_r = 0.23$.

Figure 26.- Spanwise blowing over the 45^0 swept trapezoidal wing for $\alpha = 25^0$ and $C_\mu = 0.026$; $\delta_{LE} = \delta_{TE} = 0^0$; $x_n/c_r = 0.23$.

Blowing On

Figure 27.- Spanwise blowing over the 45^0 swept trapezoidal wing for $\alpha = 25^0$ and $C_\mu = 0.042$; $\delta_{LE} = \delta_{TE} = 0^0$; $x_n/c_r = 0.23$.

Figure 28.- Spanwise blowing over the 45^0 swept trapezoidal wing for $\alpha = 25^0$ and $C_\mu = 0.042$; $\delta_{LE} = \delta_{TE} = 0^0$; $x_n/c_r = 0.23$.

Blowing On

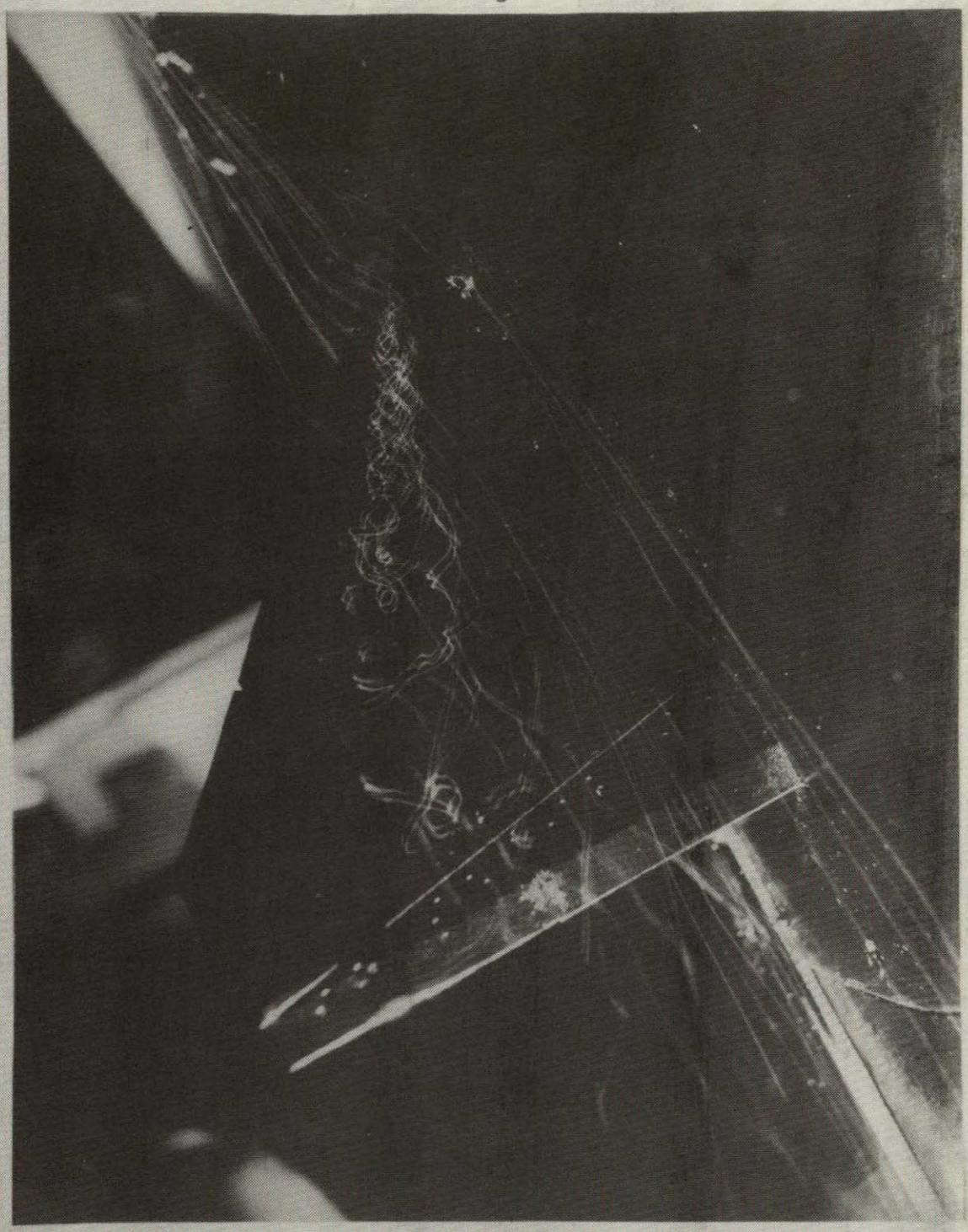

Figure 29.- Spanwise blowing over the 45^{o} swept trapezoidal wing for $\alpha = 25^{o}$ and $C_{\mu} = 0.057$; $\delta_{LE} = \delta_{TE} = 0^{o}$; $x_n/c_r = 0.23$.

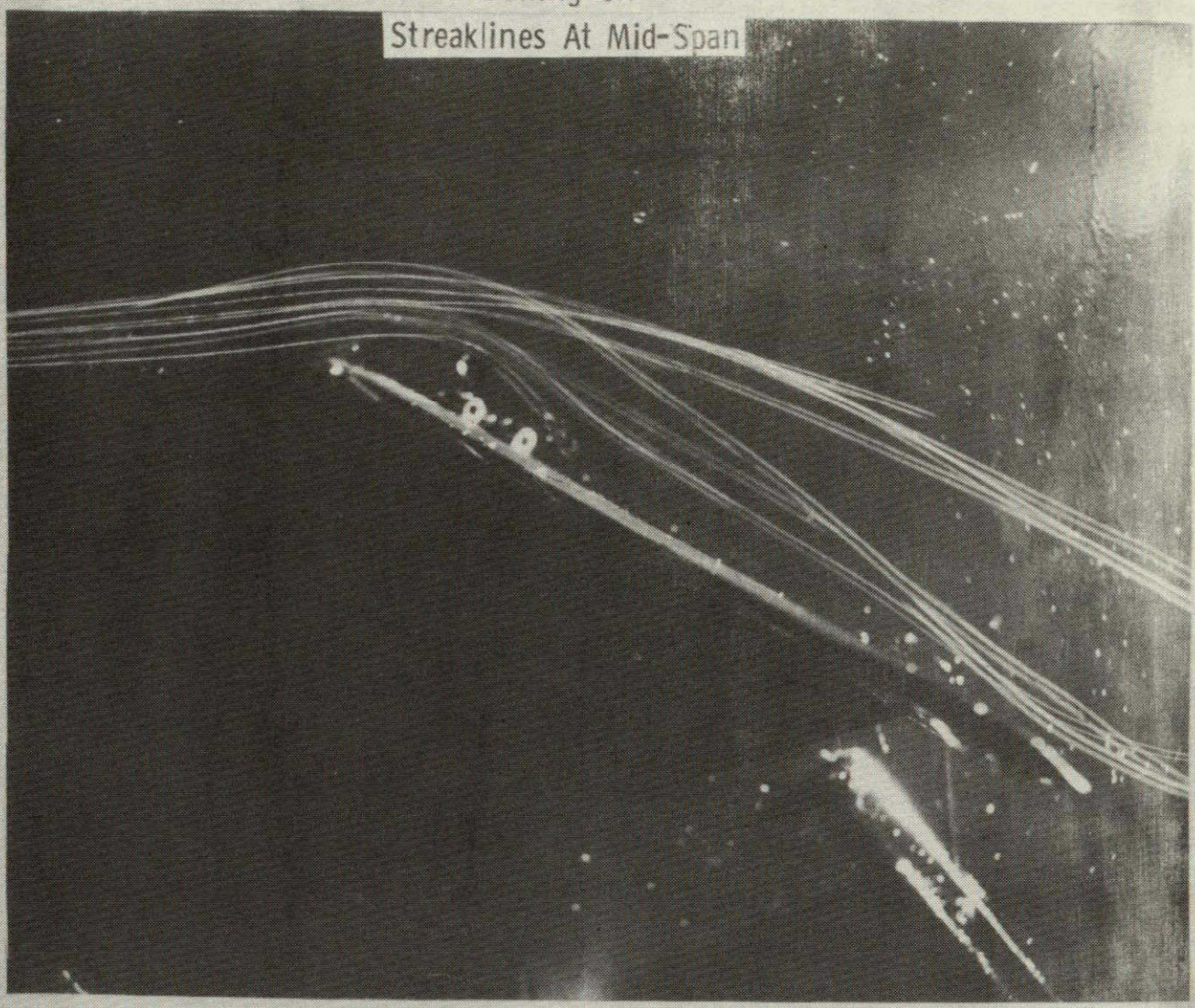

Figure 30.- Spanwise blowing over the 45^{0} swept trapezoidal wing for $\alpha = 25^{0}$ and $C_{\mu} = 0.057$; $\delta_{LE} = \delta_{TE} = 0^{0}$; 0^{0}; $x_n/c_r = 0.23$.

Blowing On

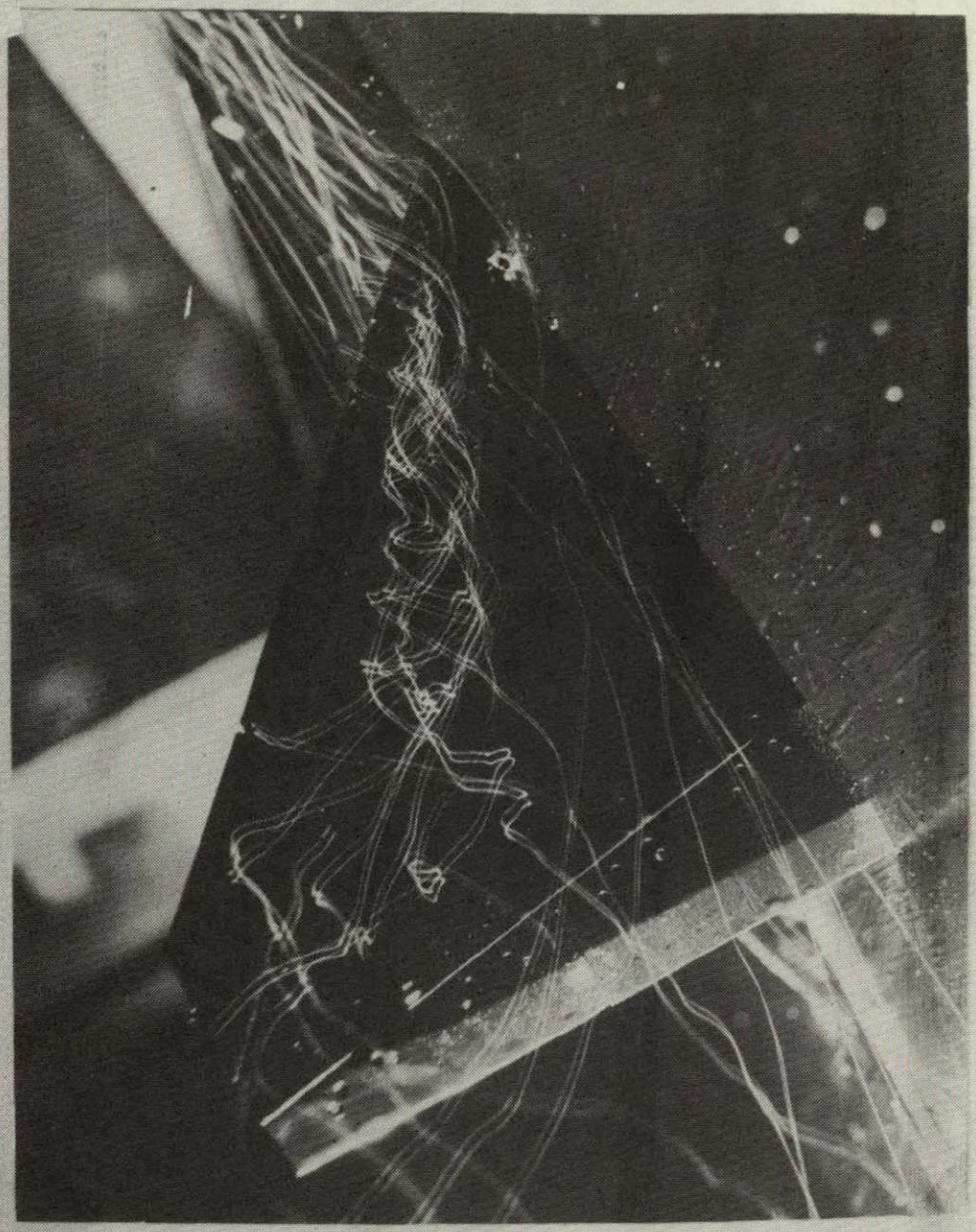

Figure 31.- Spanwise blowing over the 45^{o} swept trapezoidal wing for $\alpha = 25^{o}$ and $C_{\mu} = 0.075$; $\delta_{LE} = \delta_{TE} = 0^{o}$; $x_n/c_r = -0.23$.

Figure 32.- Spanwise blowing over the 45^{0} swept trapezoidal wing for $\alpha = 25^{0}$ and $C_{\mu} = 0.075$; $\delta_{LE} = \delta_{TE} = 0^{0}$; $x_n/c_r = 0.23$.

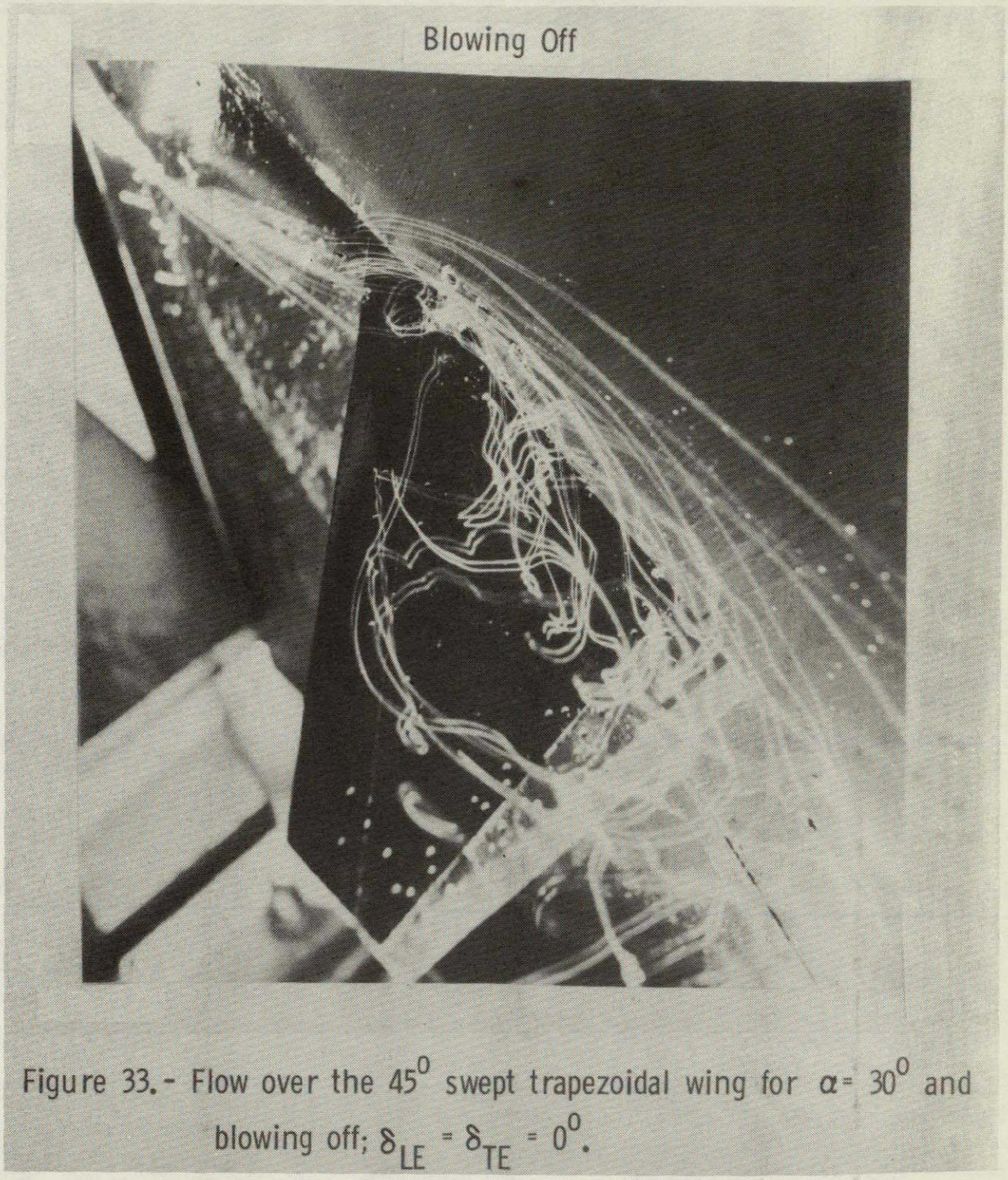

Figure 33.- Flow over the 45^{o} swept trapezoidal wing for $\alpha = 30^{o}$ and blowing off; $\delta_{LE} = \delta_{TE} = 0^{o}$.

Blowing On

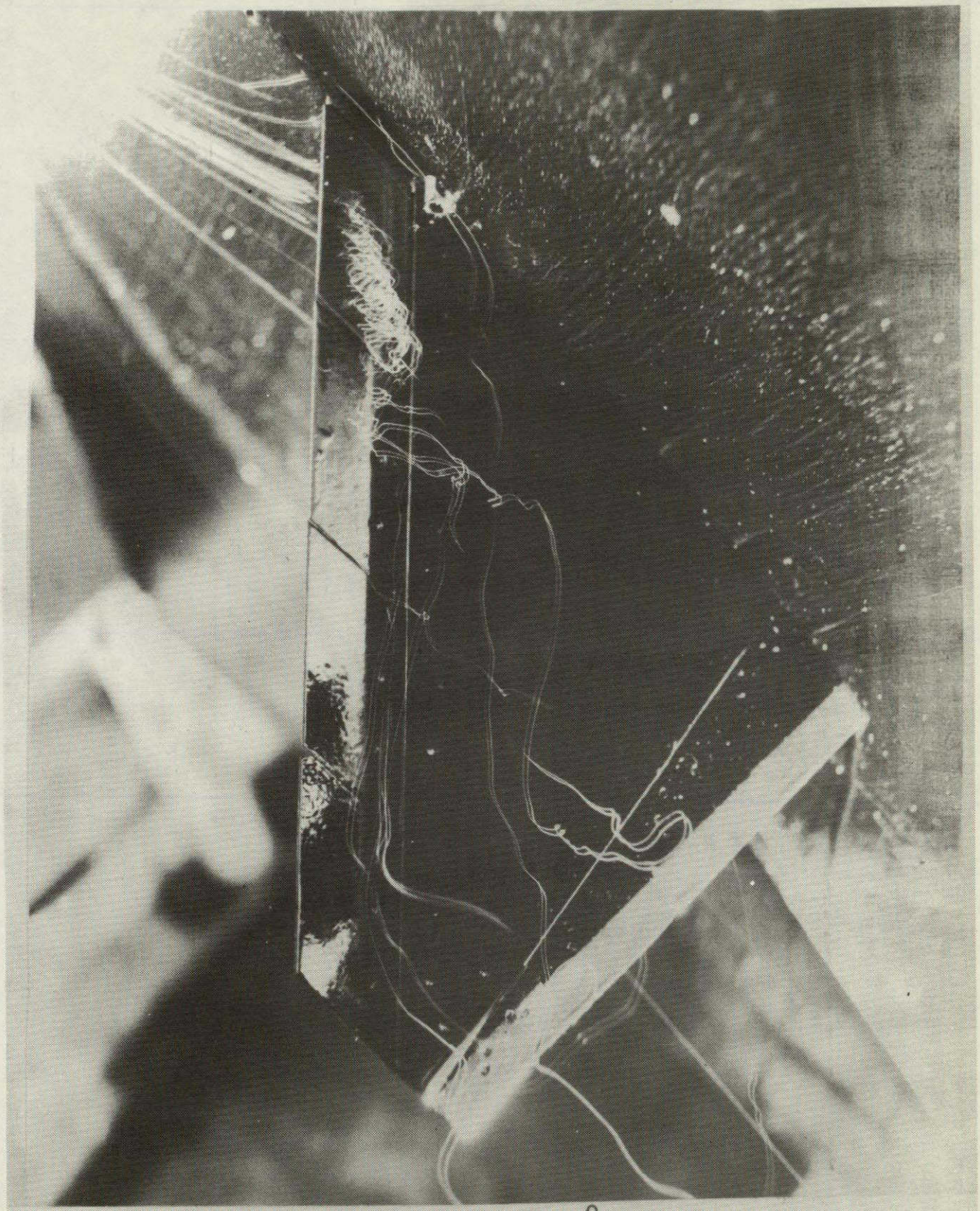

Figure 34.- Spanwise blowing over the 45^{0} swept trapezoidal wing for $\alpha = 30^{0}$ and $C_{\mu} = 0.026$; $\delta_{LE} = \delta_{TE} = 0^{0}$; $x_n/c_r = 0.23$.

Figure 35.- Spanwise blowing over the 45^{0} swept trapezoidal wing for $\alpha = 30^{0}$ and $C_{\mu} = 0.011$; $\delta_{LE} = \delta_{TE} = 0^{0}$; $x_n/c_r = 0.23$.

Blowing On

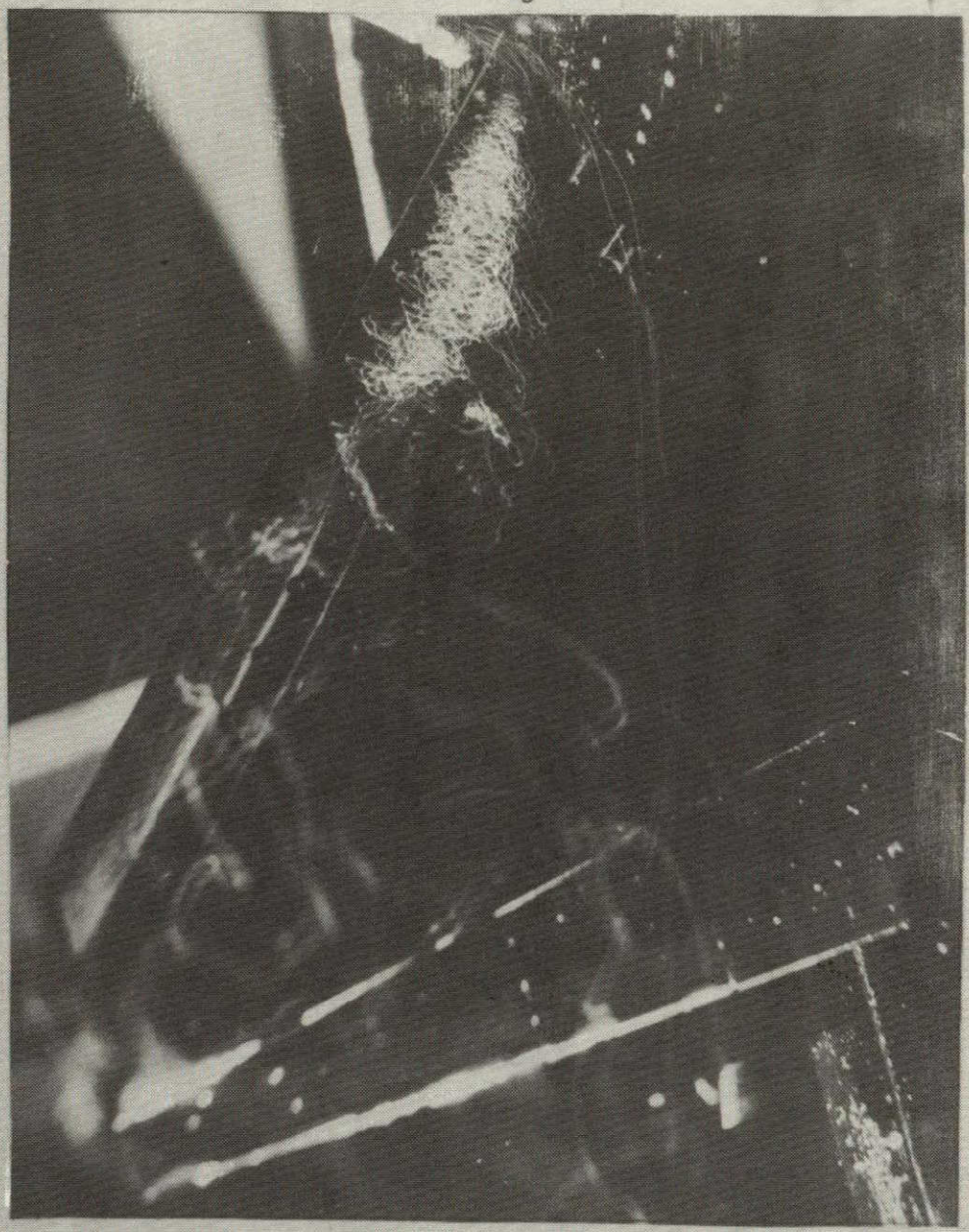

Figure 36.- Spanwise blowing over the 45^{0} swept trapezoidal wing for $\alpha = 30^{0}$ and $C_{\mu} = 0.042$; $\delta_{LE} = \delta_{TE} = 0^{0}$; $x_n/c_r = 0.23$.

Figure 37.- Spanwise blowing over the 45^{0} swept trapezoidal wing for $\alpha = 30^{0}$ and $C_{\mu} = 0.042$; $\delta_{LE} = \delta_{TE} = 0^{0}$; $x_n/c_r = 0.23$.

Figure 38.- Spanwise blowing over the 45^{0} swept trapezoidal wing for $\alpha = 30^{0}$ and $C_{\mu} = 0.057$; $\delta_{LE} = \delta_{TE} = 0^{0}$; $x_n/c_r = 0.23$.

Figure 39.- Spanwise blowing over the 45^{0} swept trapezoidal wing for $\alpha = 30^{0}$ and $C_{\mu} = 0.057$; $\delta_{LE} = \delta_{TE} = 0^{0}$; $x_n/c_r = 0.23$.

Figure 40.- Spanwise blowing over the 45^{0} swept trapezoidal wing for $\alpha = 30^{0}$ and $C_{\mu} = 0.057$; $\delta_{LE} = \delta_{TE} = 0^{0}$; $x_n/c_r = 0.23$.

Figure 41.- Spanwise blowing over the 45^0 swept trapezoidal wing for $\alpha = 30^0$ and $C_\mu = 0.075$; $\delta_{LE} = \delta_{TE} = 0^0$; $x_n/c_r = .23$.

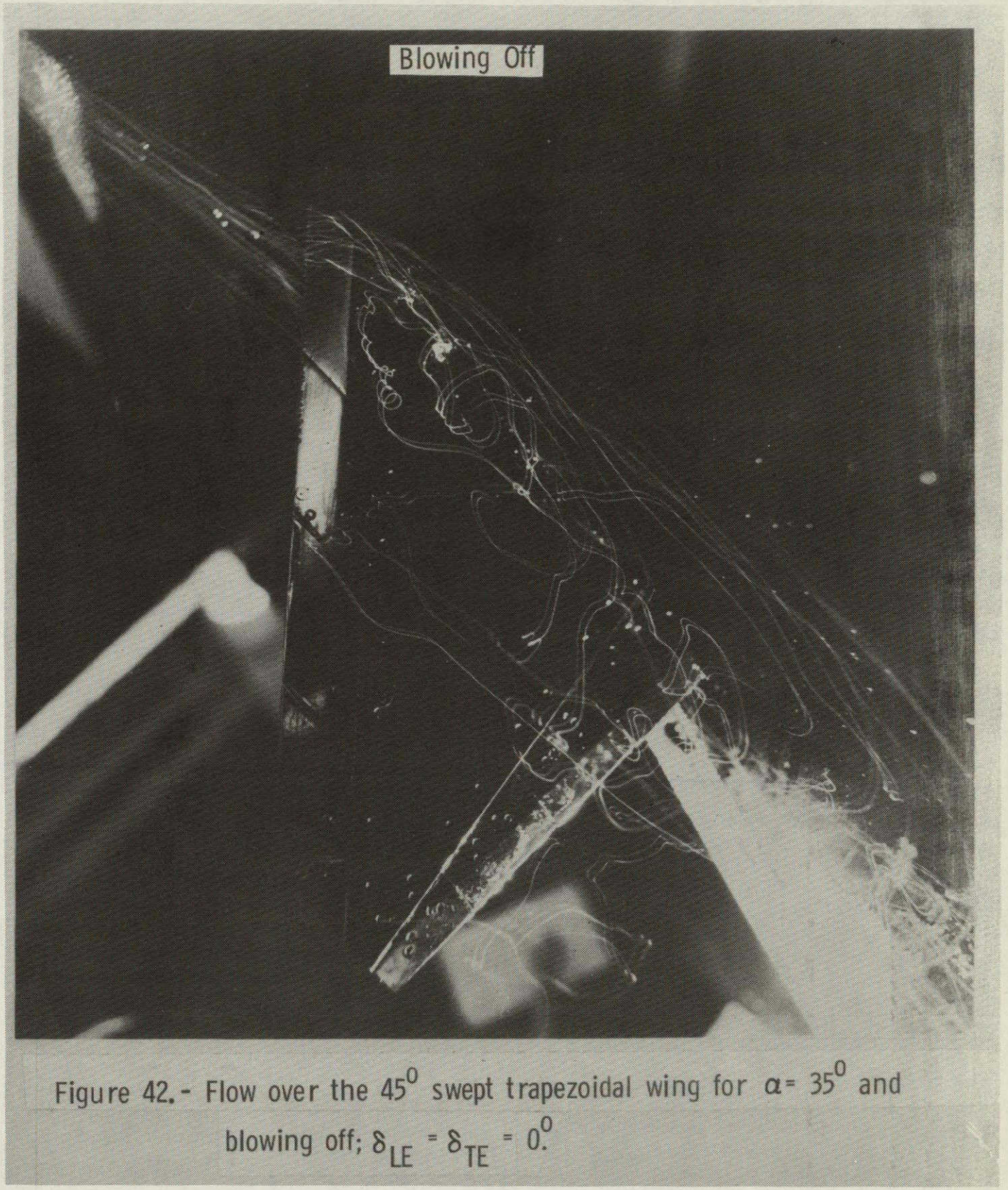

Figure 42.- Flow over the 45^{0} swept trapezoidal wing for $\alpha = 35^{0}$ and blowing off; $\delta_{LE} = \delta_{TE} = 0^{0}$.

Blowing On

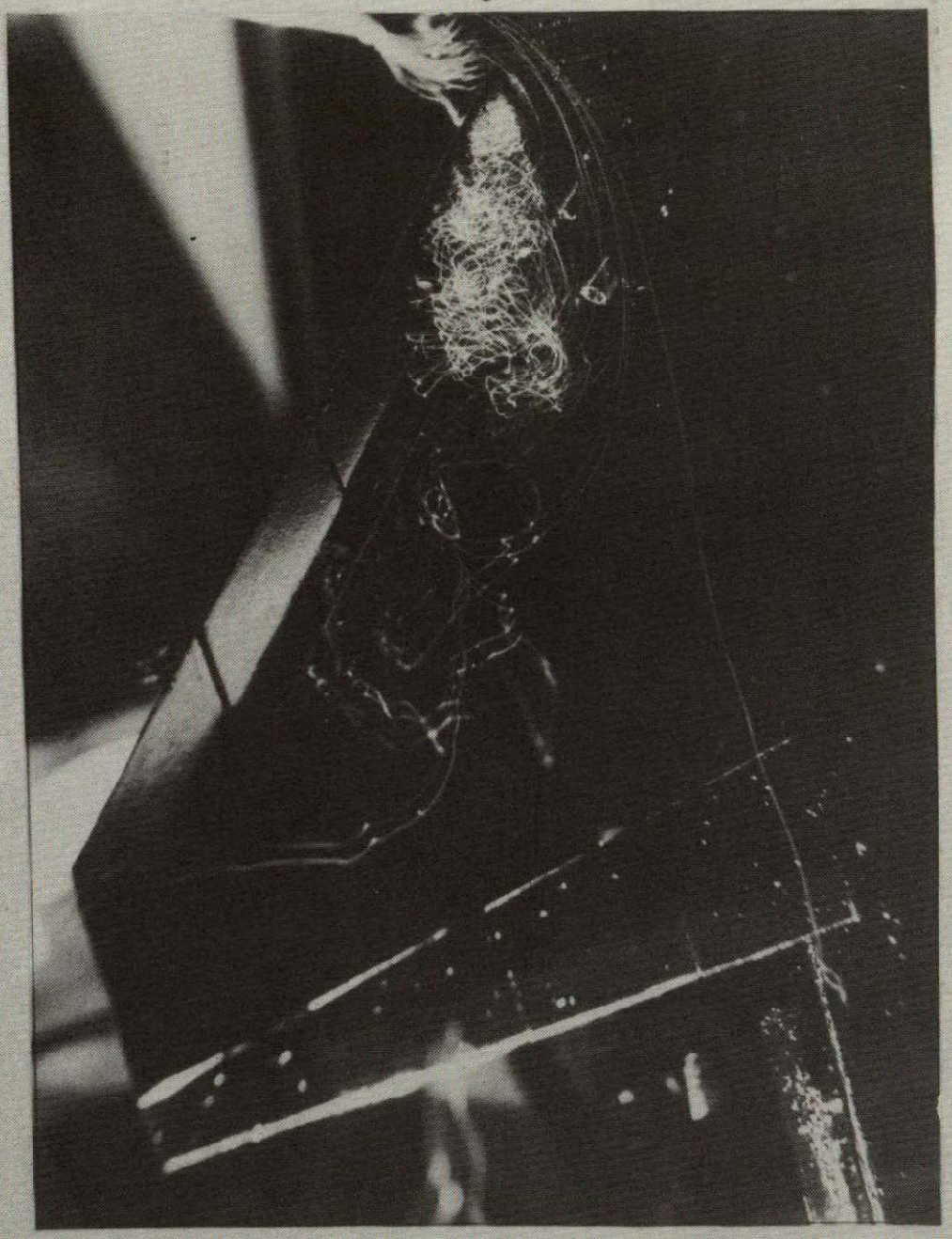

Figure 43.- Spanwise blowing over the 45^{o} swept trapezoidal wing for $\alpha = 35^{o}$ and $C_{\mu} = 0.026$; $\delta_{LE} = \delta_{TE} = 0^{o}$; $x_n/c_r = 0.23$.

Figure 44.- Spanwise blowing over the 45^{0} swept trapezoidal wing for $\alpha = 35^{0}$ and $C_{\mu} = 0.042$; $\delta_{LE} = \delta_{TE} = 0^{0}$; $x_n/c_r = 0.23$.

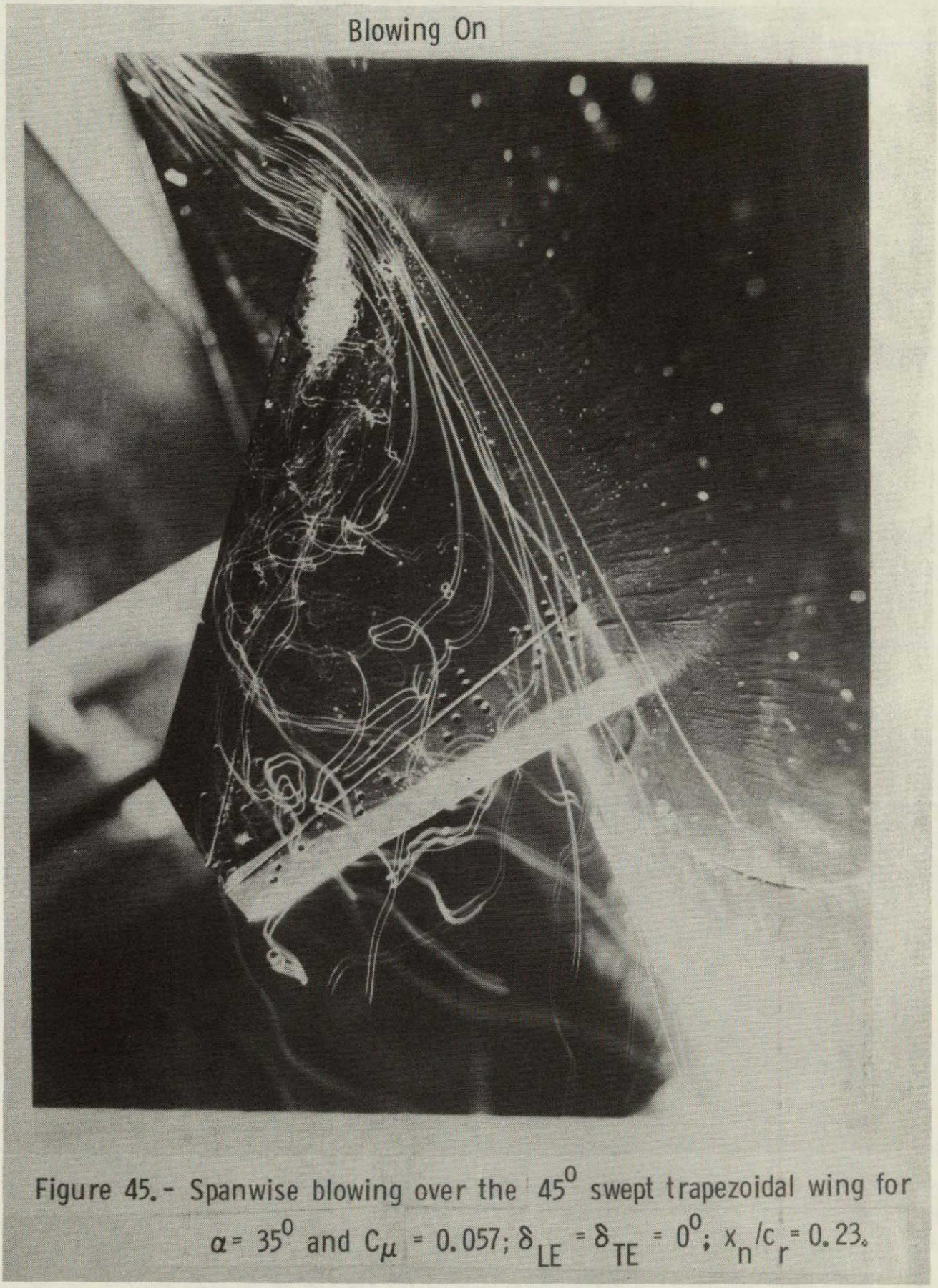

Figure 45.- Spanwise blowing over the 45^{0} swept trapezoidal wing for $\alpha = 35^{0}$ and $C_{\mu} = 0.057$; $\delta_{LE} = \delta_{TE} = 0^{0}$; $x_n/c_r = 0.23$.

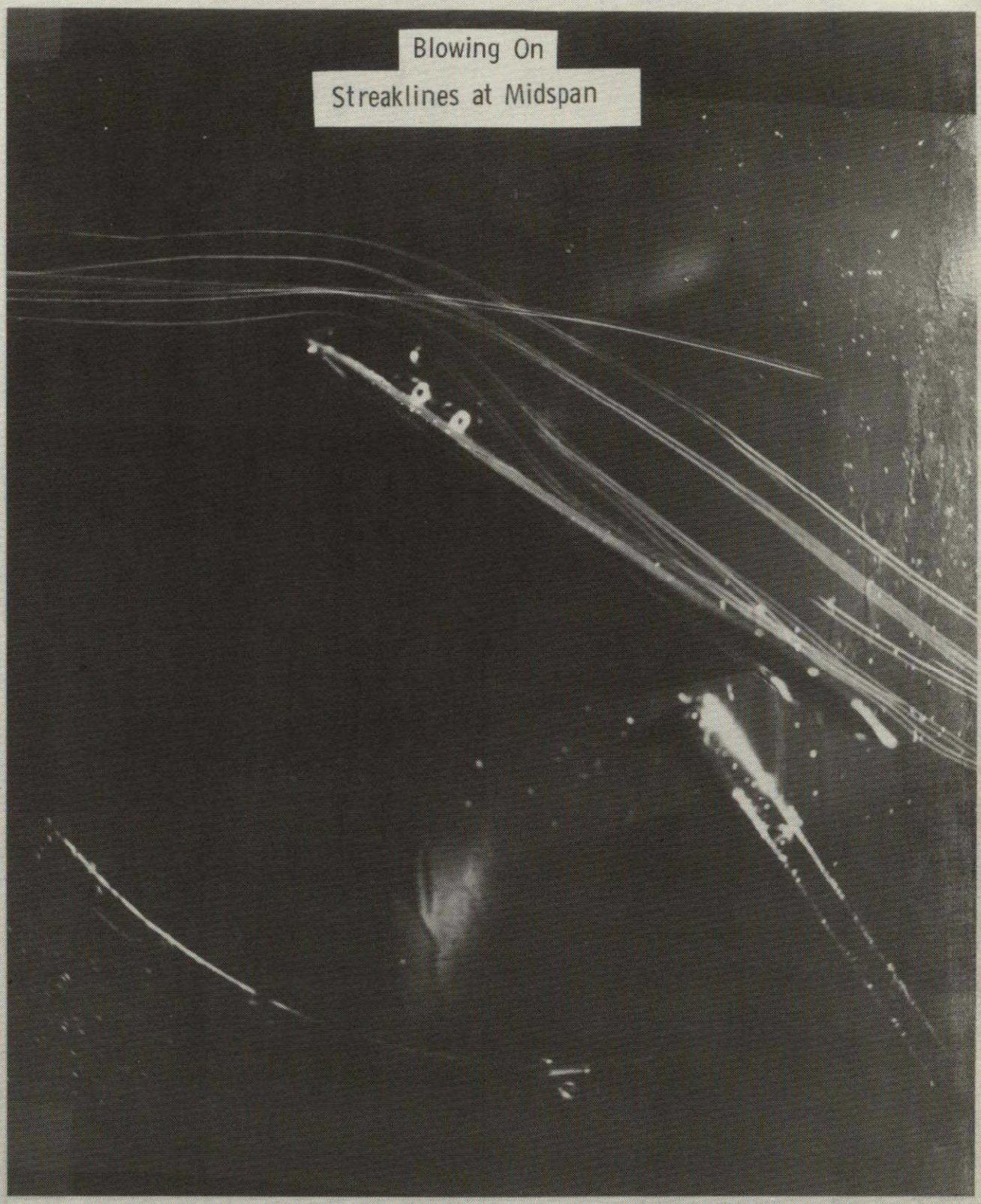

Figure 46.- Spanwise blowing over the 45° swept trapezoidal wing for $\alpha = 35^{0}$ and $C_{\mu} = 0.057$; $\delta_{LE} = \delta_{TE} = 0^{0}$; $x_n/c_r = 0.23$.

Figure 47.- Spanwise blowing over the 45^{0} swept trapezoidal wing for $\alpha = 35^{0}$ and $C_{\mu} = 0.075$; $\delta_{LE} = \delta_{TE} = 0^{0}$; $x_n/c_r = 0.23$.

Figure 48.- Spanwise blowing over the 45^{0} swept trapezoidal wing for $\alpha = 35^{0}$ and $C_{\bar{\mu}} 0.088$; $\delta_{LE} = \delta_{TE} = 0^{0}$; $x_n/c_r = 0.23$.

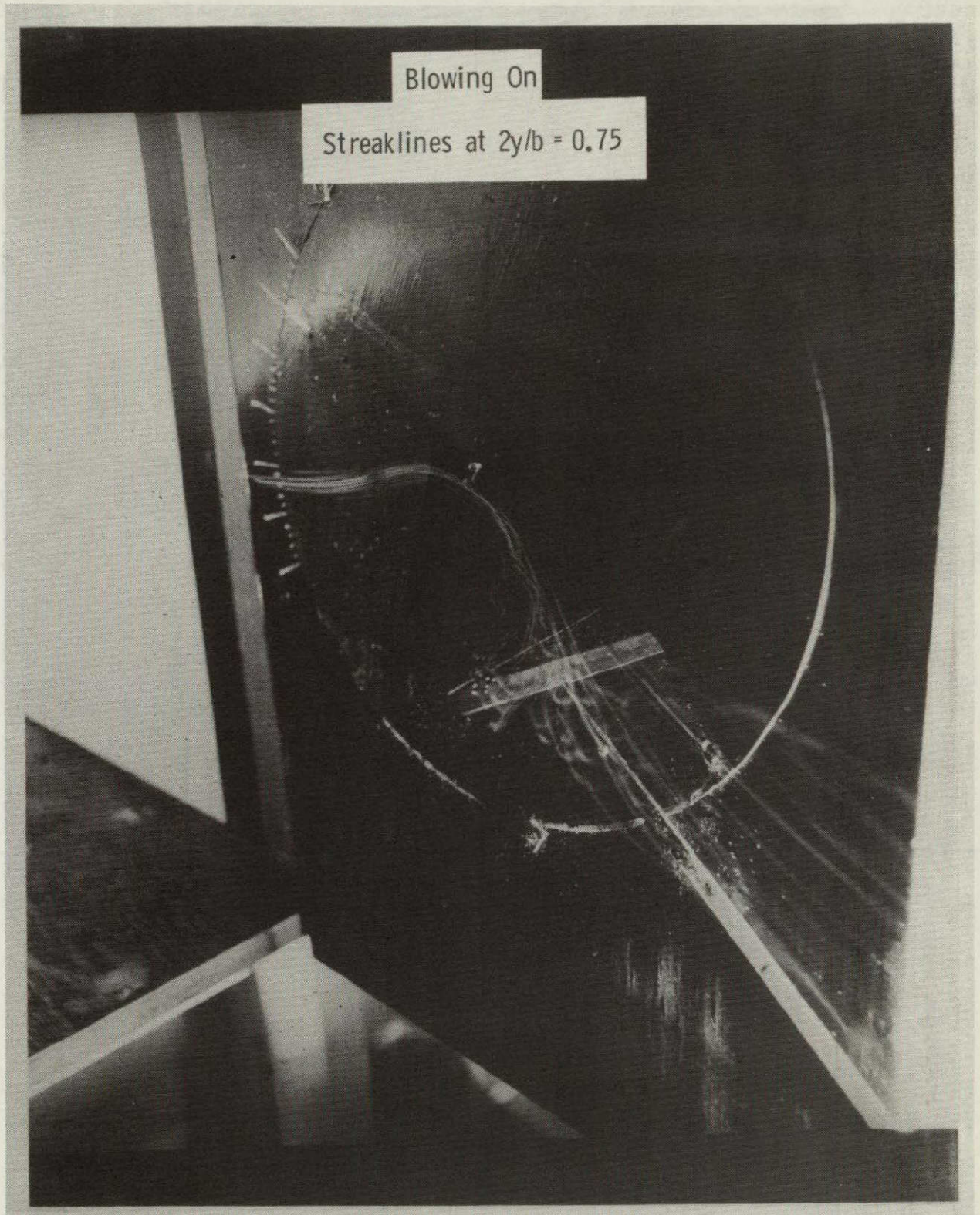

Figure 49.- Spanwise blowing over the 45^{0} swept trapezoidal wing for $\alpha = 35^{0}$ and $C_{\mu} = 0.088$; $\delta_{LE} = \delta_{TE} = 0^{0}$; $x_n/c_r = 0.23$.

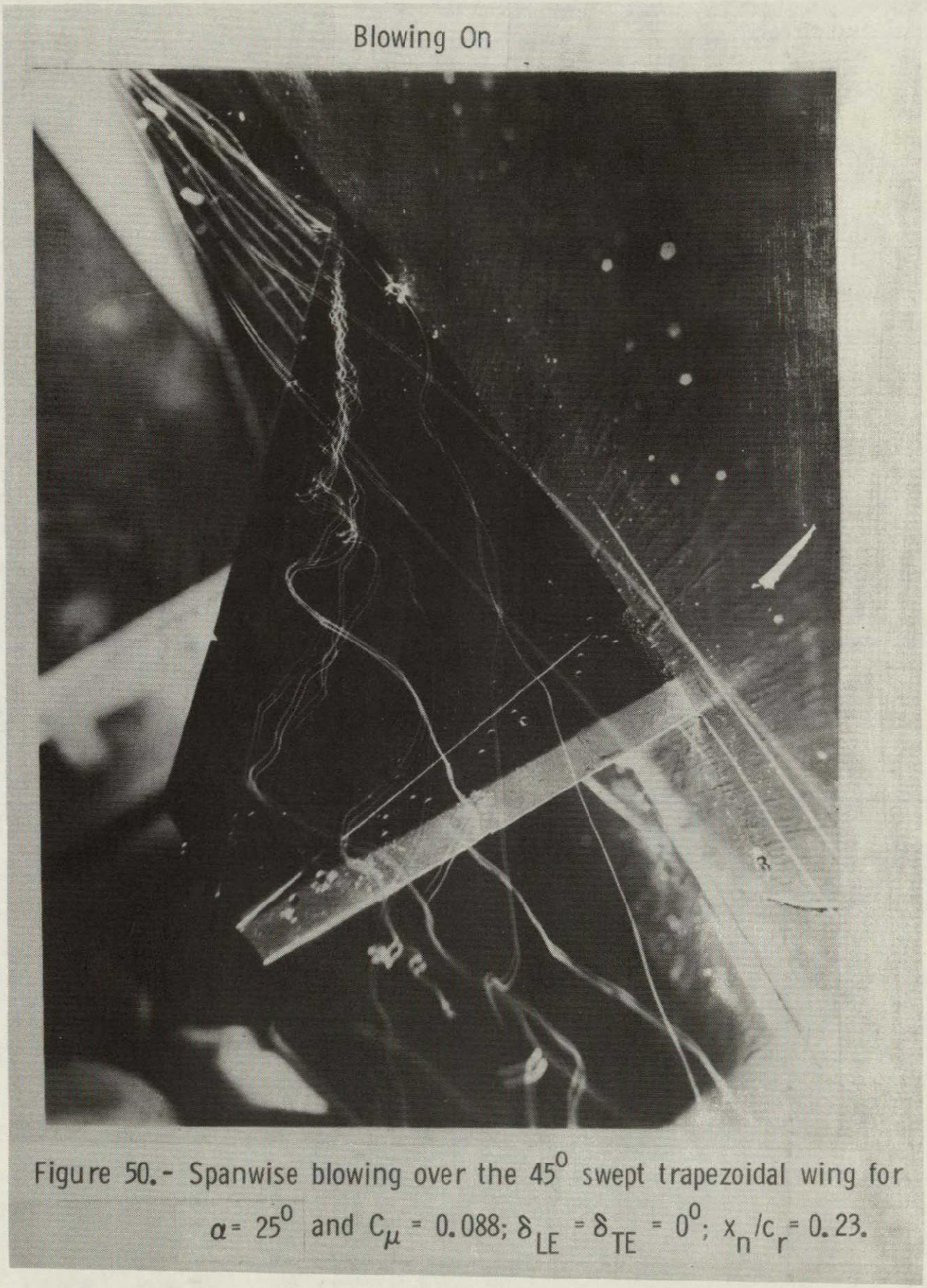

Figure 50.- Spanwise blowing over the 45° swept trapezoidal wing for $\alpha = 25^{\circ}$ and $C_{\mu} = 0.088$; $\delta_{LE} = \delta_{TE} = 0^{\circ}$; $x_n/c_r = 0.23$.

Blowing On

Figure 51.- Spanwise blowing over the 45^{0} swept trapezoidal wing for $\alpha = 25^{0}$ and $C_{\mu} = 0.088$; $\delta_{LE} = \delta_{TE} = 0^{0}$; $x_n/c_r = 0.32$.

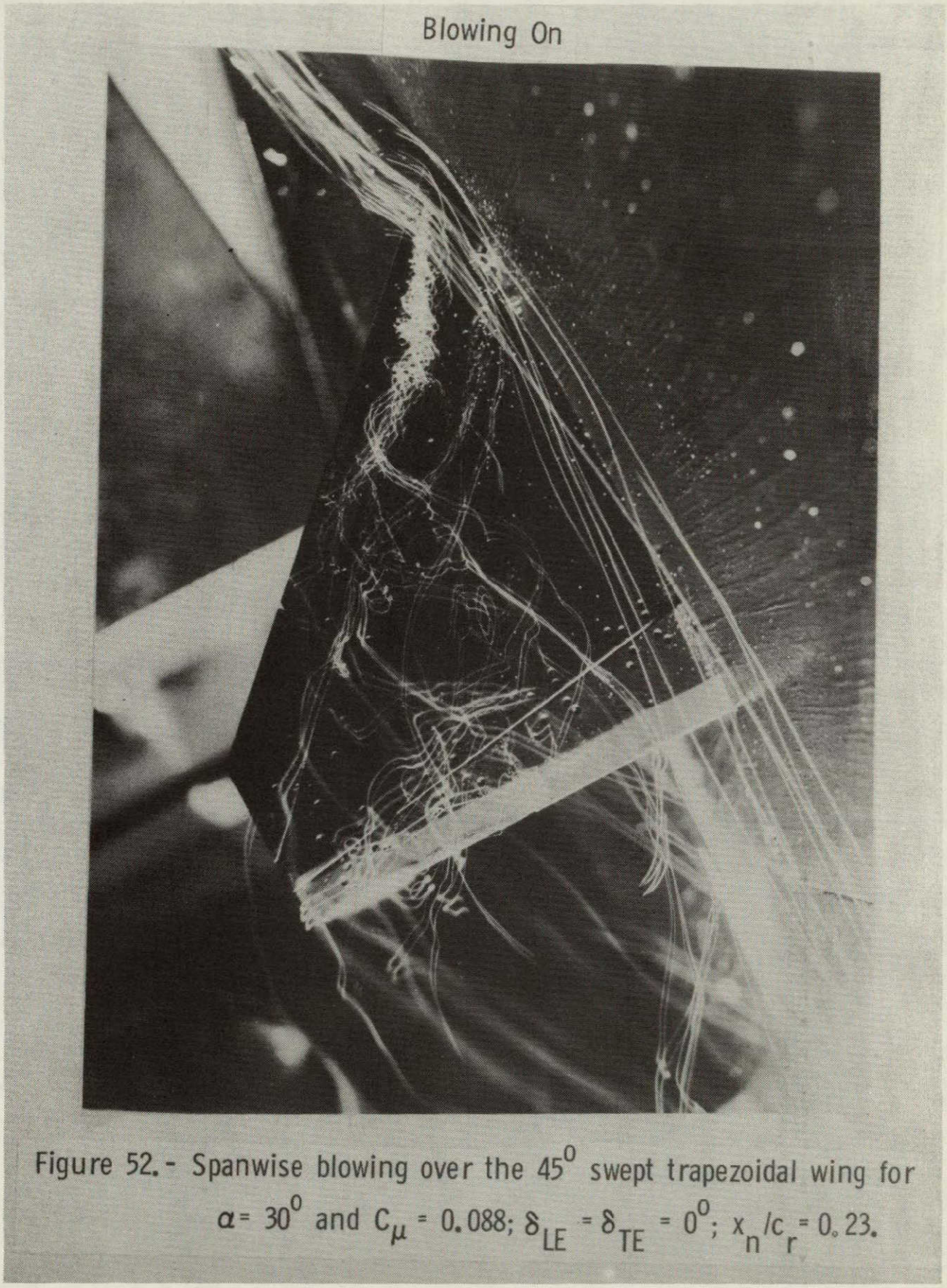

Figure 52.- Spanwise blowing over the 45^{0} swept trapezoidal wing for $\alpha = 30^{0}$ and $C_{\mu} = 0.088$; $\delta_{LE} = \delta_{TE} = 0^{0}$; $x_n/c_r = 0.23$.

Figure 53.- Spanwise blowing over the 45^{0} swept trapezoidal wing for $\alpha = 30^{0}$ and $C_{\mu} = 0.088$; $\delta_{LE} = \delta_{TE} = 0^{0}$; $x_n/c_r = 0.32$.

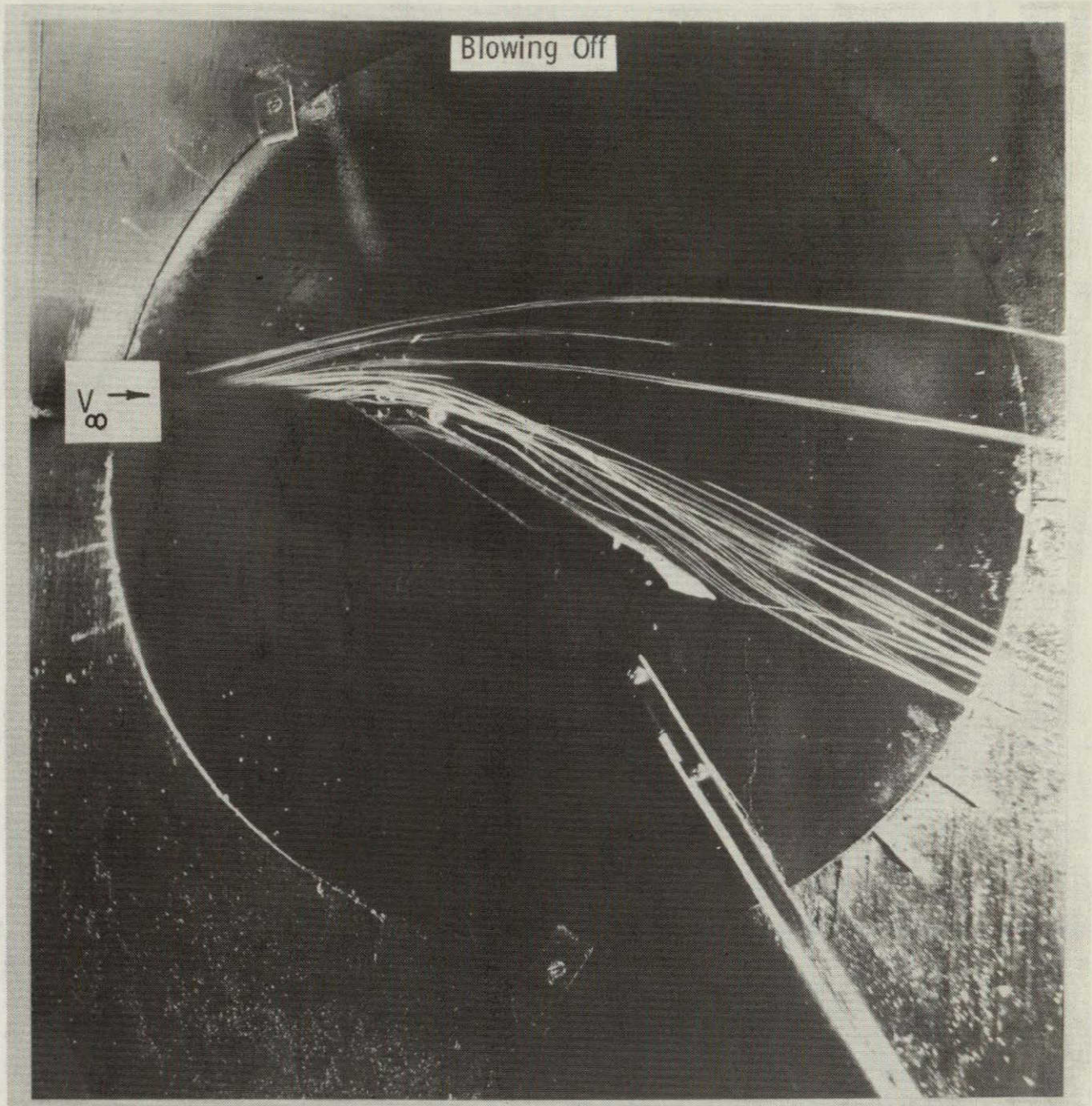

Figure 54.- Flow over the 45^0 swept trapezoidal wing with deflected LE flap for $\alpha = 20^0$ and blowing off; $\delta_{LE} = 20^0$; $\delta_{TE} = 0^0$.

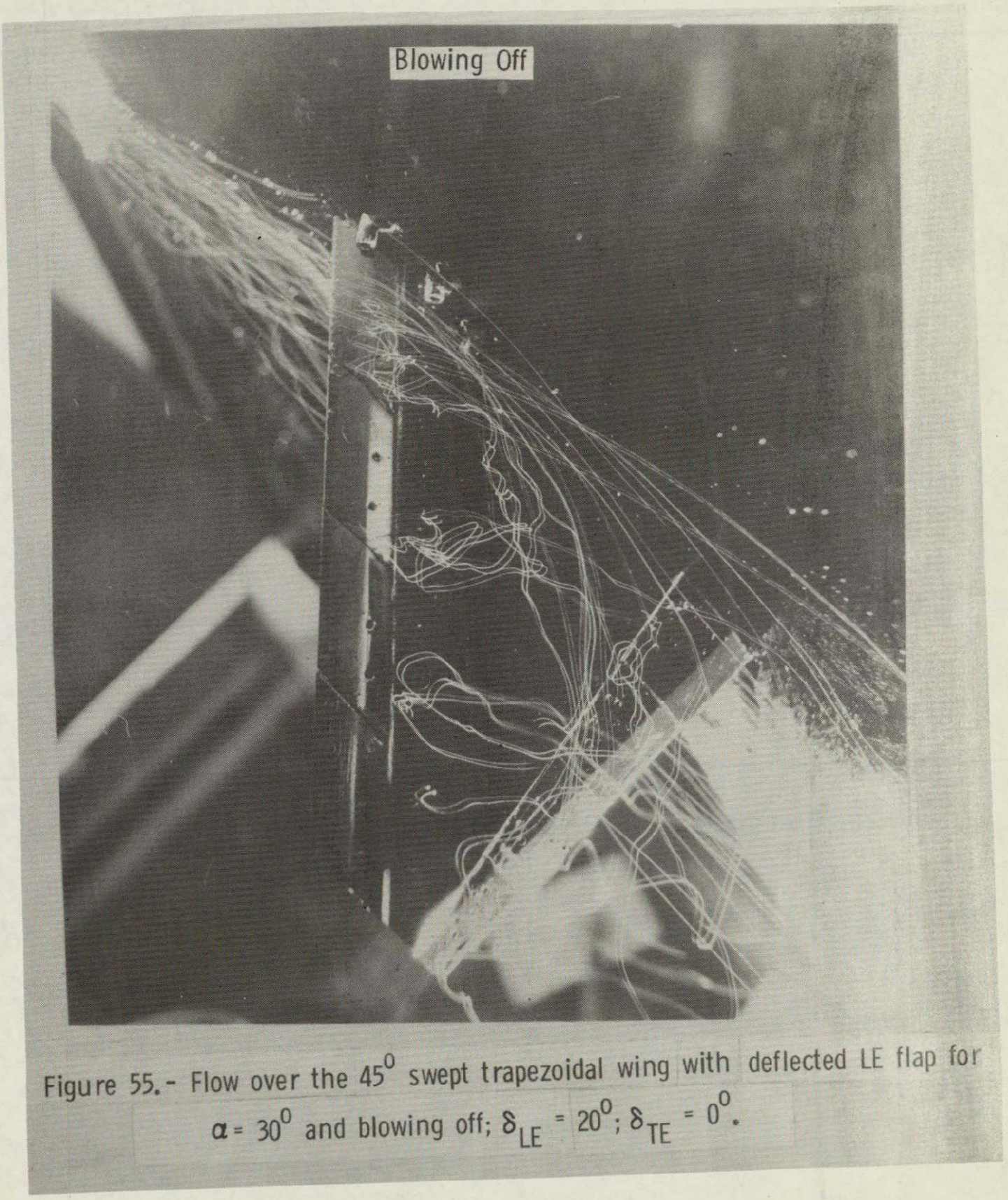

Figure 55.- Flow over the 45^{0} swept trapezoidal wing with deflected LE flap for $\alpha = 30^{0}$ and blowing off; $\delta_{LE} = 20^{0}$; $\delta_{TE} = 0^{0}$.

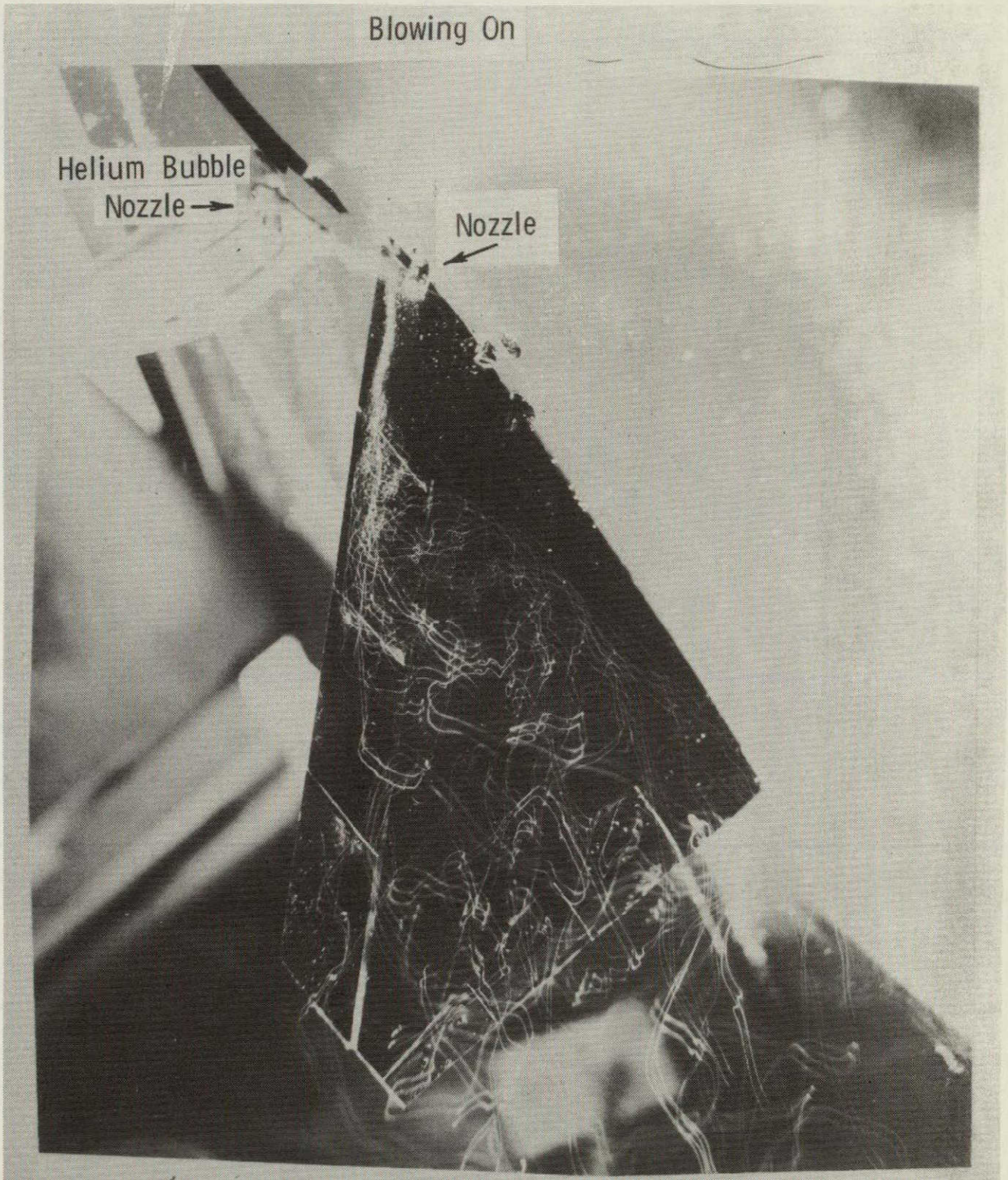

Figure 56.- Spanwise blowing over the 45^{0} swept trapezoidal wing with deflected LE flap for $\alpha = 30^{0}$ and $C_{\mu} = 0.057$; $\delta_{LE} = 20^{0}$; $\delta_{TE} = 0^{0}$; $x_n/c_r = 0.08$.

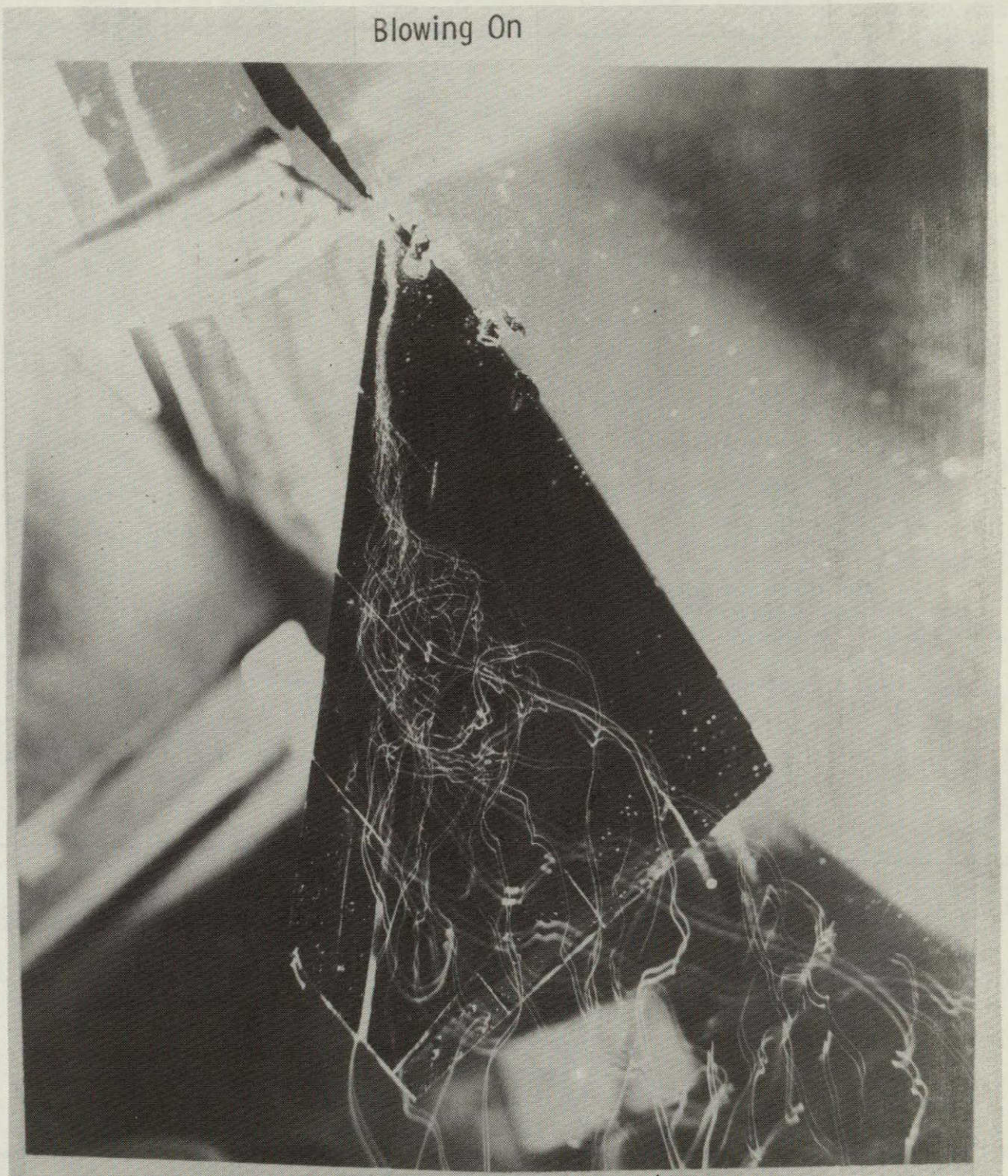

Figure 57.- Spanwise blowing over the 45^{o} swept trapezoidal wing with deflected LE flap for $\alpha = 30^{o}$ and $C_{\mu} = 0.075$; $\delta_{LE} = 20^{o}$; $\delta_{TE} = 0^{o}$; $x_n/c_r = 0.08$.

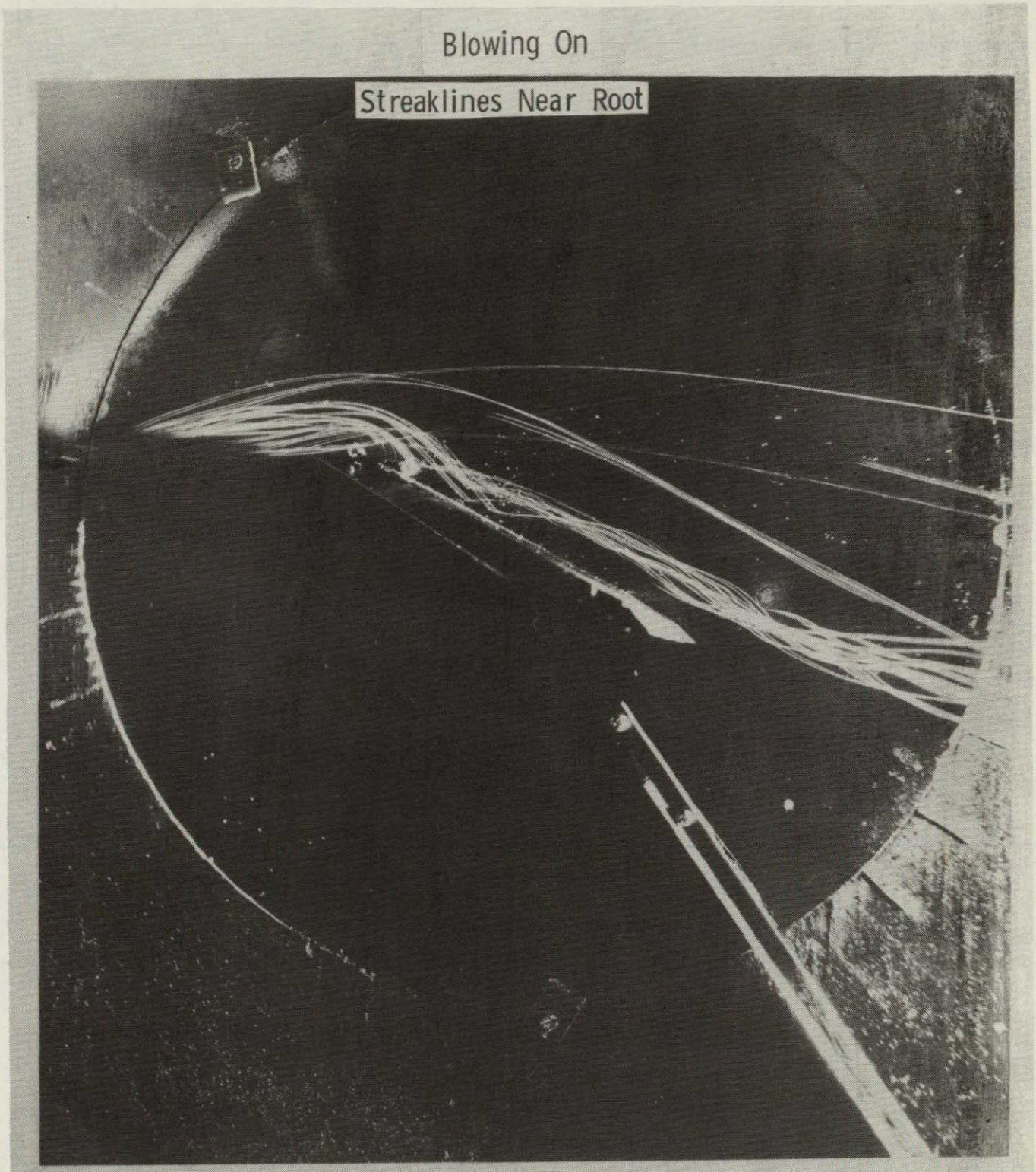

Figure 58.- Spanwise blowing over the 45^{0} swept trapezoidal wing with deflected LE flap for $\alpha = 30^{0}$ and $C_{\mu} = 0.057$; $\delta_{LE} = 20^{0}$; $\delta_{TE} = 0^{0}$; $x_n/c_r = 0.08$.

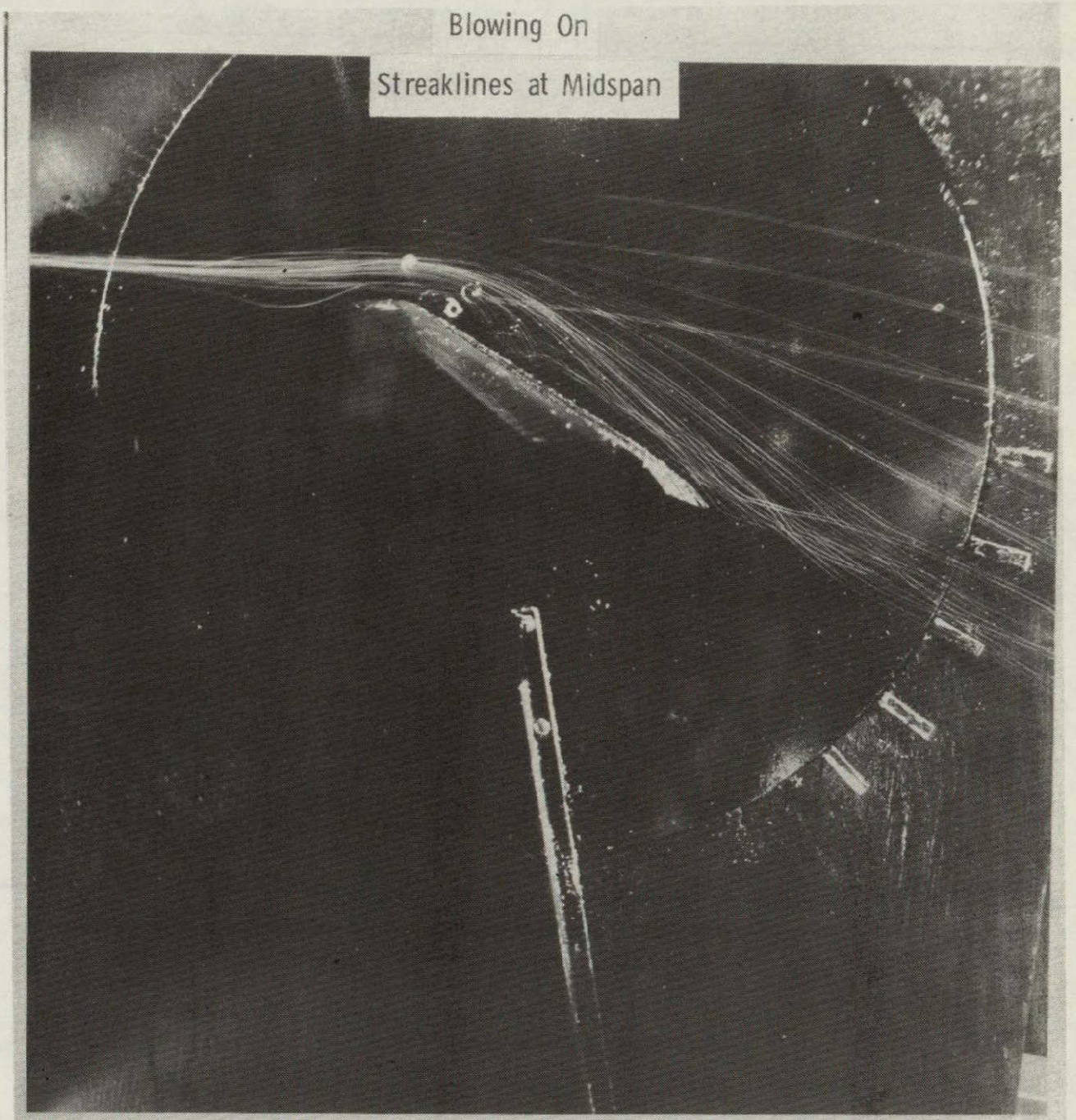

Figure 59.- Spanwise blowing over the 45^{0} swept trapezoidal wing with deflected LE flap for $\alpha = 30^{0}$ and $C_{\mu} = 0.057$; $\delta_{LE} = 20^{0}$; $\delta_{TE} = 0^{0}$; $x_n/c_r = 0.08$.

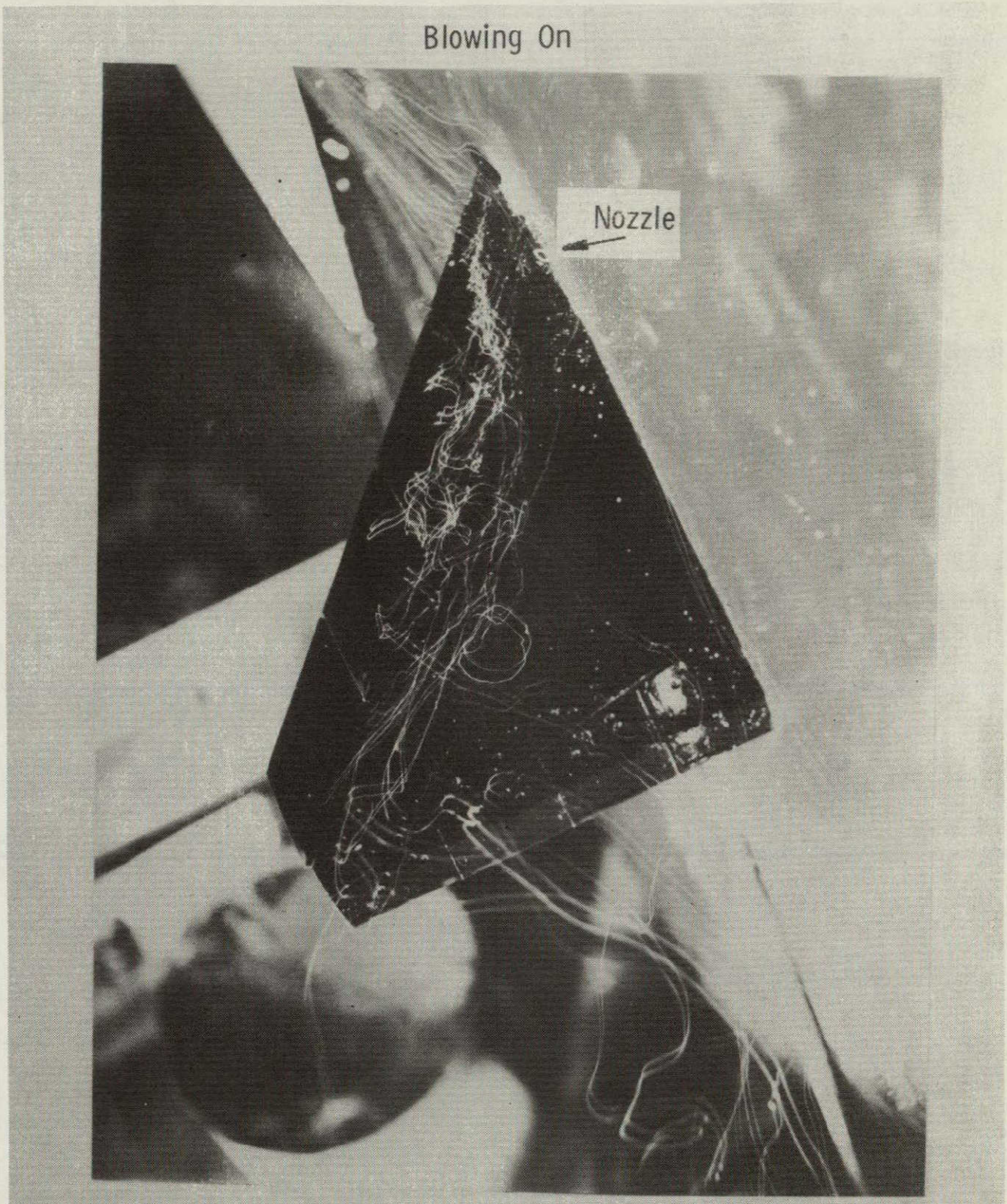

Figure 60.- Spanwise blowing over the 45^0 swept trapezoidal wing with deflected LE flap for $\alpha = 30^0$ and $C_\mu = 0.057$; $\delta_{LE} = 20^0$; $\delta_{TE} = 0^0$; $x_n/c_r = 0.23$.

Figure 61.- Spanwise blowing over the 45^{0} swept trapezoidal wing with deflected LE flap for $\alpha = 30^{0}$ and $C_{\mu} = 0.075$; $\delta_{LE} = 20^{0}$; $\delta_{TE} = 0^{0}$; $x_n/c_r = 0.23$.

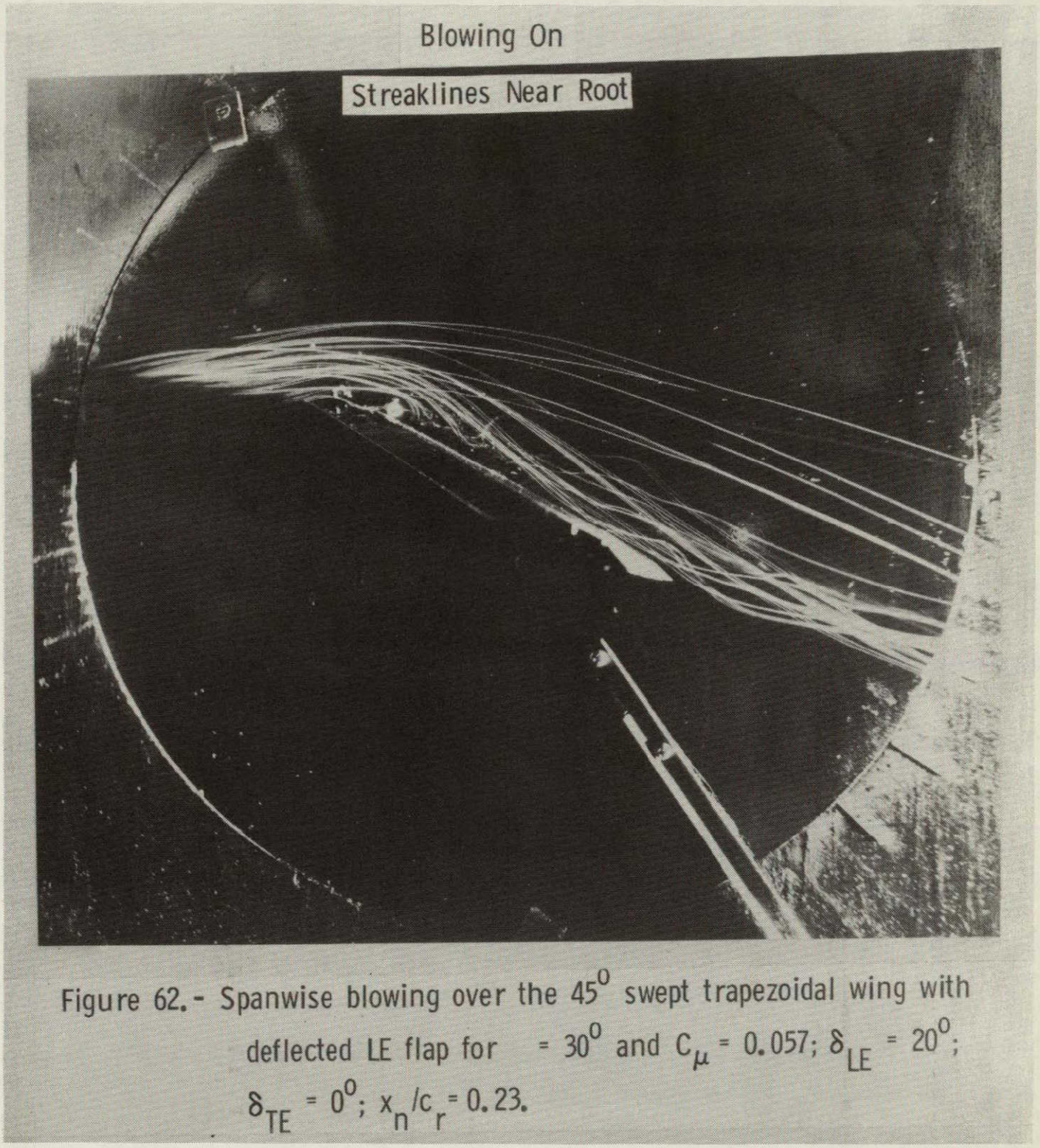

Figure 62.- Spanwise blowing over the 45° swept trapezoidal wing with deflected LE flap for $= 30^{\circ}$ and $C_{\mu} = 0.057$; $\delta_{LE} = 20^{\circ}$; $\delta_{TE} = 0^{\circ}$; $x_n/c_r = 0.23$.

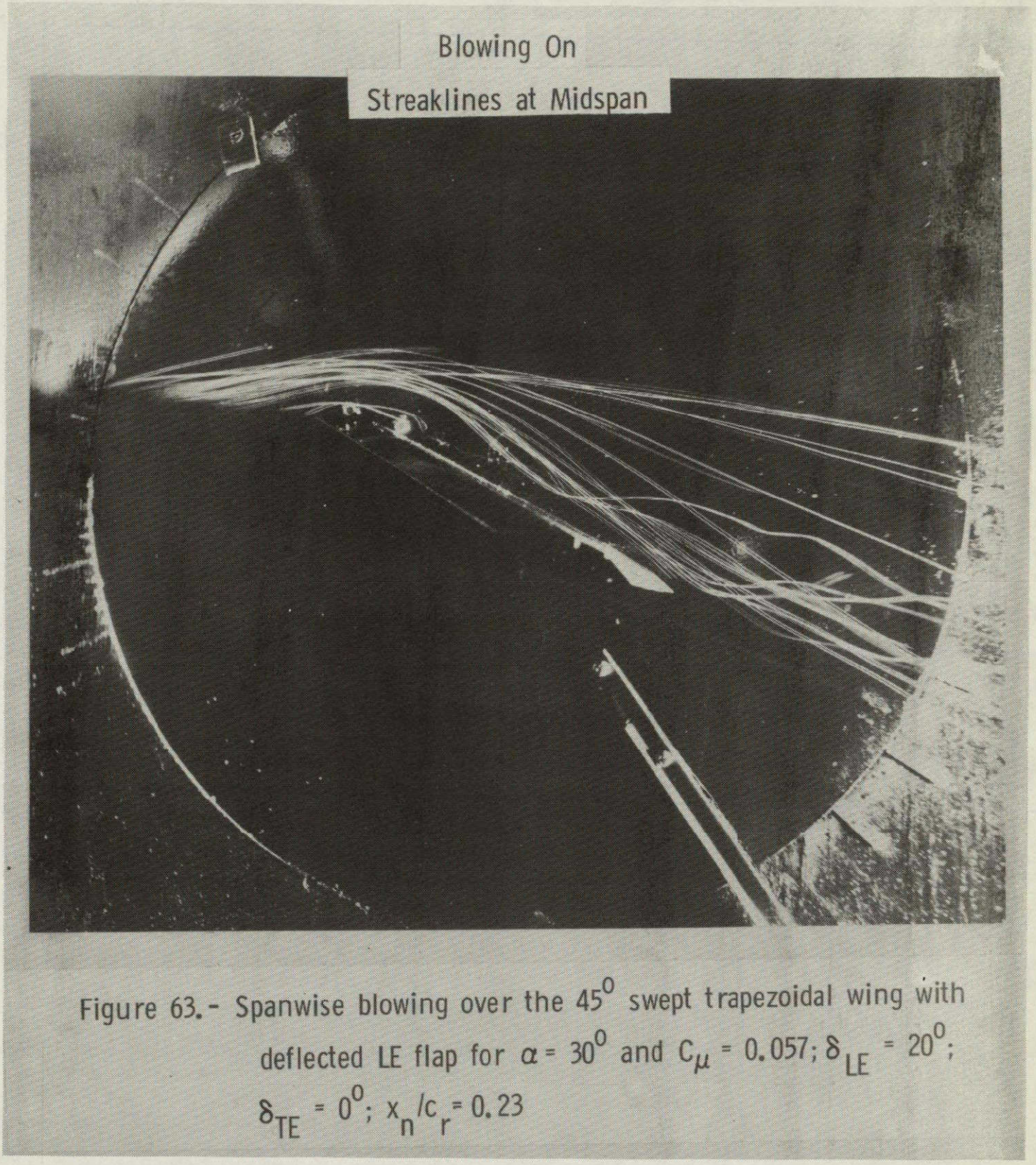

Figure 63.- Spanwise blowing over the 45^{0} swept trapezoidal wing with deflected LE flap for $\alpha = 30^{0}$ and $C_{\mu} = 0.057$; $\delta_{LE} = 20^{0}$; $\delta_{TE} = 0^{0}$; $x_n/c_r = 0.23$

Blowing Off

Figure 64.- Flow over the 45^{0} swept trapezoidal wing with deflected LE flap for $\alpha = 35^{0}$ and blowing off; $\delta_{LE} = 20^{0}$; $\delta_{TE} = 0^{0}$.

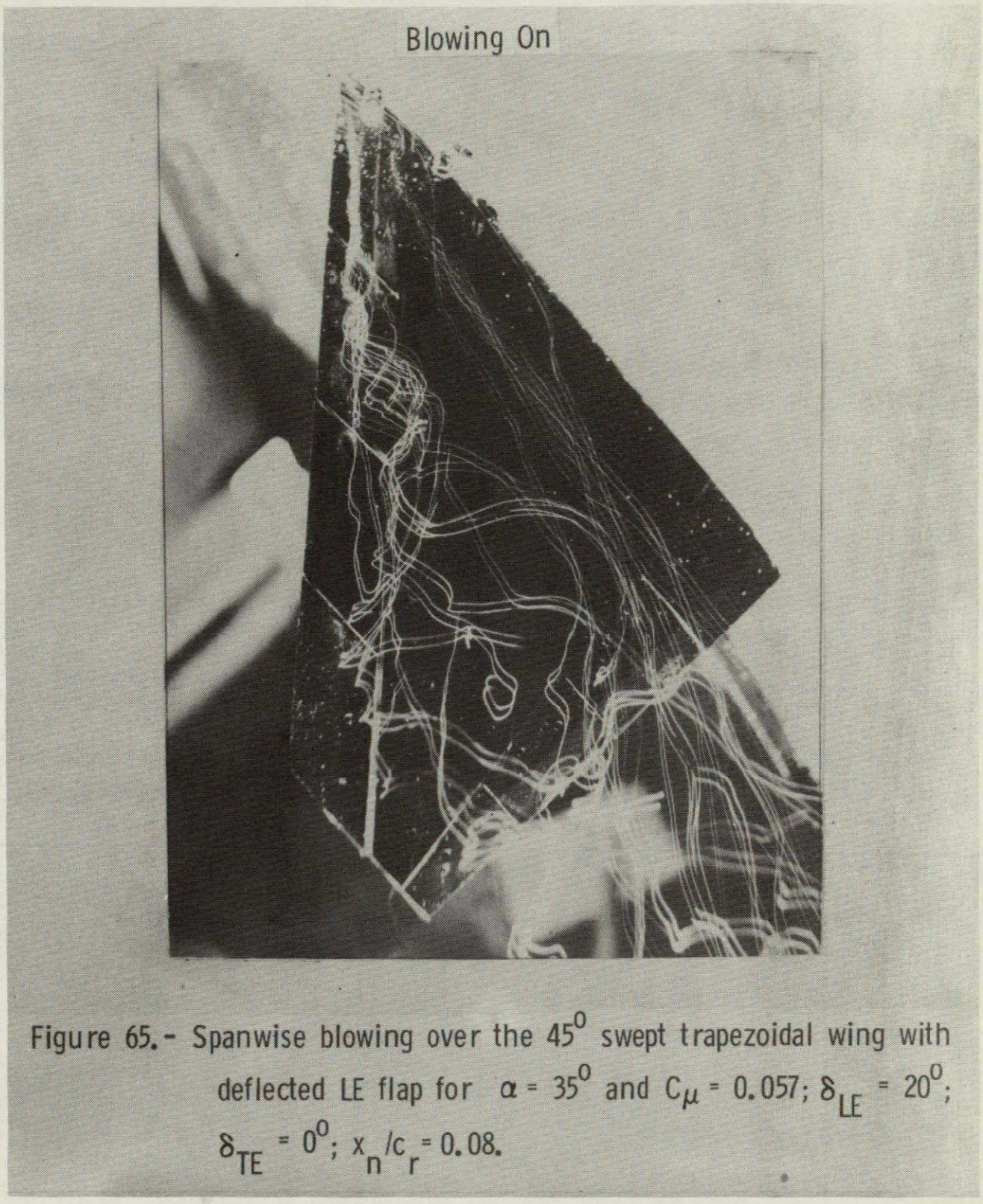

Figure 65.- Spanwise blowing over the 45^{o} swept trapezoidal wing with deflected LE flap for $\alpha = 35^{o}$ and $C_{\mu} = 0.057$; $\delta_{LE} = 20^{o}$; $\delta_{TE} = 0^{o}$; $x_n/c_r = 0.08$.

Figure 66.- Spanwise blowing over the 45^{0} swept trapezoidal wing with deflected LE flap for $\alpha = 35^{0}$ and $C_{\mu} = 0.075$; $\delta_{LE} = 20^{0}$; $\delta_{TE} = 0^{0}$; $x_n/c_r = 0.08$.

Blowing On

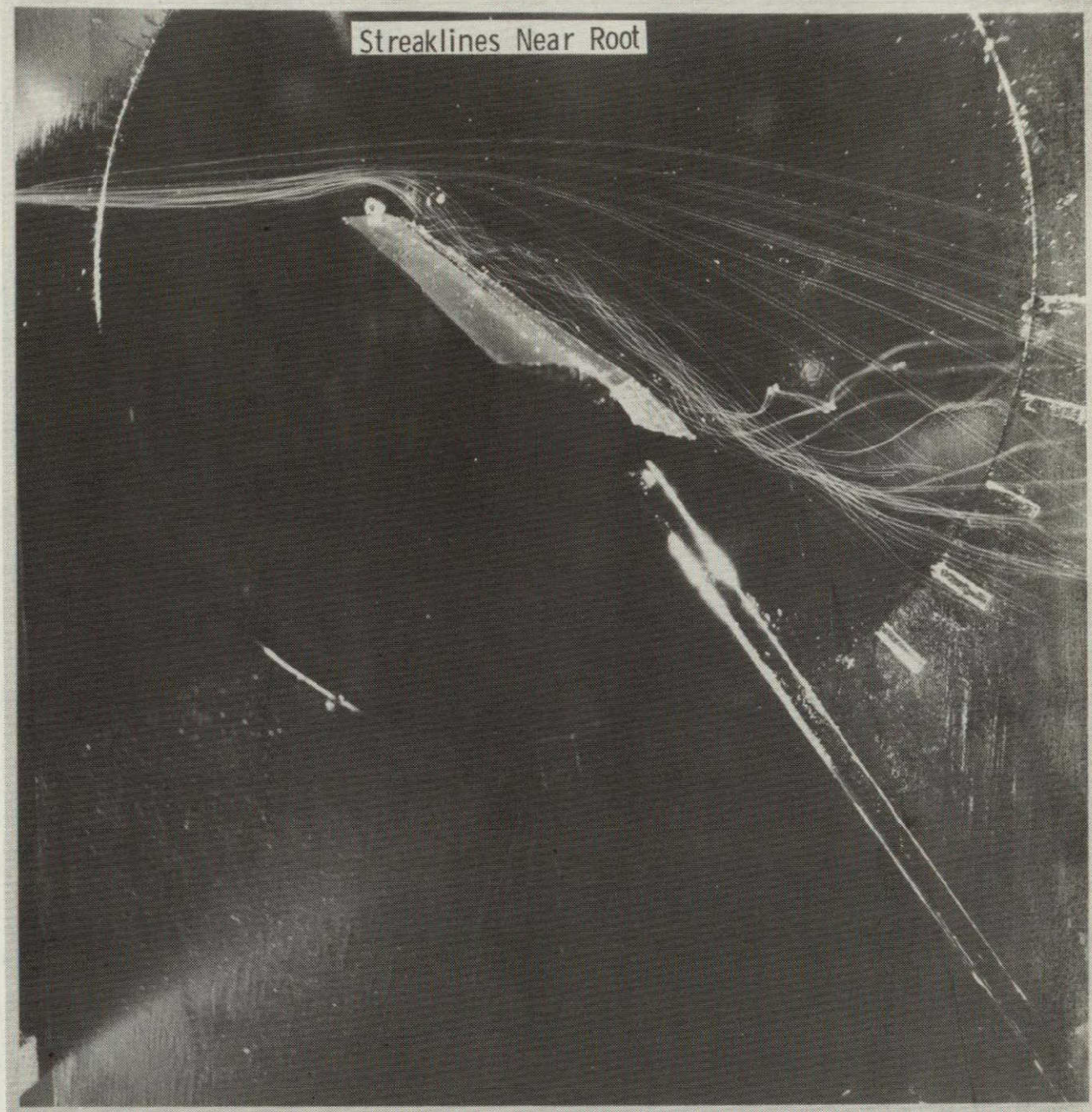

Figure 67.- Spanwise blowing over the 45° swept trapezoidal wing with deflected LE flap for $\alpha = 35^{\circ}$ and $C_{\mu} = 0.057$; $\delta_{LE} = 20^{\circ}$; $\delta_{TE} = 0^{\circ}$; $x_n/c_r = 0.08$.

Blowing On

Streaklines at Midspan

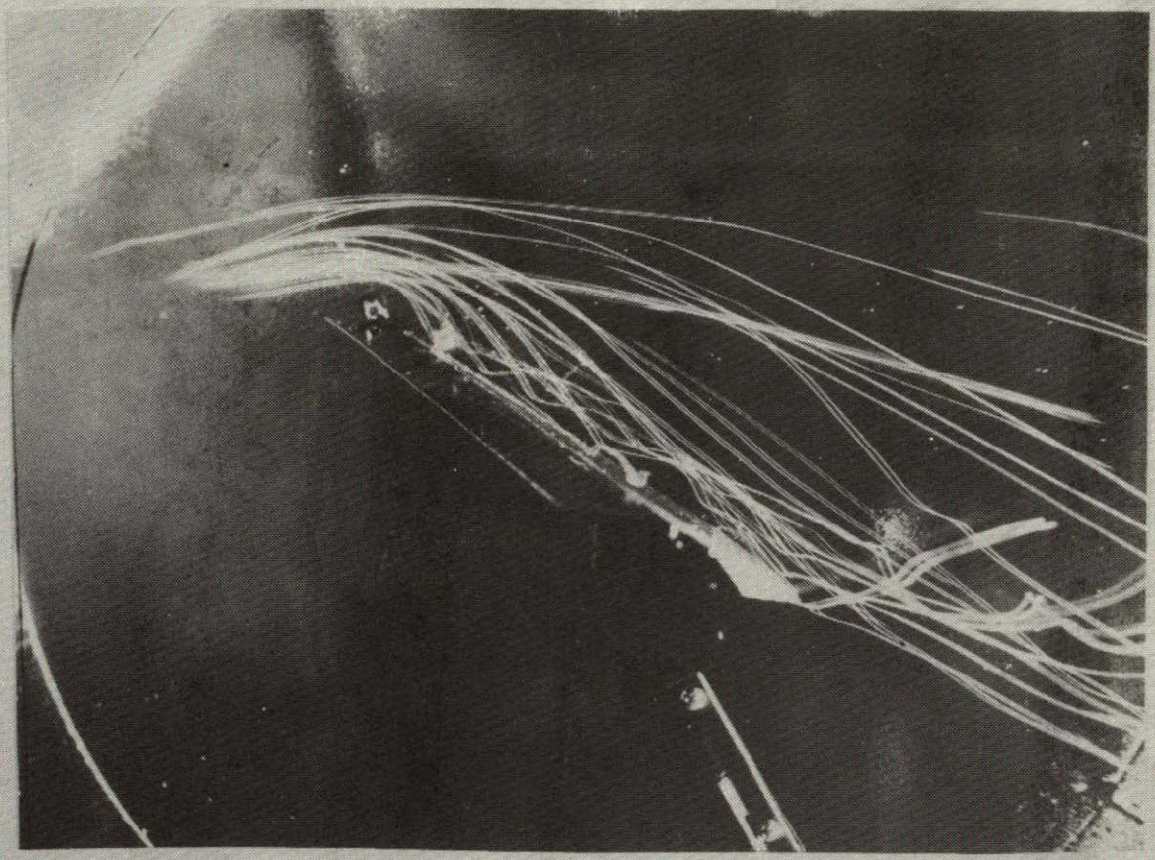

Figure 68.- Spanwise blowing over the 45^0 swept trapezoidal wing with deflected LE flap for $\alpha = 35^0$ and $C_\mu = 0.057$; $\delta_{LE} = 20^0$; $\delta_{TE} = 0^0$; $x_n/c_r = 0.08$.

Blowing On

Figure 69.- Spanwise blowing over the 45^0 swept trapezoidal wing with deflected LE flap for $\alpha = 35^0$ and $C_\mu = 0.057$; $\delta_{LE} = 20^0$; $\delta_{TE} = 0^0$; $x_n/c_r = 0.23$.

Figure 70.- Spanwise blowing over the 45^{o} swept trapezoidal wing with deflected LE flap for $\alpha = 35^{o}$ and $C_{\mu} = 0.075$; $\delta_{LE} = 20^{o}$; $\delta_{TE} = 0^{o}$; $x_n/c_r = 0.23$.

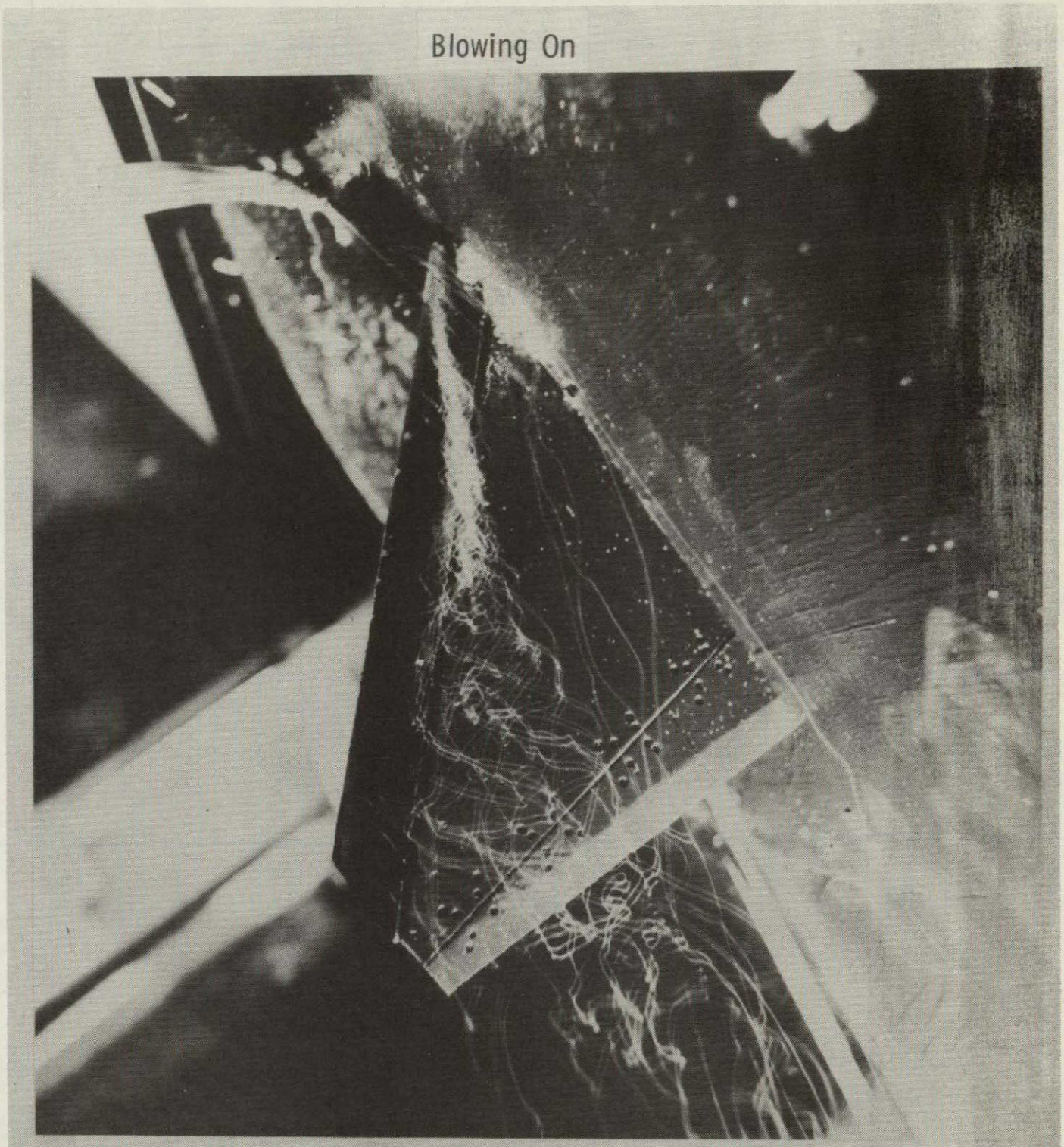

Figure 71.- Spanwise blowing over the 45^{0} swept trapezoidal wing with deflected LE flap for $\alpha = 35^{0}$ and $C_{\mu} = 0.088$; $\delta_{LE} = 20^{0}$; $\delta_{TE} = 0^{0}$; $x_n/c_r = 0.23$.

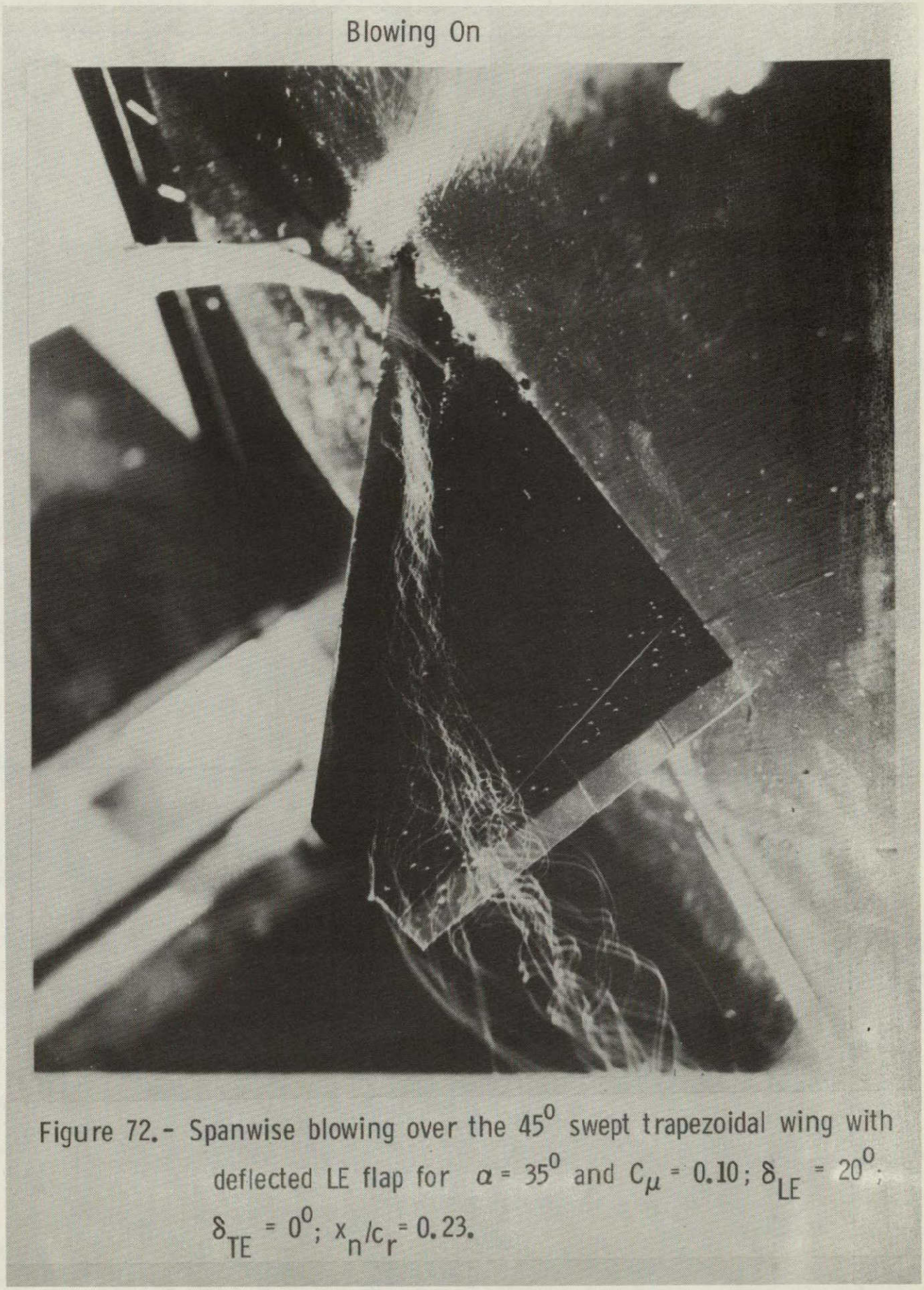

Figure 72.- Spanwise blowing over the 45^{0} swept trapezoidal wing with deflected LE flap for $\alpha = 35^{0}$ and $C_{\mu} = 0.10$; $\delta_{LE} = 20^{0}$; $\delta_{TE} = 0^{0}$; $x_n/c_r = 0.23$.

Figure 73.- Spanwise blowing over the 45^{0} swept trapezoidal wing with deflected LE flap for $\alpha = 35^{0}$ and $C_{\mu} = 0.057$; $\delta_{LE} = 20^{0}$; $\delta_{TE} = 0^{0}$; $x_n/c_r = 0.23$.

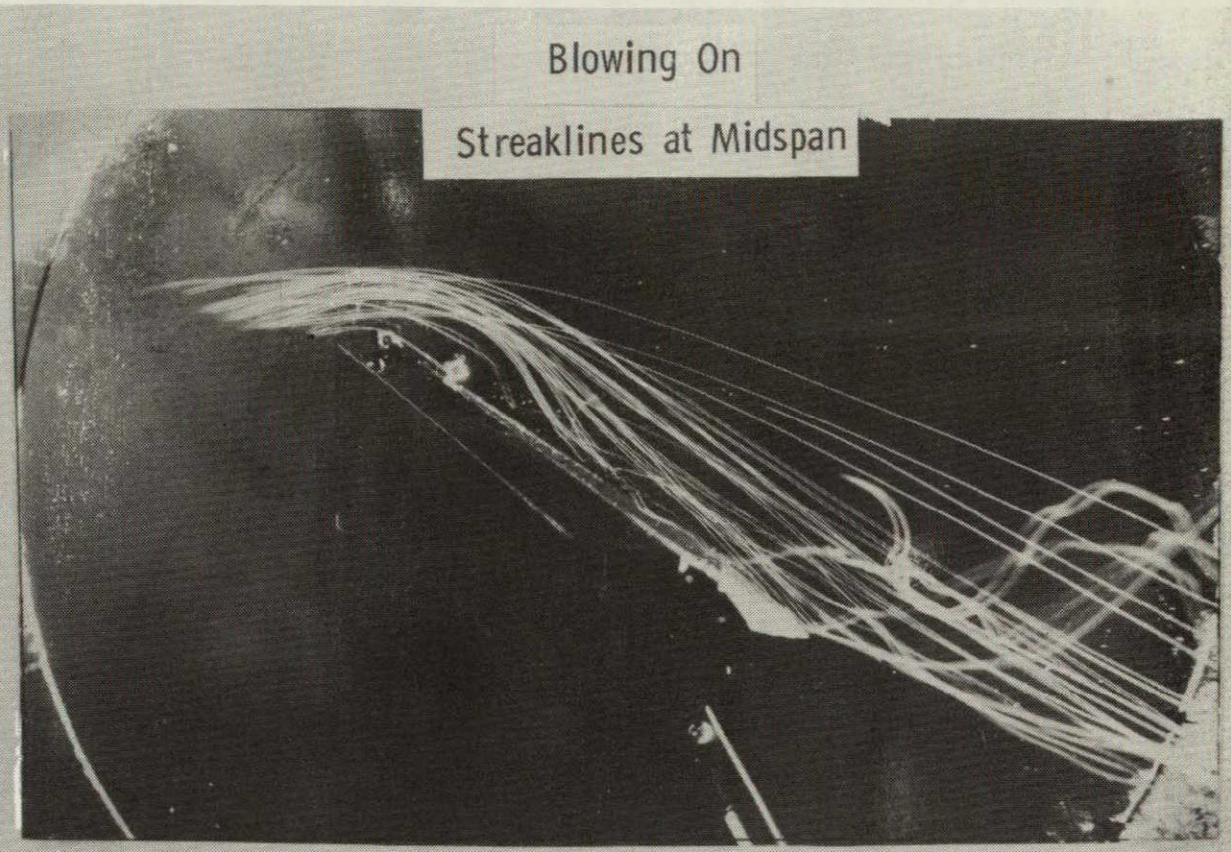

Figure 74.- Spanwise blowing over the 45^0 swept trapezoidal wing with deflected LE flap for $\alpha = 35^0$ and $C_\mu = 0.057$; $\delta_{LE} = 20^0$; $\delta_{TE} = 0^0$; $x_n/c_r = 0.23$.

Blowing Off

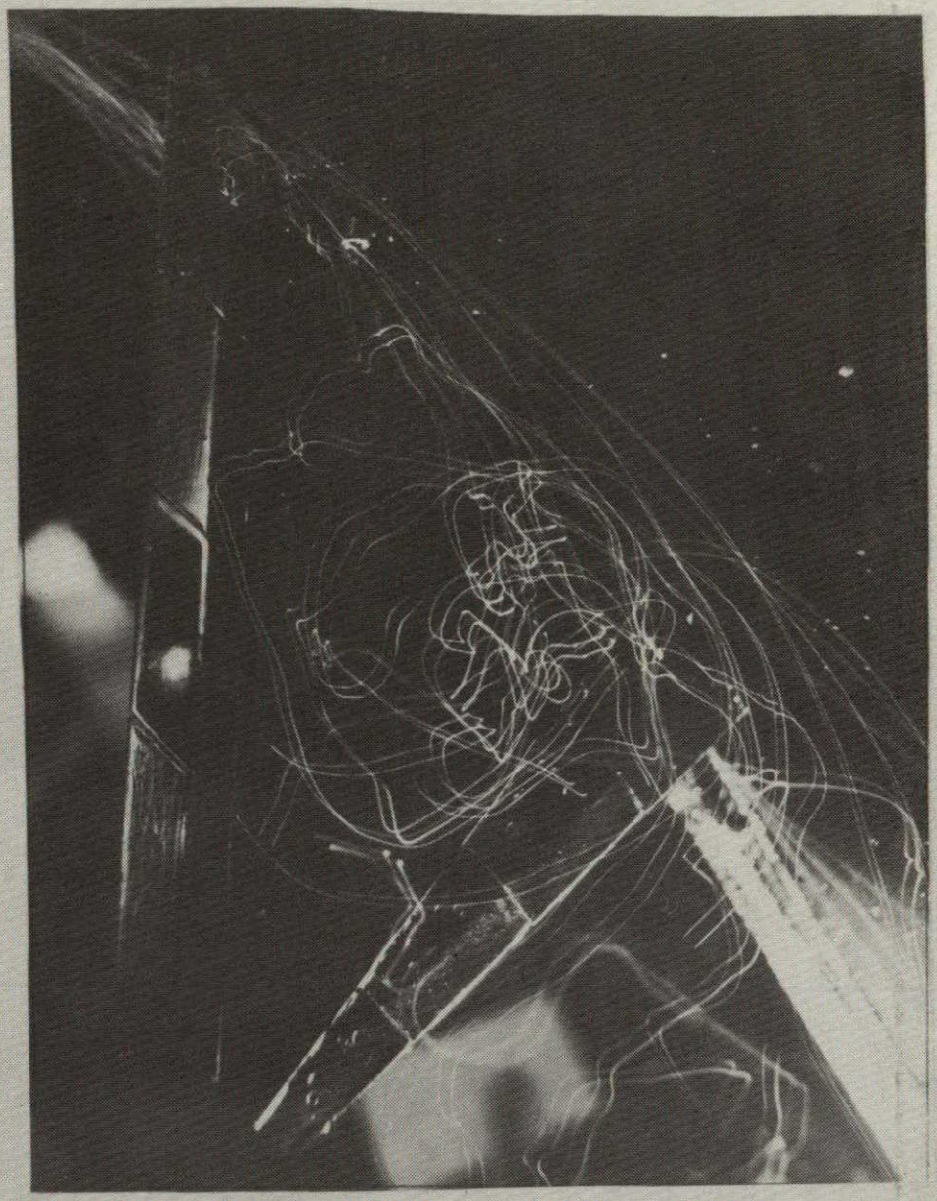

Figure 75.- Flow over the 45^{0} swept trapezoidal wing with deflected LE flap for $\alpha = 40^{0}$ and blowing off; $\delta_{LE} = 20^{0}$; $\delta_{TE} = 0^{0}$.

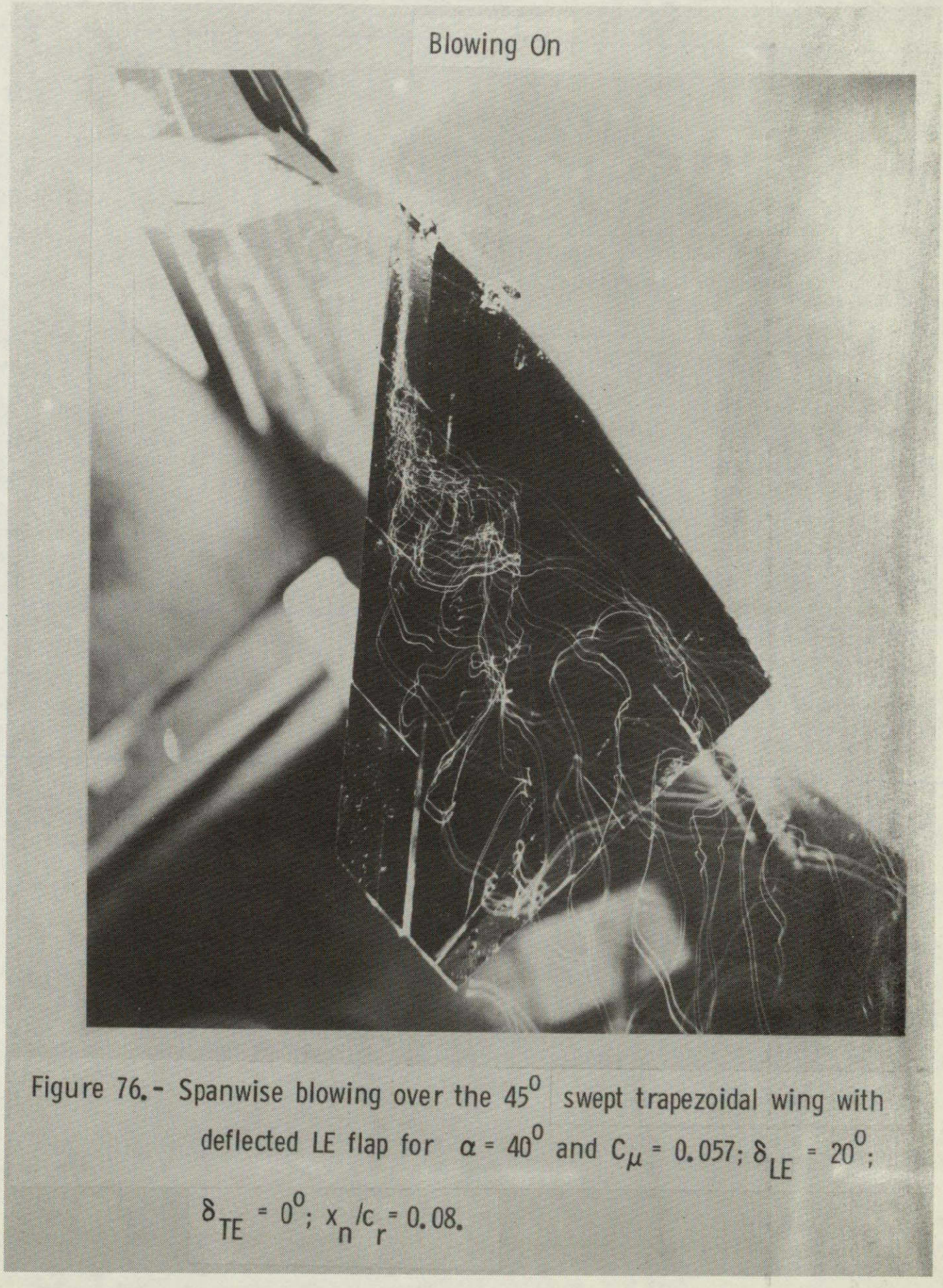

Figure 76.- Spanwise blowing over the 45^{o} swept trapezoidal wing with deflected LE flap for $\alpha = 40^{o}$ and $C_{\mu} = 0.057$; $\delta_{LE} = 20^{o}$; $\delta_{TE} = 0^{o}$; $x_n/c_r = 0.08$.

Blowing On

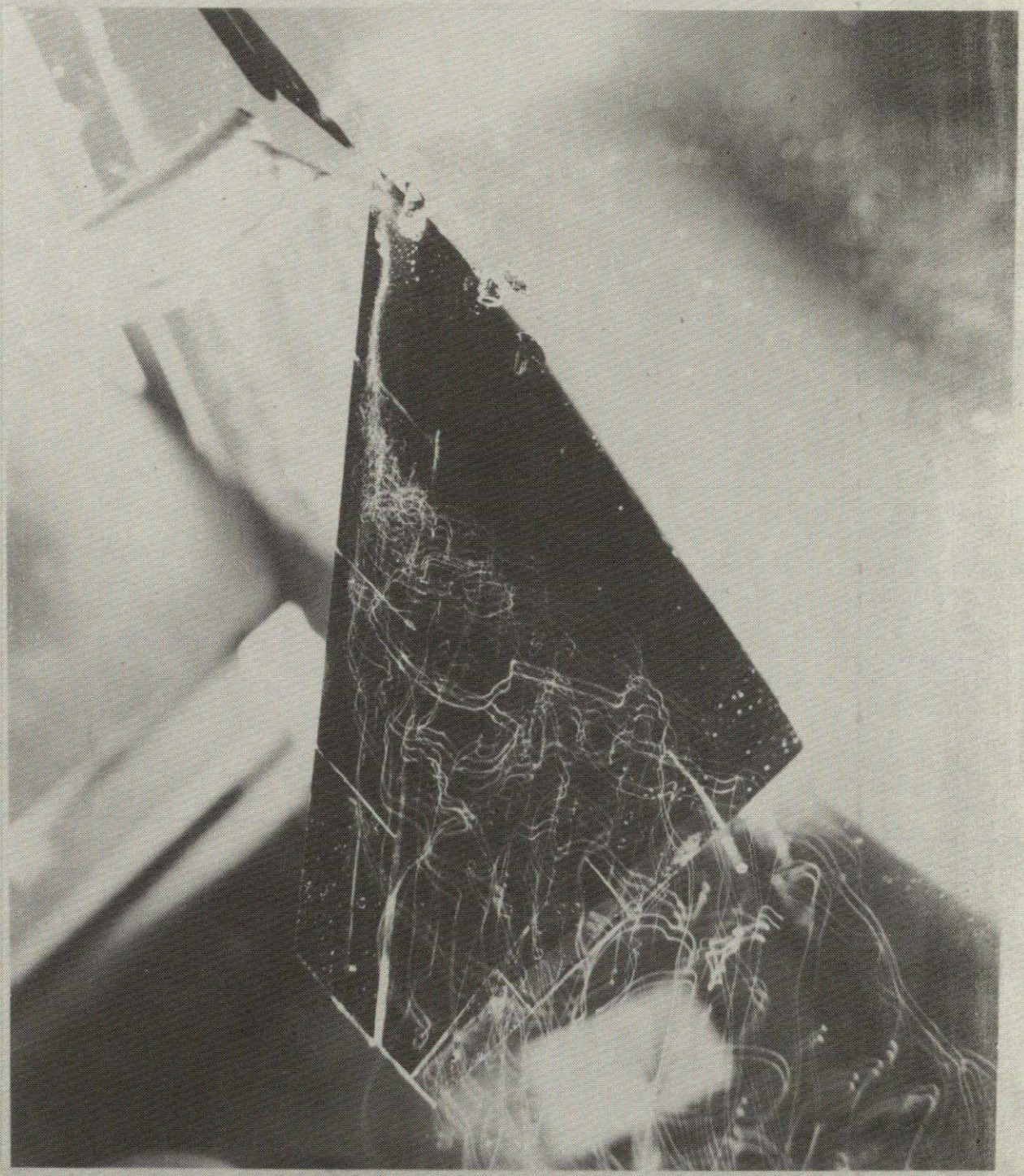

Figure 77.- Spanwise blowing over the 45^{o} swept trapezoidal wing with deflected LE flap for $\alpha = 40^{o}$ and $C_{\mu} = 0.075$; $\delta_{LE} = 20^{o}$; $\delta_{TE} = 0^{o}$; $x_n/c_r = 0.08$.

Figure 78.- Spanwise blowing over the 45^{0} swept trapezoidal wing with deflected LE flap for $\alpha = 40^{0}$ and $C_{\mu} = 0.075$; $\delta_{LE} = 20^{0}$; $\delta_{TE} = 0^{0}$; $x_n/c_r = 0.08$.

C-2

Blowing On

Streaklines at Midspan

Figure 79.- Spanwise blowing over the 45° swept trapezoidal wing with deflected LE flap for $\alpha = 40^{\circ}$ and $C_{\mu} = 0.075$; $\delta_{LE} = 20^{\circ}$; $\delta_{TE} = 0^{\circ}$; $x_n/c_r = 0.08$.

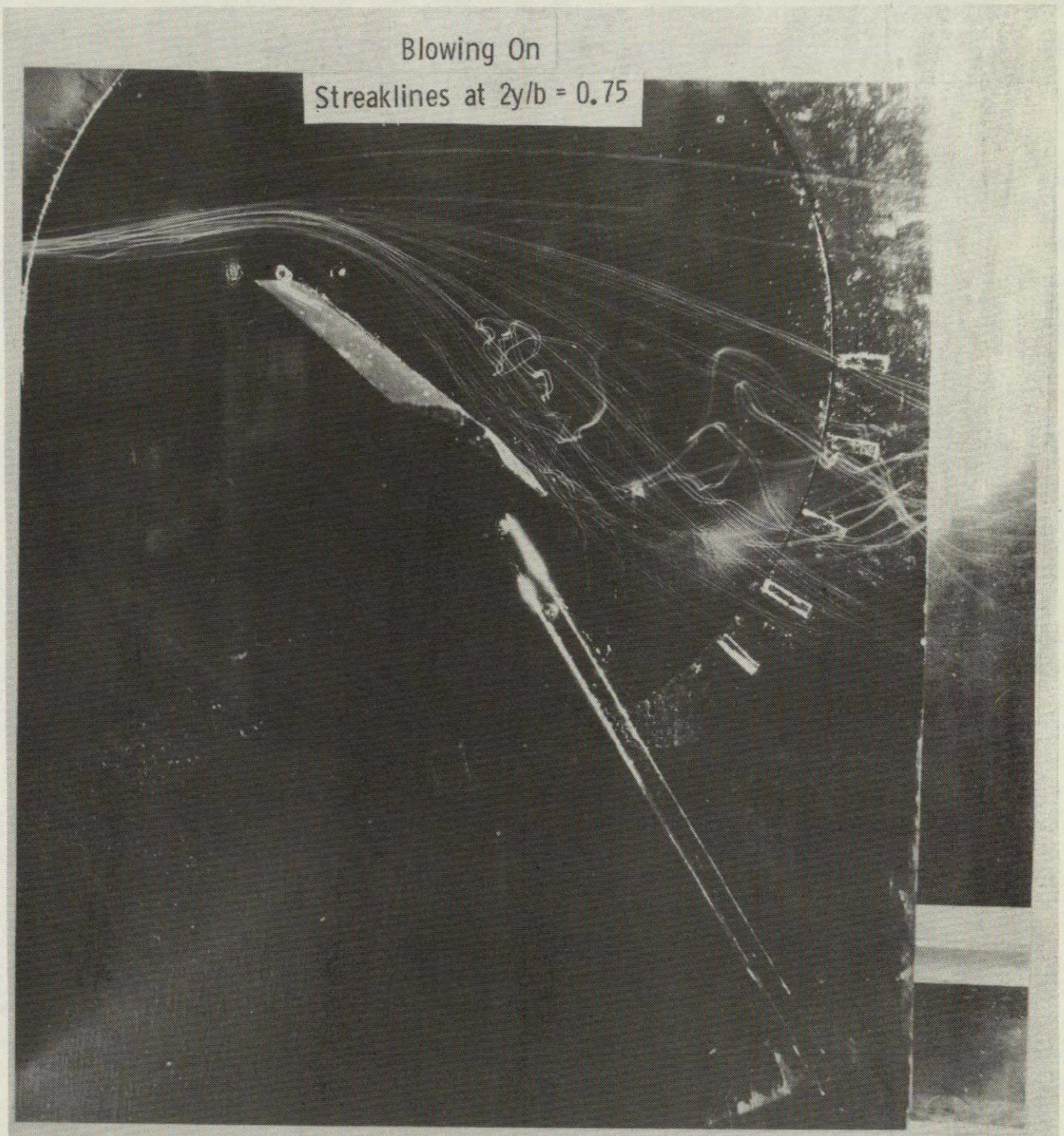

Figure 80.- Spanwise blowing over the 45^0 swept trapezoidal wing with deflected LE flap for $\alpha = 40^0$ and $C_\mu = 0.075$; $\delta_{LE} = 20^0$; $\delta_{TE} = 0^0$; $x_n/c_r = 0.08$.

Figure 81.- Spanwise blowing over the 45^{o} swept trapezoidal wing with deflected LE flap for $\alpha = 40^{o}$ and $C_{\mu} = 0.057$; $\delta_{LE} = 20^{o}$; $\delta_{TE} = 0^{o}$; $x_n/c_r = 0.23$.

Blowing On

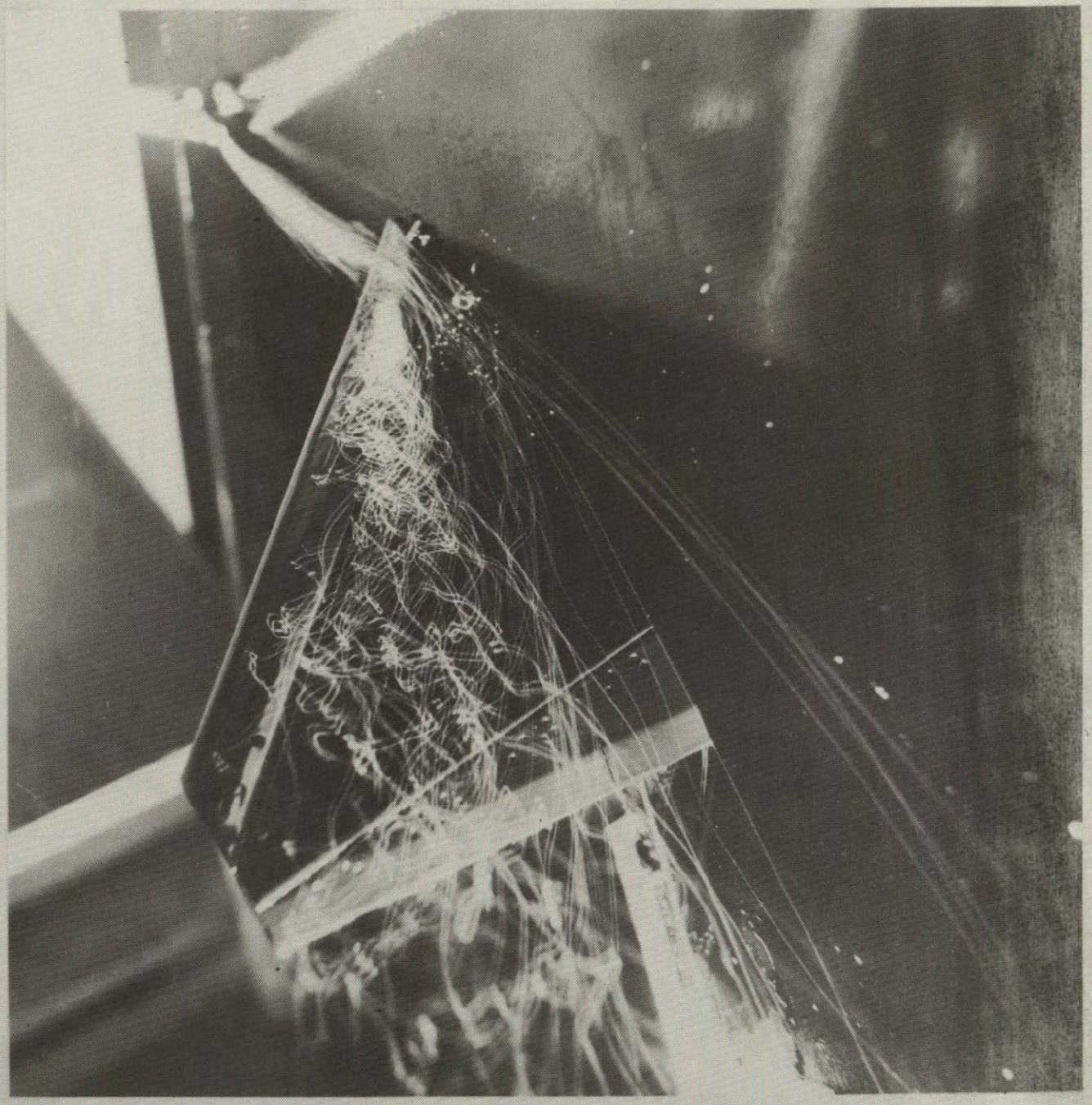

Figure 82.- Spanwise blowing over the 45^{0} swept trapezoidal wing with deflected LE flap for $\alpha = 40^{0}$ and $C_{\mu} = 0.075$; $\delta_{LE} = 20^{0}$; $\delta_{TE} = 0^{0}$; $x_n/c_r = 0.23$.

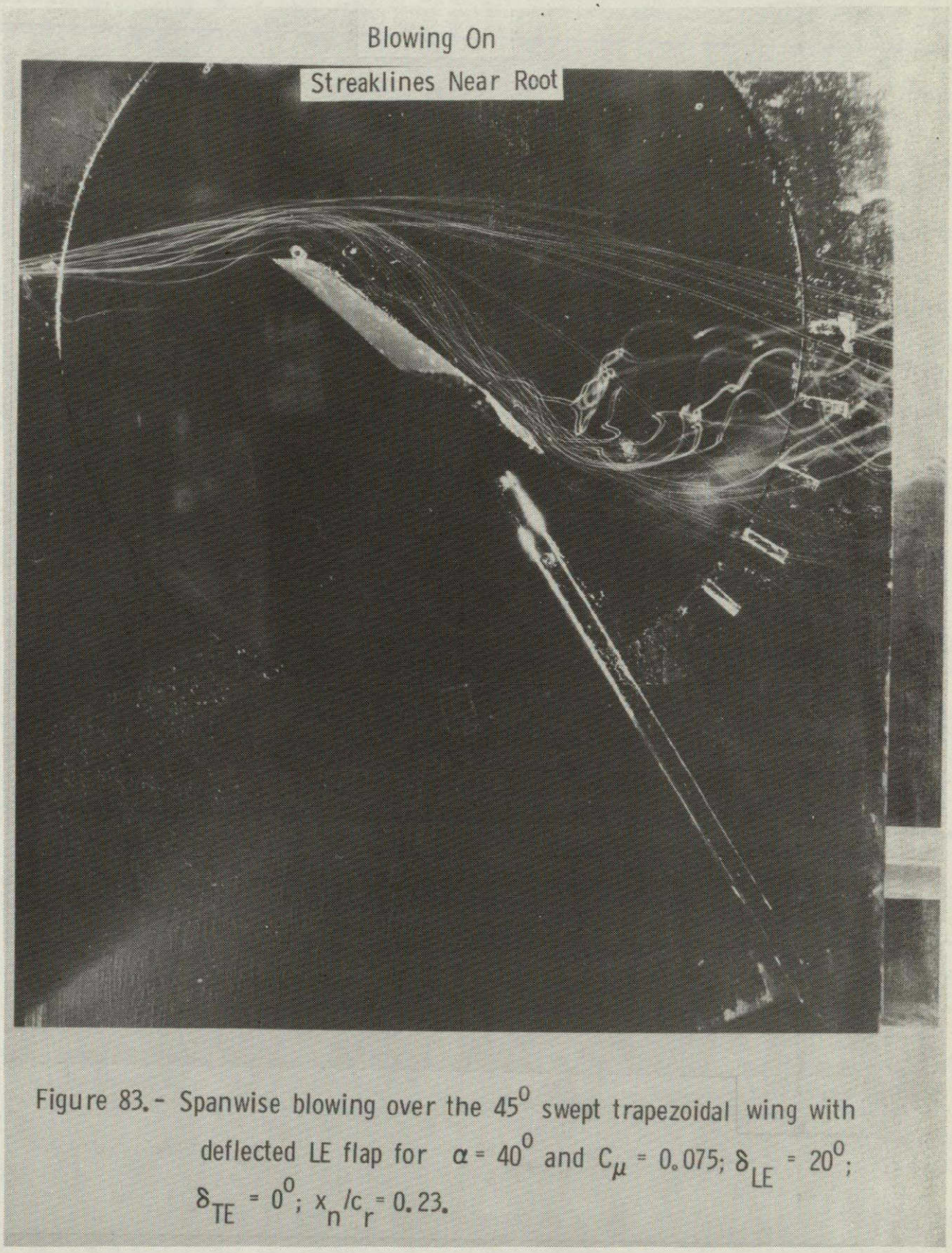

Figure 83.- Spanwise blowing over the 45^{0} swept trapezoidal wing with deflected LE flap for $\alpha = 40^{0}$ and $C_{\mu} = 0.075$; $\delta_{LE} = 20^{0}$; $\delta_{TE} = 0^{0}$; $x_n/c_r = 0.23$.

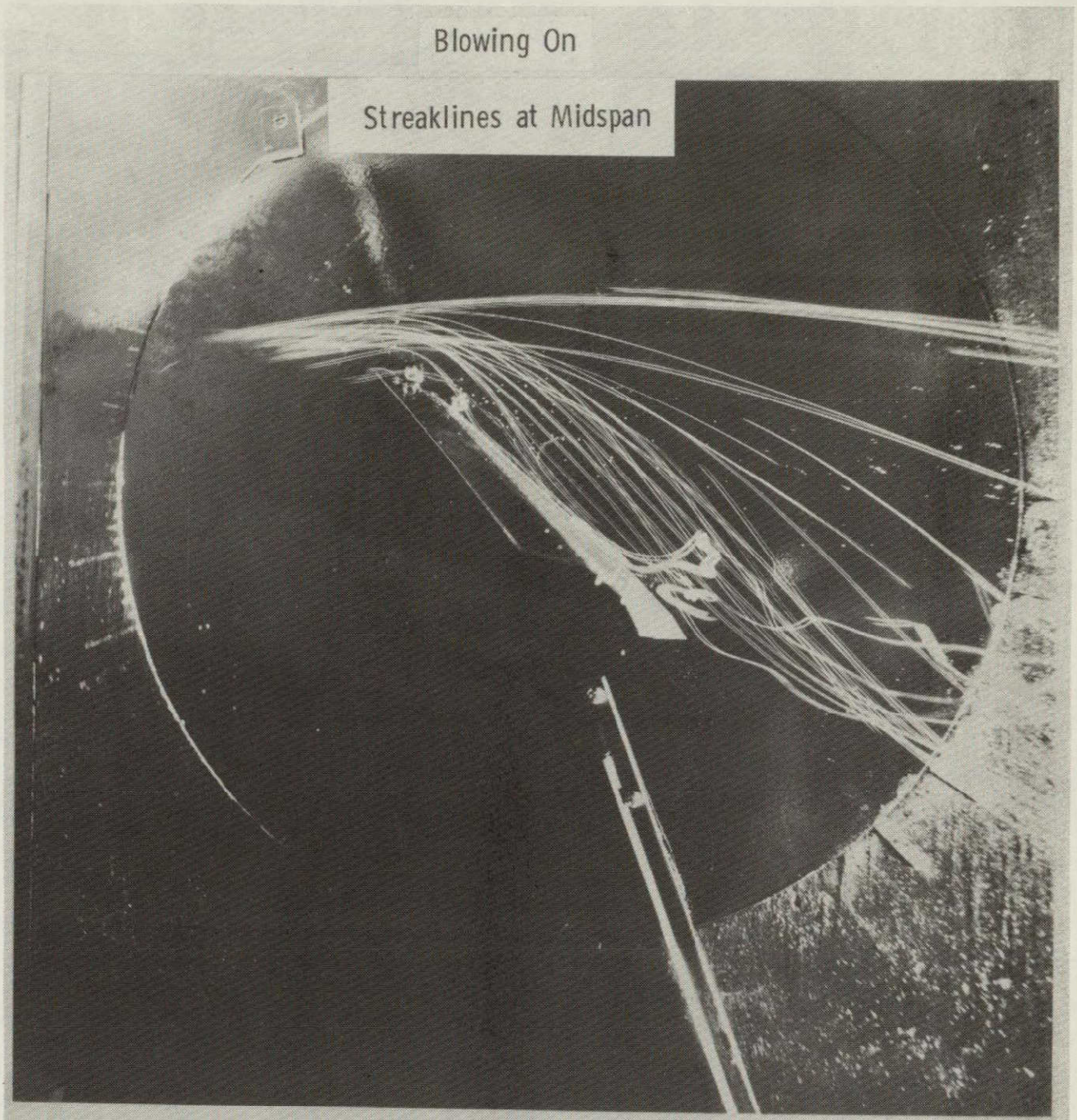

Figure 84.- Spanwise blowing over the 45^0 swept trapezoidal wing with deflected LE flap for $\alpha = 40^0$ and $C_\mu = 0.075$; $\delta_{LE} = 20^0$; $\delta_{TE} = 0^0$; $x_n/c_r = 0.23$.

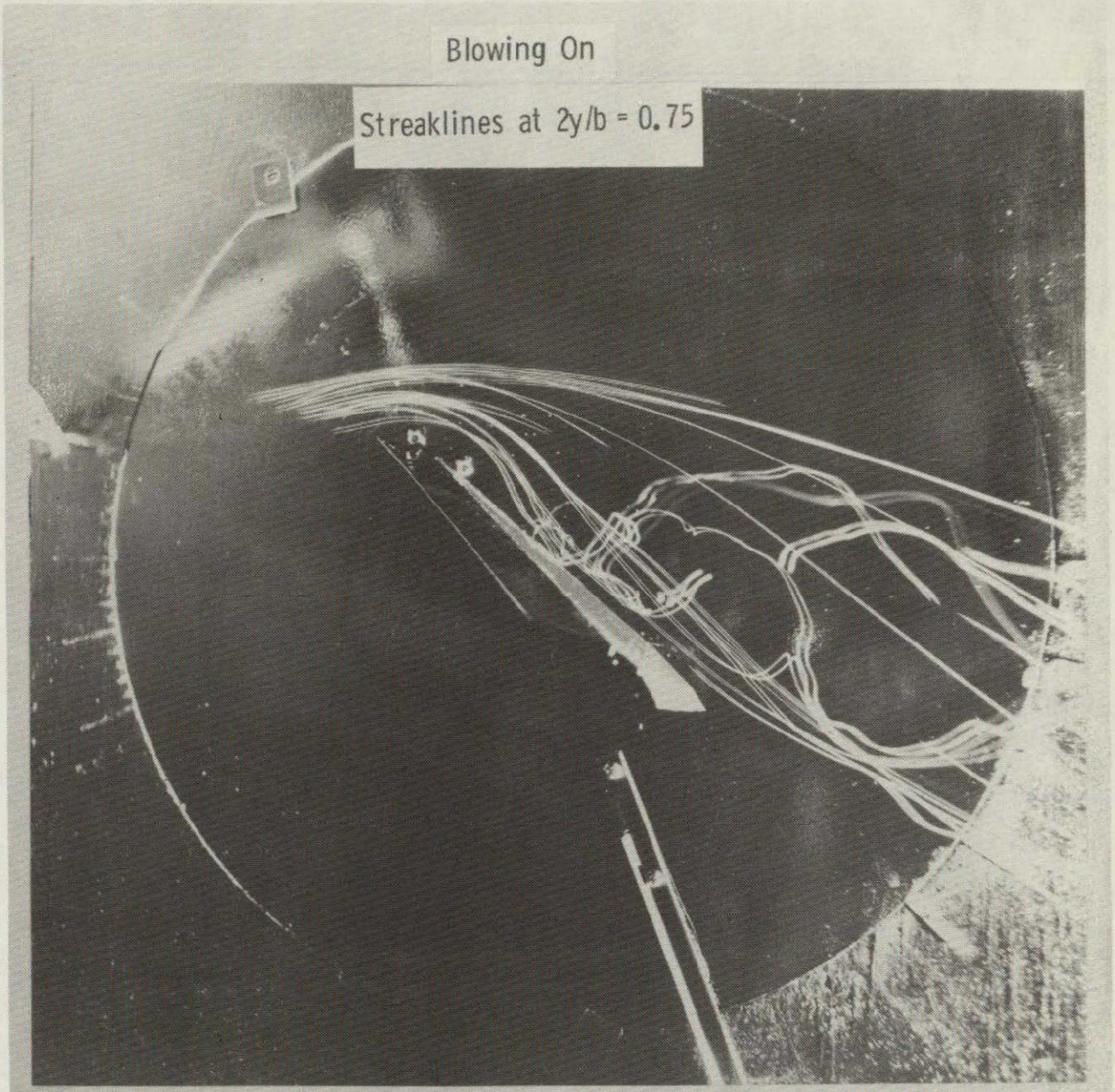

Figure 85.- Spanwise blowing over the 45^{0} swept trapezoidal wing with deflected LE flap for $\alpha = 40^{0}$ and $C_{\mu} = 0.075$; $\delta_{LE} = 20^{0}$; $\delta_{TE} = 0^{0}$; $x_n/c_r = 0.23$.

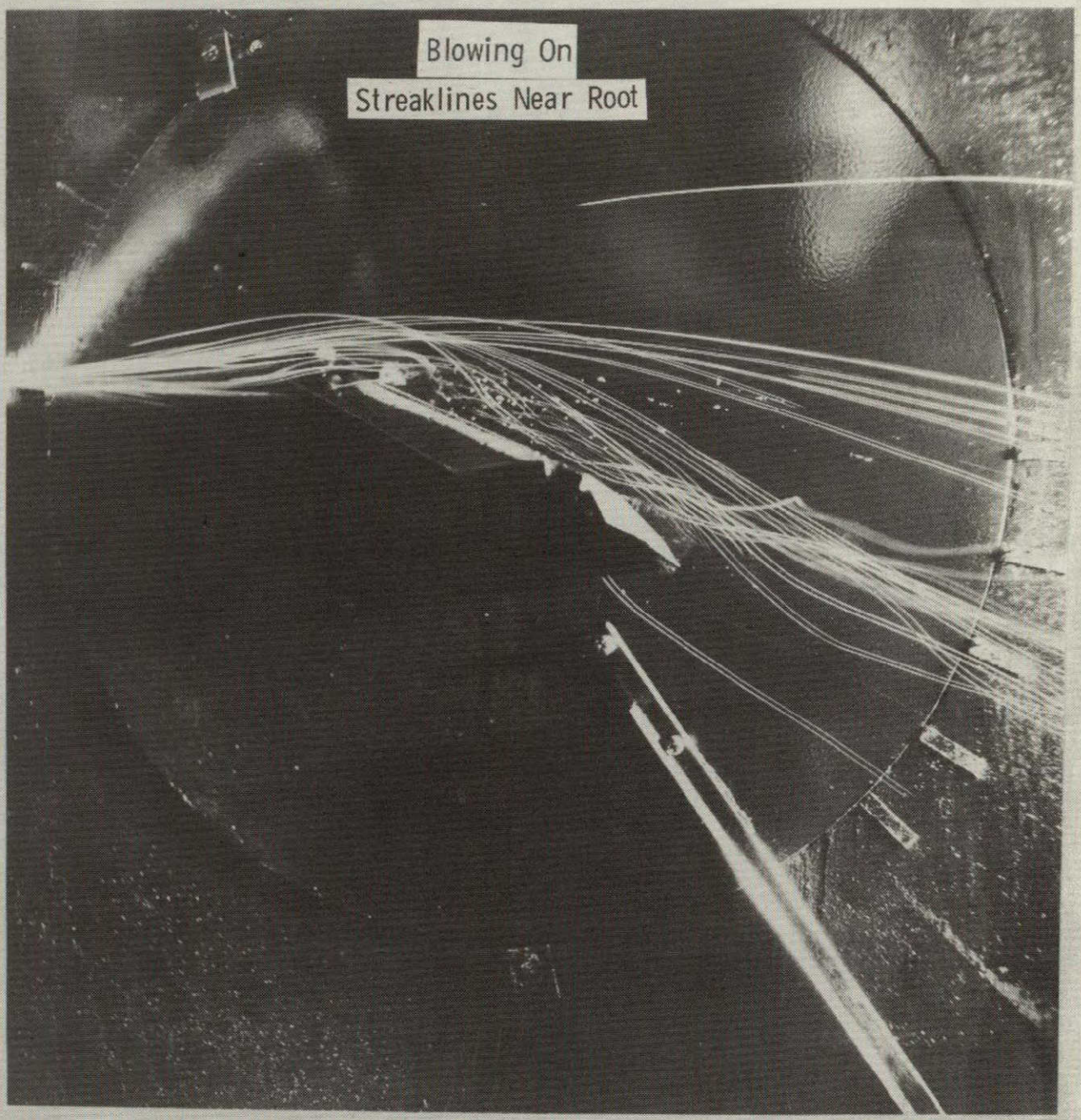

Figure 86.- Spanwise blowing over the 45^{0} swept trapezoidal wing with deflected LE and TE flaps for $\alpha = 25^{0}$ and $C_{\mu} = 0.011$; $\delta_{LE} = 20^{0}$; $\delta_{TE} = 30^{0}$; $x_n/c_r = 0.23$.

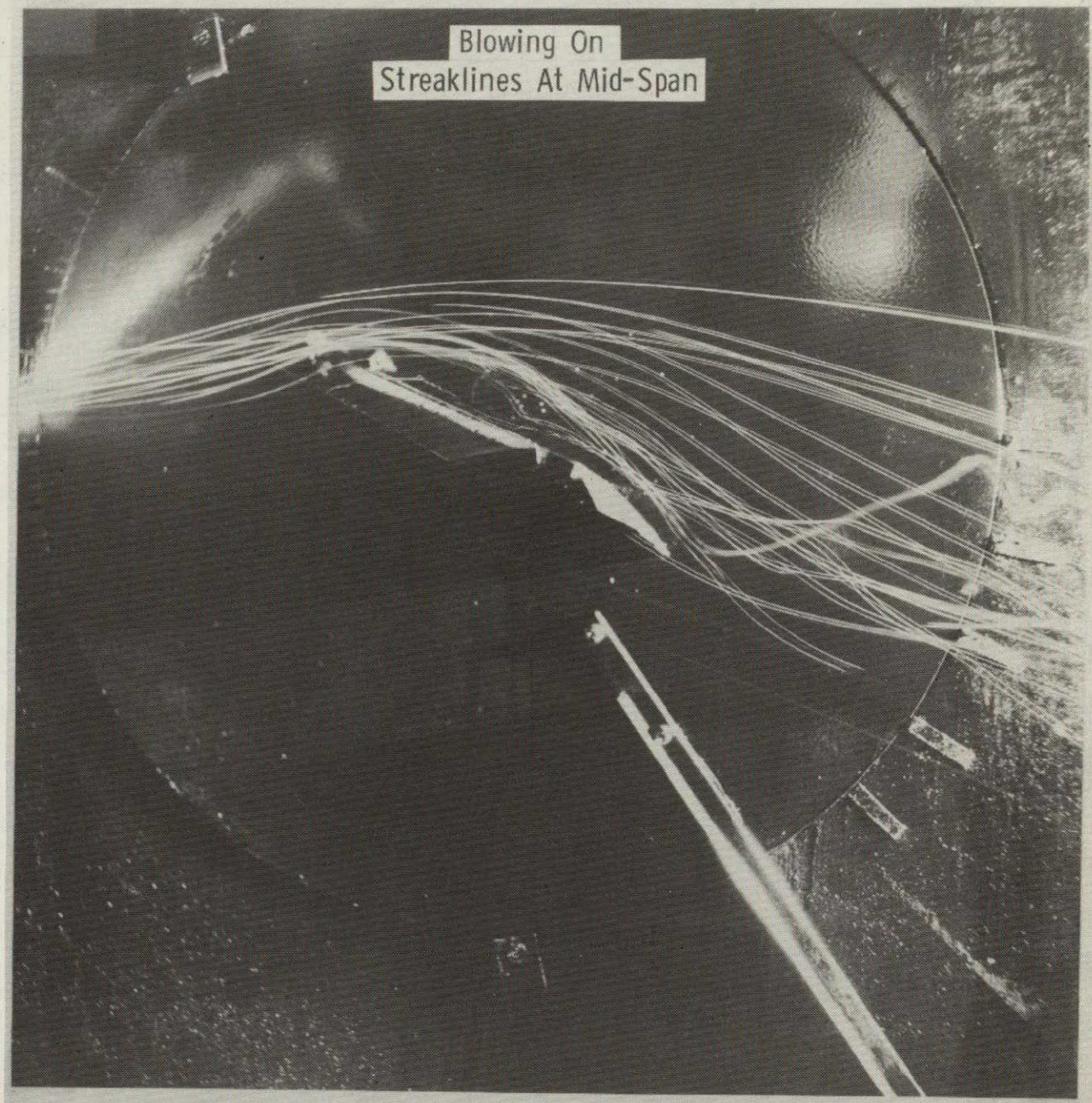

Figure 87.- Spanwise blowing over the 45^{0} swept trapezoidal wing with deflected LE and TE flaps for $\alpha = 25^{0}$ and $C_{\mu} = 0.011$; $\delta_{LE} = 20^{0}$; $\delta_{TE} = 30^{0}$; $x_n/c_r = 0.23$.

Figure 88.- Spanwise blowing over the 45^{0} swept trapezoidal wing with deflected LE and TE flaps for $\alpha = 30^{0}$ and $C_{\mu} = 0.026$; $\delta_{LE} = 20^{0}$; $\delta_{TE} = 30^{0}$; $x_n/c_r = 0.23$.

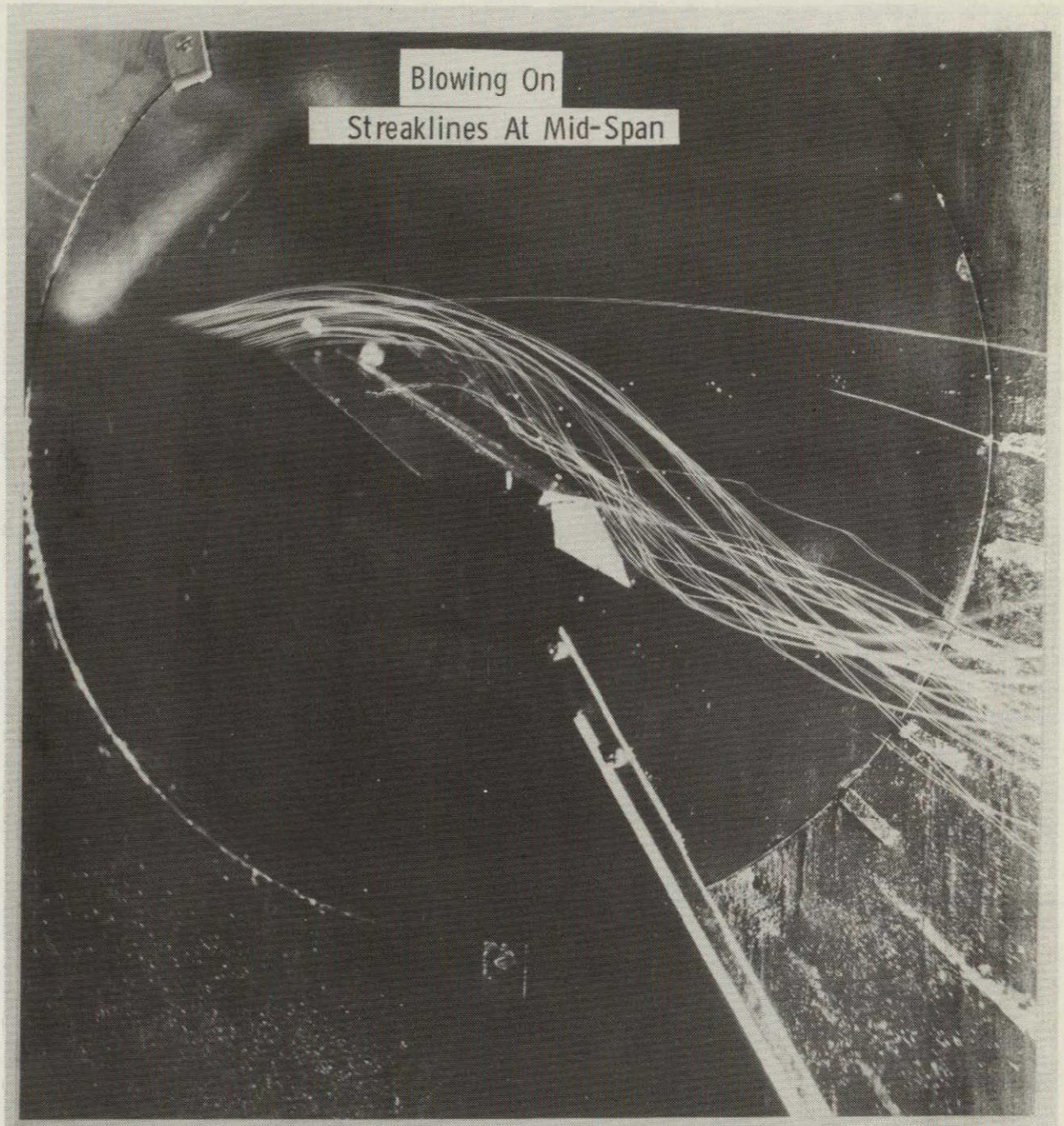

Figure 89.- Spanwise blowing over the 45^{0} swept trapezoidal wing with deflected LE and TE flaps for $\alpha = 30^{0}$ and $C_{\mu} = 0.026$; $\delta_{LE} = 20^{0}$; $\delta_{TE} = 30^{0}$; $x_n/c_r = 0.23$.